Structure/function analysis of the Huntingtin N-terminus encoded by *Htt* exon 1 using knock-in mouse models

Emily Ann André
Virginia Beach, Virginia
B.S. Biology, Biochemistry Minor James Madison University 2006

A Dissertation presented to the Graduate Faculty of the University of Virginia in Candidacy for the Degree of Doctor of Philosophy

Neuroscience Graduate Program
University of Virginia
May 2017

Scott Zeitlin, Ph.D. _____
(Dissertation Advisor)
Bettina Winckler, Ph.D. _____
(Executive committee member)
George Bloom, Ph.D. _____

Jim Mandell, M.D. _____

Madaline Harrison, M.D. _____

Abstract

Huntington's disease (HD) is a neurodegenerative disorder that effects up to 1 in every 10,000 people and it is caused by an expansion of the polyglutamine (polyQ) stretch within the Huntingtin (HTT) protein [1]. The HTT polyQ in mammals is flanked by a highly conserved 17 amino acid N-terminal domain (N17), and a proline-rich region (PRR) [2-4]. The PRR is a binding site for many HTT-interacting proteins [5-7], and the N17 domain regulates several normal HTT functions, including HTT's ability to associate with membranes and organelles [8, 9].

This study investigates the consequence of deleting mouse Huntingtin's (Htt's) N17 domain (ΔN17), deleting a combination of its polyQ stretch and PRR (ΔQP), or deleting all three N-terminal domains (ΔNQP) on normal murine Htt function and in the context of an HD mouse model (Q140). $Htt^{\Delta N17}$, $Htt^{\Delta QP}$, and $Htt^{\Delta NQP}$ knock-in mice were generated, and their behavior, autophagy function, and neuropathology were evaluated. Homozygous and hemizygous $Htt^{\Delta N17/\Delta N17}$, $Htt^{\Delta QP/\Delta QP}$, $Htt^{\Delta NQP/\Delta NQP}$, $Htt^{\Delta N17/-}$, and $Htt^{\Delta QP/-}$ mice were generated at the expected Mendelian frequency. $Htt^{\Delta QP/\Delta QP}$ mutants exhibit improvements in motor coordination compared to controls ($Htt^{+/+}$) while in contrast, $Htt^{\Delta N17/\Delta N17}$ mutants do not exhibit any changes in motor coordination, but they do display variable changes in spatial learning and memory. Neither mutant exhibited any changes in basal autophagy in comparison to controls, but thalamostriatal synapses in the dorsal striatum of 24-month-old $Htt^{\Delta N17/\Delta N17}$ mice were decreased compared to controls. These findings support the hypothesis that Htt's N17, polyQ, and PRR domains are dispensable for its critical functions during early embryonic development, but are likely more important for Htt functions in CNS development or maintenance.

In order to investigate the effects of the N-terminal domain deletions in the context of an HD mouse model, $Htt^{\Delta N17}$ and $Htt^{\Delta QP}$ mice were also crossed with Q140 mice to generate $Htt^{140Q/\Delta N17}$ and $Htt^{140Q/\Delta QP}$ mice. $Htt^{140Q/\Delta N17}$ and $Htt^{140Q/\Delta QP}$ mice demonstrated exacerbated rotarod and activity cage phenotypes, but improvements in spatial learning and memory. Investigation of primary striatal neurons from $Htt^{140Q/\Delta N17}$ and $Htt^{140Q/\Delta QP}$ mice exposed a deficit in autophagic flux in comparison to controls that was not observed in primary cortical neurons, suggesting that normal Htt's functions may be somewhat altered in different regions of the brain. Additionally, $Htt^{140Q/\Delta N17}$ primary striatal and cortical neurons had elevated basal p62 immunostaining. These results suggest that expression of the Htt domain deletions *in trans* with 140Q-Htt can elicit autophagy phenotypes in cortical and striatal neurons.

Acknowledgements

I would first and foremost like to thank Scott Zeitlin and Jeh-Ping Liu for their scientific guidance, technical expertise and continual support. Thank you for always pushing me to be a better scientist, and for your patience during the times when things were not working out the way we wanted. I would also like to thank my committee members: Dr. Bettina Winckler, Dr. Jim Mandell, Dr. Madaline Harrison, and Dr. George Bloom for their support and direction over the years. I would also like to thank the NGP Administrators: Tracy Mourton and Nadia Cempre, and NGP Directors: Dr. Sue Moetner, Dr. Bettina Winkler, Dr. Manoj Patel, and Dr. Chris Deppmann.

I would like to thank Jonathan Kipnis, Noel Derecki, and Alban Gaultier for sharing essential equipment. I also would like to thank Ellie Braatz for significant help with data collection, analysis, and editing of this and other manuscripts, and Stephen Grado for his help collecting activity cage data. This work was supported by NIH/NINDS F31NS083289 (E. Andre), NS043466, and NS077926 (S. Zeitlin).

Finally I would like to thank my incredible network of friends and my wonderful family. They have all been so unbelievably supportive over the past 7½ years, and I would not have made it through to this point with out their encouragement and love.

Table of Contents

Chapter I: Introduction

Huntington's disease (HD) is an autosomal dominant neurodegenerative disorder that is caused by an expansion of a CAG nucleotide repeat within the *Huntingtin* (*HTT*) gene that encodes an expanded polyglutamine (polyQ) stretch in the Huntingtin (HTT) protein. Although the *HTT* gene was discovered almost a quarter century ago [1, 10], there is still no effective treatment or cure for HD. HD is one of nine neurodegenerative disorders that are caused by expanded CAG repeat-encoded polyQ expansions [1]. Although each of these disorders exhibit common features, different neuronal populations are affected in each disease [1]. Thus, the protein context surrounding the polyQ expansion could be important in determining the mechanism of pathogenesis for each disorder.

i. HD neuropathology and symptoms

1. Diagnosis and symptoms

Patients develop HD when the polyQ stretch within the HTT protein expands to >39Q. Most HD patients are diagnosed between 35 and 50 years-of-age, but ~10% develop juvenile onset HD and are diagnosed before they are 20 years old [1]. Although HD is classified as a movement disorder, patients exhibit cognitive and psychiatric deficits in addition to motor impairments [11].

Early motor decline in HD patients is largely dominated by chorea, an involuntary "dance-like" dyskinesia, but as the disease progresses, bradykinesia, dystonia, and rigidity become increasingly more common, and may in fact cause more severe physical impairment that results in serious falls [11, 12]. During the later disease stages, many

patients develop dysarthria (difficulty in speaking) and dysphagia (difficulty in swallowing) that often leads to aspiration pneumonia. Disturbances in the sleep/wake cycle and gradual cognitive decline in comprehension, reasoning, judgment, and memory precede motor impairment in most patients [1, 11]. This decline in cognitive function may even develop into a progressive dementia in some patients [1, 11]. Psychiatric impairments in HD are usually related to depression and irritability, but can also include apathy, social withdrawal, bi-polar disorder, and manic episodes [11, 12]. Additionally, a variety of peripheral symptoms can manifest due to the fact that mutant HTT (mHTT) is expressed throughout the entire body [13]. Weight loss, cardiomyopathy and skeletal muscle atrophy are common in HD patients, and mHTT aggregates can be found in many different cell types, including cardiomyocytes, skeletal muscle, and peripheral immune cells [13, 14]. Death occurs approximately 15-20 years post-symptomatic onset [1, 11, 12].

2. Neuropathology

a) mHTT aggregation

Widespread neuronal loss is observed in post-mortem brains of HD patients, but the most significant neuronal death occurs in the basal ganglia and in the cortex [1, 15]. There are many hypotheses for the selective vulnerability of these two populations of neurons, but it is clear that cellular dysfunction occurs in nearly all cell types in the brain and in many cells in the periphery. For many years, it has been known that mHTT is inefficiently cleared, leading to the formation of toxic mHTT oligomers, fibrils, and aggregates in many neuronal sub-types [16-19]. To a lesser extent, mHTT aggregates can

also be found in oligodendrocytes and astrocytes, and at a very low level in microglia [20]. N-terminal mHTT fragments containing the expanded polyQ stretch are thought to be especially toxic and can be generated through cleavage by several different proteases at multiple locations within the HTT protein (Fig. 1-1A) [21-24]. For example, caspase-6 cleavage of the full-length mHTT protein has been hypothesized to be required for neuronal dysfunction and degeneration in mice [21]. In addition to full-length HTT, these N-terminal fragments generated by protease cleavage of mHTT readily form oligomers and fibrils that can then aggregate into larger nuclear inclusions or cytoplasmic aggregates [24].

Recent evidence also suggests that some neuropathology can be attributed to aberrant Repeat Associated Non-ATG (RAN) translation of both sense and anti-sense *mHTT* RNA transcripts containing the CAG (or CUG) repeats [25]. RAN translation of the triplet repeats within the *mHTT* transcripts can generate polyalanine, polyserine, polyleucine, and polycysteine that aggregate readily and, like the mHTT aggregates, can also accumulate within the nucleus and cytoplasm of neurons, astrocytes, and microglia [25]. Additionally, *HTT* primary RNA transcripts contain a cryptic polyadenylation signal within the first intron [26]. The expanded CAG repeat within the *mHTT* mRNA can suppress recognition of the first intron's 5′splice site leading to activation of the cryptic polyadenylation signal within the intron [26]. This leads to the generation of a truncated *mHTT* mRNA that is translated into a toxic N-terminal fragment of mHTT encoded by the first exon [26]. The expression and accumulation of the different species of mHTT protein and RAN translation products can lead to extensive and wide-ranging cellular dysfunction in the brain, as illustrated in Figure 1-1.

Interestingly, while mHTT oligomers and fibrils have been shown to be toxic, there is significant debate in the field over whether or not large mHTT aggregates cause cellular dysfunction, or whether aggregation is a mechanism for cells to sequester toxic mHTT fragments into a form where they can do less harm [1, 27]. One possible mechanism for aggregate toxicity, however, may be through aberrant mHTT interactions leading to sequestration and local depletion of wild type HTT, transcription factors, and motor proteins, resulting in altered transcriptional regulation and disrupted axonal transport (Fig. 1-1B,E,F) [28, 29].

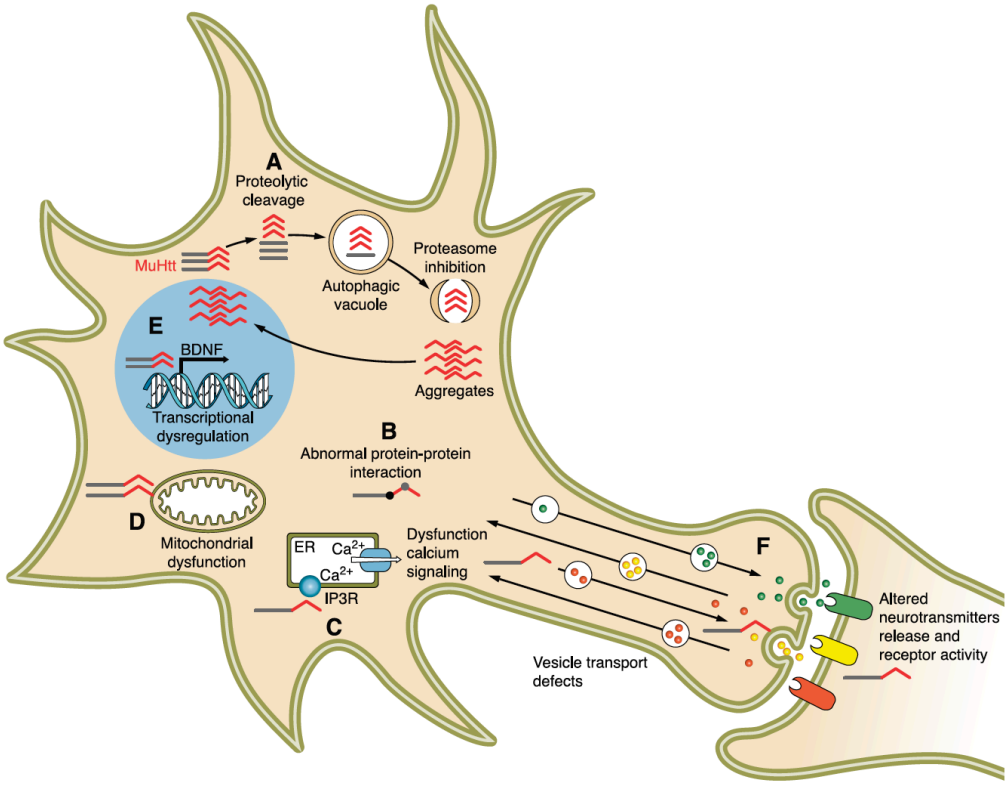

Figure 1-1. Summary of the cellular processes that are disrupted in HD. Adapted from Zuccato et al. [1]

In addition to the generation of aberrant protein products due to proteolysis of full-length mHTT, activation of a cryptic polyadenylation site, and RAN translation,

aggregates also accumulate because clearance of cellular waste through degradative pathways is defective in HD [1, 16, 30]. Failure of autophagosomes to efficiently recognize cytosolic cargo has been observed in HD models [30]. This cargo recognition failure results in the generation of empty autophagosomes, leading to decreased protein and organelle degradation in neurons [30]. Additionally, inefficient transport of autophagosomes has been described in HD mouse models [31]. Interestingly, lysosomes maintain a diffuse distribution throughout the cell body of wild type cells, but in HD cells, lysosomes adopt an aberrant perinuclear distribution [32]. Because autophagosomes that are generated in the distal tips of axons mature as they are transported retrogradely towards the cell body for fusion with lysosomes and eventual degradation [33], inefficient transport of autophagosomes and the altered localization of lysosomes can lead to defective clearance of aggregates, proteins, and organelles in HD [31, 32].

b) Metabolic and cellular pathway dysfunction in HD

Alteration of cerebral glucose consumption can be detected in early clinical stage HD patients by Positron Emission Tomography (PET) scans illustrating metabolic deficits likely due to dysfunctional mitochondrial bioenergetics [34]. Indeed, deficits can be observed in mitochondrial fission, fusion, and transport in HD mouse models resulting in the appearance of fragmented mitochondria (Fig. 1-1D) [35, 36]. Mitochondrial respiration efficiency has also been shown to be affected in HD models through changes in electron transport chain protein levels and activity [37-39].

Synaptic dysregulation and consequential neuronal excitotoxicity are also

observed in HD [1]. Wild type HTT interacts with PSD-95, a synaptic density anchoring protein that modulates long-term potentiation (LTP) and long-term depression (LTD) through its regulation of NMDA-receptor clustering at the post-synaptic density [40]. mHTT's interaction with PSD-95 is reduced, leading to increased availability of PSD-95 in the post-synaptic density that could contribute to NMDA-modulated excitotoxicity [40]. Excitotoxicity in HD may also be caused by alterations in NMDA receptor subunit expression levels and decreased glutamate transporter levels in astrocytes, both of which can be detected in HD patient post-mortem tissue [41]. Q140 HD knock-in mouse model mice have a reduced number of thalamostriatal synapses at 1 month-of-age, and decreased corticostriatal synapses can be observed at 12 months-of-age [42, 43]. Additionally, BACHD mice have a decreased number of dendritic spines on medium spiny neurons by 18 months of age [44]. Decreased brain-derived neurotrophic factor (BDNF) mRNA and protein, and altered Ca^{2+} homeostasis also contribute to cellular dysfunction in HD [45-47]. The considerable number of cellular pathways that are affected by mHTT complicate our understanding of pathogenic mechanism; furthermore, there is substantial evidence that loss of wild type HTT function may also contribute to HD pathogenesis.

ii. Wild type HTT structure and function

1. Evolution of HTT

HTT is an ancient gene that is found in organisms as far back as *Heliocidaris herithrogramma* (Sea urchin) [1, 4]. Analysis of the *HTT* sequence throughout evolution suggests that the C-terminal portion of the protein is the most conserved region within

HTT, and that it confers a more primordial function that is hypothesized to be essential for HTT's essential role in embryonic development [1, 4]. Loss of this evolutionarily conserved function in development can therefore explain the embryonic lethality that is observed in *Htt* $^{-/-}$ mice [1, 4]. Because the N-terminal region appears to have evolved more recently coincident with new neuronal activities in deuterostomes, it is thought that the N-terminus confers a specific neuronal function to HTT [4]. Indeed, when *Htt*$^{+/-}$ mice are crossed with mice expressing an N-terminal fragment of mouse Htt containing the first 208 amino acids of Htt, progeny hemizygous for expression of this fragment exhibit embryonic lethality, similar to *Htt*$^{-/-}$ embryos. [48]. As chordates began to evolve more complex nervous systems similar to vertebrates, HTT distribution became more restricted to neural plate cells, implicating an essential role for HTT in neural development [3]. Interestingly, HTT expression in humans is highest in cortical pyramidal neurons from layers III and V that project to the striatum [49].

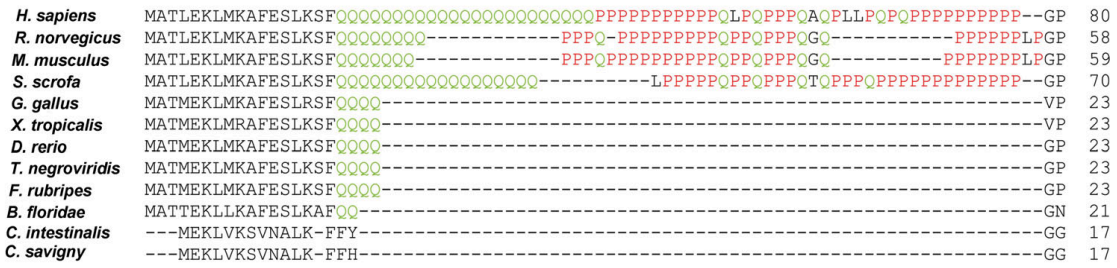

Figure 1-2. Diagram showing the evolution of the amino acid sequence encoded by exon 1. The polyQ domain can first be observed in *B. floridae*, the lancelet. Adapted from Candiani et al [3].

In mammals, the polyQ stretch of HTT is flanked by two domains that can modulate polyQ structure and toxicity [2, 50-53]: a highly conserved 17 amino acid N-terminal domain (N17) and a proline-rich region (PRR) adjacent to the C-terminus of the polyQ stretch. The polyQ stretch of HTT has expanded in size during its evolution from more ancient species to mammals (Fig. 1-2) [4]. The N17 domain has retained strict

sequence conservation in nearly all vertebrates [4]. As HTT evolved in mammals, the polyQ region continued to elongate concurrent with the appearance of an adjacent PRR (Fig. 1-2) [4]. These domains continued to increase in size during mammalian evolution with the PRR increasing in length as the polyQ stretch expanded from 7Q in rodents to an average of 20Q in humans [4]. This suggests that the PRR may have a role in modulating the structure and function of the polyQ stretch in mammals [4].

2. Structure of HTT

HTT is a large (~350kD) protein, and it is partly because of its size that both the structure and function of the protein have been so difficult to study. Seven different conformations have been characterized for the N-terminus of HTT that encodes the N17, polyQ and PRR domains [50, 54]. The N17 region adopts an α-helix that induces the closest 10-15 Q within the polyQ region into a similar secondary structure [50, 54]. The remainder of the polyQ region forms a random coil that eventually devolves into an extended loop [50]. The PRR forms two polyproline helices, but the structure of the more C-terminal amino acids of exon 1 were not solved [50]. The flexibility of the polyQ region could be a factor in HTT's ability to form so many alternate conformations [54]. Indeed, as the polyQ region expands, there is a higher probability for this region to form a β-sheet structure, thus, increasing its tendency to form intermolecular aggregates [2]. Additionally, the polyQ region can form a polar zipper that facilitates its interaction with polyQ domain-containing transcription factors, enabling HTT to modulate gene transcription and expression [55, 56].

Previous studies have shown that the amphipathic α-helical HTT N17 domain is

capable of associating with organelle membranes, and is critical for HTT's function in cellular stress responses [8, 9, 57-59]. The N17 domain is also a target for multiple post-translational modifications that can influence HTT subcellular localization and stability, and contains a CRM1-dependent nuclear export signal (Fig. 1-3) [8, 9, 57, 58, 60]. The HTT PRR interacts with both WW domain- and Src homology 3 (SH3)-containing proteins, and can influence post-translational modifications of the HTT N17 domain [5-7, 61, 62]. Additionally, the HTT N17 and PRR domains can interact with each other [63-65].

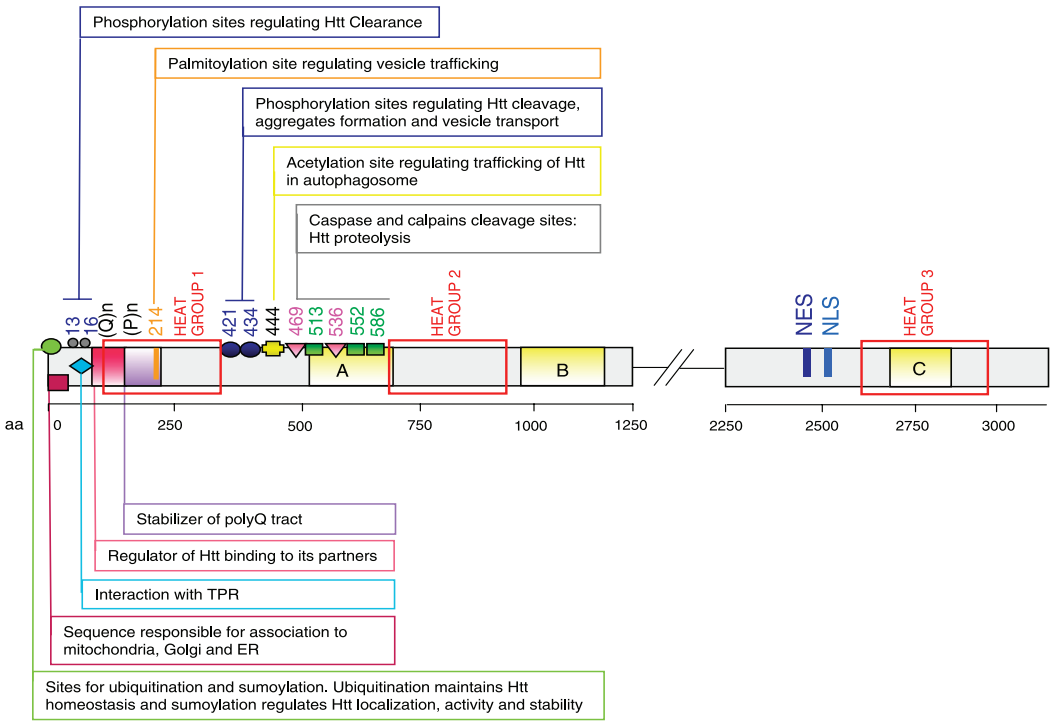

Figure 1-3. Important HTT functional regions and post-translational modification sites. Adapted from Zucatto et al. [1].

HTT can interact with hundreds of different proteins, and HTT's HEAT repeat structure (named for the group of proteins in which they were initially described:

Huntingtin, Elongation factor 3, protein phosphatase 2A, and target of rapamycin (TOR1) kinase) can potentially regulate several of these interactions [1, 4, 66, 67]. HTT has 36 HEAT and HEAT-like repeats, about 40 amino acids each, which are organized into 3-4 different regions within the protein (Fig. 1-3) [68, 69]. HEAT repeats form 3-dimensional structures called α-RODs, which can associate with other α-RODs [4, 68]. This could allow for intramolecular association of HEAT repeats within HTT, homodimerization of HTT, and also intermolecular associations of HTT with α-RODs in other proteins [68].

The HTT C-terminus contains both a nuclear localization signal (NLS) and a nuclear export signal (NES), which allow for its movement in and out of the nucleus and provide a mechanism for HTT-mediated transcriptional regulation [70].

Post-translational modifications of HTT have extremely diverse effects on HTT function (Fig. 1-3). For example, there are multiple phosphorylation sites within HTT, and phosphorylation of serine 13 and 16 have been shown to increase clearance of HTT, to regulate interaction of the N17 domain with the PRR, to regulate HTT's subcellular localization, and to decrease toxicity of mHTT [60, 64, 71, 72]. Furthermore, phosphorylation of HTT at serine 434, 1181 and 1201 result in decreased proteolytic cleavage at residue 513 resulting in decreased toxicity in HD models [73]. Additionally, phosphorylation at serine 421 regulates the directionality of HTT-modulated microtubule-based transport in axons [74]. Ubiquitination of HTT can target it to the proteasome for degradation, and acetylation can induce its clearance by autophagy [75, 76]. Sumoylation of HTT can also affect HTT's localization and stability within the cell [76]. When mHTT is sumoylated, decreased aggregation leads to increased

transcriptional repression and toxicity *in vitro* and in *Drosophila* HD models [76]. Furthermore, repression of sumoylation modifications in HTT results in improved neuropathological and motor phenotypes in HD mouse models [77]. Finally, palmitoylation of HTT at cysteine 214 can enhance its membrane association [78].

HTT can be cleaved by caspases, calpains, and aspartyl proteases at specific amino acid residues [79]. Different proteolytic cleavages are favored in specific cell types, perhaps conferring vulnerability to specific neuronal cell populations [16, 80]. The normal function of these cleavage events is currently unknown, however it has been demonstrated that alterations in the pattern of these cleavages can exacerbate toxicity of mHTT [22].

3. Wild type Huntington Functions

HTT is a scaffolding protein that is involved in multiple cellular functions [65, 81, 82]. The generation and characterization of *Htt* knock-out mice revealed that Htt has an essential function during early embryonic development [83-85]. Homozygous *Htt* knock-out embryos (*Htt* $^{-/-}$) die between E8 and E10 [83-85]. Subsequent experiments using hypomorphic *Htt* knock-in mice that express significantly reduced levels of Htt during development, and Cre/*loxP*-mediated knock-out of *Htt* expression in the developing forebrain at mid-gestation and at postnatal day 5, revealed that Htt is involved in neurogenesis and adult neuronal homeostasis [86, 87]. In the hypomorphic *Htt* knock-in mice, global reduction of Htt expression below 50% normal levels led to abnormal cranial formation and gross CNS developmental phenotypes [86]. A similar reduction in Htt expression also leads to defects during generation of the neural tube and later in

development, severe structural phenotypes were observed in the cortex [88]. In chimeras generated with Htt knock-out ES cells, very few descendants of the knockout cells were found in the thalamus, striatum, cortex, and certain layers of the cerebellum [89]. Cells lacking Htt in these regions were not able to survive during development, demonstrating that Htt not only plays a major role in embryonic development but also in the overall formation of the CNS [89]. Recent MRI studies of pre-symptomatic gene-positive individuals have identified subtle structural abnormalities years before disease onset, lending support to the hypothesis that HD is both a neurodevelopmental and neurodegenerative disease [90].

HTT is also involved in the regulation of synaptic development and maintenance. In addition to its post-synaptic interactions with PSD-95, HTT can associate with a variety of other synaptic complexes including clathrin-coated vesicles via an association with HIP1, and with PACSIN 1 a protein that modulates synaptic vesicle recycling in synaptic boutons [40, 91-93]. HTT also interacts with several Cytomatrix at Active Zone (CAZ) proteins in the pre-synaptic terminal including Bassoon, Piccolo, and Ahnak that modulate vesicular endo- and exocytosis [94]. When *Htt* is conditionally inactivated in cortical neurons, an increased number of $Vglut1^{+}PSD\text{-}95^{+}$ corticostriatal synapses can be detected in the dorsal striatum of 21-day-old mice, while an increase in both corticostriatal synapses and $Vglut2^{+}PSD\text{-}95^{+}$ thalamostriatal synapses can be observed in 5-week-old mice [95]. These data suggest that there is a role for Htt in synaptic development and maintenance.

It is hypothesized that HTT may have evolved through the fusion of 3 yeast cytoplasm to vacuole targeting (Cvt) autophagy genes (Atg23, Vac8, and Atg11), which

regulate selective macroautophagy [65, 75]. HTT has been shown to promote selective macroautophagy through its interaction with several autophagy pathway members including p62/SQSTM1 (p62), Ubiquitin (Ub) and microtubule associated protein 1A/1B-light chain 3 (LC3) [81]. "Bulk" non-selective macroautophagy (a.k.a. starvation-induced autophagy) is regulated by mTORC1 association with and repression of ULK1 [81, 96-98]. Under cellular stress, however, HTT can compete with mTORC1 for binding to ULK1 [81]. The subsequent interaction of the HTT-ULK1 complex with p62, LC3, and Ub leads to the assembly of autophagosomes around specific cargo [81]. Interestingly, decreased ULK1 activity is seen in HD models because large amounts of the protein become sequestered into the insoluble protein fraction, resulting in decreased macroautophagy and decreased degradation of cellular debris [99]. In addition to the initiation of selective macroautophagy, HTT's interaction with p62 and ubiquitinated substrates enhances binding of p62 to its cargo and increases the efficiency of autophagosome assembly [81]. When Htt is conditionally deleted from the forebrain of mice, $p62^{+}$ ubiquitinated protein aggregates accumulate in an age-dependent manner, further emphasizing the importance of Htt in neuronal selective macroautophagy [65].

Axonal transport of cargos and organelles to and from the soma is yet another important function for HTT in neuronal cells [100]. Htt is thought to be involved in the process of forming the motor complex onto microtubules during dynein- and kinesin-1-mediated vesicular transport, with the help of other proteins such as HAP1[100]. Through this interaction, Htt can modulate autophagosomal and mitochondrial transport, perinuclear positioning of late endosomes and lysosomes, and transport of BDNF-containing vesicles [29, 31, 101-105]. One explanation for the observation that MSNs are

particularly vulnerable in HD is that decreased Htt levels can lead to decreased production of BDNF in the cortex and lower levels of striatal BDNF [106]. Htt expression regulates BDNF promoter II, which contains a DNA response element called RE1/NRSE that is recognized and silenced by the REST/NRSF co-repressor complex [56]. mHtt is unable to form its normal association with REST/NRSF which, when bound to Htt, is sequestered in the cytoplasm of the cell, allowing transcription of BDNF to occur [56]. There is likely an entire subset of genes, both neuronal and non-neuronal, that could be regulated by HTT through RE1/NRSE promoter sequences [56].

Another HTT function that is dependent on its interaction with HAP1 is the transport of ciliary proteins to the peri-centriolar material (PCM), which surrounds the basal body where cilia biogenesis and anchoring occur [107]. Loss of wild type Htt leads to decreased primary and secondary ciliogenesis in neurons and glia, and dispersion of the PCM proteins [107]. Interestingly, mHtt causes hyperactive ciliogenesis that leads to altered motile secondary cilia orientation in ependymal cells and disrupted flow of the cerebrospinal fluid (CSF) in the ventricles [107]. Reduced CSF flow could be especially harmful in the HD brain given that both removal of waste and delivery of growth factors and nutrients could be affected in this disorder.

An unexpected function for Htt during mitosis has now been demonstrated in two independent laboratories [58, 108]. Htt localizes to mitotic spindle poles from prophase to anaphase, to the spindle mid-zone during anaphase, and to the cell furrow during cytokinesis [58, 108]. Depletion of Htt disrupts spindle orientation and alters assembly of mitotic proteins at the spindle poles [108]. Altered spindle orientation can affect how mouse neural progenitors divide, ultimately influencing their cell fate and causing

progenitors to differentiate into neurons prematurely at the expense of maintaining the progenitor cell population in the ventricular zone [108].

The Htt polyQ stretch does not appear to contribute to its essential functions, as its deletion in mice does not perturb embryonic development or result in motor or neuropathological deficits in adults [109]. Deletion of the polyQ stretch resulted in improved motor coordination, and a significantly increased lifespan [109, 110]. Moreover, deletion of the normal Htt polyQ stretch in the context of an HD mouse model (*Htt*$^{140Q/\Delta Q}$ mice) resulted in increased autophagic clearance of mHtt aggregates and amelioration of behavioral phenotypes (Fig. 1-4) [110]. These results suggest that enhancing selective macroautophagy may be beneficial for organisms in general, not only in the context of disease [109, 110].

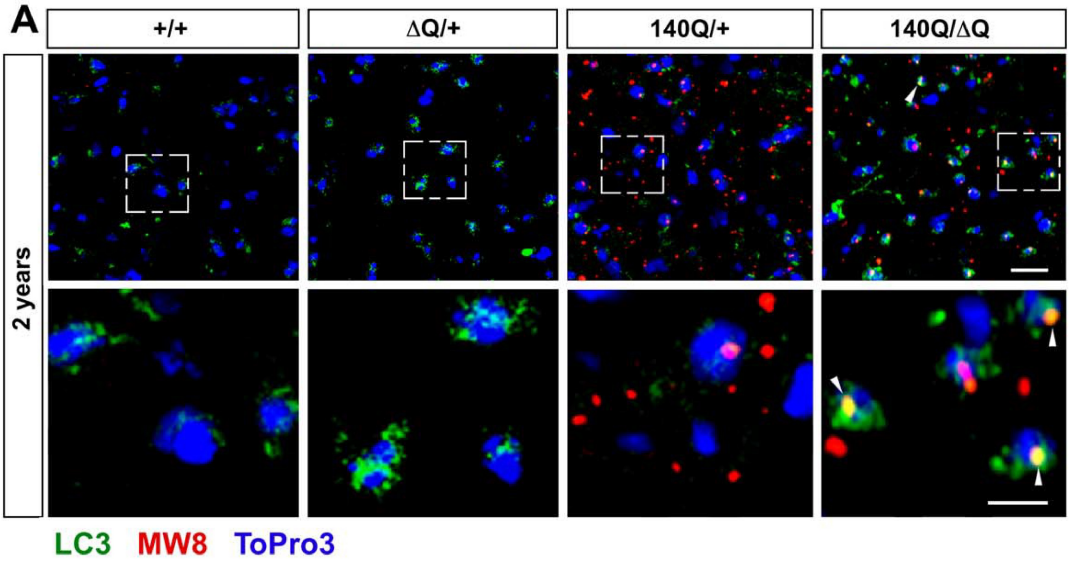

Figure 1-4. Increased LC3 immunostaining in the striatum of 2-year-old *Htt*$^{140Q/\Delta Q}$ mice compared to *Htt*$^{140Q/+}$ mice. Figure adapted from Zheng et al. [110]

ER stress and autophagy regulation are closely interconnected. ER stress can induce autophagy to help in the catabolism of unfolded proteins or damaged organelles

[111, 112]. Htt's association with the ER is stress-sensitive, and during acute stress events (e.g. the unfolded protein response, temperature stress, and DNA/RNA damage), Htt dissociates from the ER and vesicles, is phosphorylated at serine 13 and serine 16, and can subsequently enter the nucleus [57, 58, 113]. These phosphorylation events in the N17 domain also result in reduced nuclear export and increased nuclear retention [58]. Cofilin-1, an actin modulating protein, is also transported into the nucleus during acute stress events [114]. Together, cofilin and Htt bind nuclear actin and form many small cofilin-actin rods [114, 115]. This process temporarily halts nuclear actin treadmilling, resulting in decreased ATP consumption and increased availability of cellular ATP that can subsequently contribute to additional cellular stress response mechanisms to aid in recovery from acute stress events [114, 115]. Knock-down of wild type Htt can cause changes in the dynamic assembly and disassembly of these cofilin-actin rods [114].

Additionally, under conditions of heat shock stress, Htt rapidly localizes to $Rab5C^{+}$ early endosomes in the cytoplasm of neurons in as little as 10 minutes post-stress induction [116]. Coincident with Htt's re-localization, a halt in early to recycling and early to late endosomal trafficking can be observed [116]. This can also result in a decrease in ATP consumption, comparable to that of halting nuclear actin treadmilling [116]. Importantly, the secondary structure and post-translational modifications of the N17 domain were shown to be critical for these neuronal stress responses [60, 114, 116]. Moreover, expression of mHtt was shown to significantly delay recovery from these stress response events [114, 116].

Recent work has demonstrated that the Htt N17 domain can act as a sensor for reactive oxygen species (ROS) [117]. During conditions of oxidative stress, the sulfur

side group on methionine 8 in the N17 domain is oxidized and leads to Htt dissociation from the ER membrane, phosphorylation of serine 13 and 16, and accumulation of Htt within the nucleus [117]. Subsequent work showed that upon entering the nucleus, Htt can also localize to sites of oxidative DNA damage and may act as a scaffold for DNA base excision repair machinery [82].

The N17 domain has also been proposed to be required for mHTT oligomerization and aggregate formation, and its loss leads to decreased cellular viability *in vitro* [118, 119]. The enhanced toxicity of mHTT lacking its N17 domain may be due to the fact that this domain modulates HTT's interaction with multiple chaperone proteins that affect the size, density, and location of HTT aggregates through acetylation, ubiquitination, and sumoylation of this domain [118, 120, 121].

Solid-state NMR investigation of the N17 domain has also suggested that the long-hypothesized α-helical structure of the N17 domain is in fact relatively prone to devolve into a disordered state under physiological temperature and pH conditions [122]. Additionally, computational modeling indicates that once the N17 domain has transformed into a more disordered state, the entire N-terminal exon 1 fragment of mHTT is much more likely to form aggregates, suggesting a crucial role for the N17 domain in mHTT aggregation dynamics [122]. Additionally, phospho-mimicry of serine 13 and serine 16 has been shown to decrease the α-helical content of the N17 domain [60].

The PRR is a WW-domain and SH3 protein interaction domain that modulates HTT's interaction with many proteins and protein complexes [5-7, 62]. Several of these proteins are transcription factors, or are involved in pre-mRNA splicing, implicating HTT in multiple mRNA biogenesis pathways [5]. Additionally, the PRR has been shown to

enable Htt's interaction with Epidermal Growth Factor Receptor signaling complexes, linking Htt to the modulation of tyrosine receptor-mediated signaling, including cell proliferation, migration, and adhesion [6]. The interactions of both PACSIN 1 and PSD-95 with Htt are mediated through the SH3 domain of each protein; therefore, they likely interact with Htt through the PRR [40, 93].

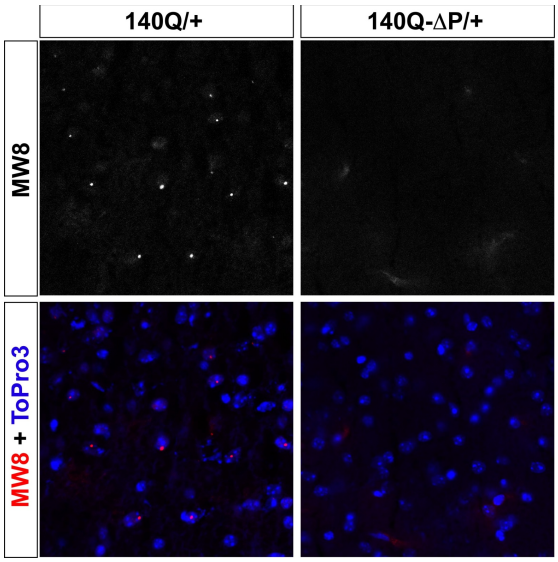

Figure 1-5. Nuclear aggregate formation is modulated by the PRR. The Q140 HD mouse model develops nuclear inclusions by 6 months of age (detected with the MW8 antibody). When the PRR is deleted in the context of the 140Q stretch (*Htt* $^{140Q\text{-}\Delta P/+}$ mice), MW8^{+}-aggregates are not detected at 6 months of age. Liu et al. in preparation.

Substantial *in vitro* evidence suggests that the PRR helps to stabilize the polyQ region against conformational collapse and can reduce mHtt toxicity [2, 51, 52, 54]. Thus, its deletion should result in enhanced toxicity in an HD disease model. *In vivo* data suggests that deletion of the PRR in wild type Htt has no impact on embryonic development, but does result in spatial learning and memory deficits in 18-month-old male mice [61]. In *Htt*$^{140Q\Delta P/+}$ mice, deletion of the PRR leads to a reduction and delay in the formation of large 140QΔPRR-Htt aggregates and to differential effects in motor tests (Fig. 1-5) and Liu et al., in preparation

4. Wild type Htt modulation of HD pathogenesis

Results from several studies suggest that decreasing normal HTT expression in the context of mHTT expression enhances pathogenesis and accelerates disease progression [88, 123]. A transgenic mouse model of HD on a *Htt*-null background (YAC128-*Htt*$^{-/-}$ mice) exhibit more severe phenotypes in comparison to mice with normal levels of wild type Htt [123]. The YAC128 mice lacking normal Htt exhibit more striatal atrophy in comparison to the control YAC128 mice, and they perform worse in motor coordination tests [123]. Thus, wild type Htt expression can modulate the deleterious effects of mHtt expression. While symptoms in HD can be generally attributed to the toxicity of mHTT, it is likely that complete amelioration of symptoms can only be accomplished by also restoring normal Htt's functions [123]. Therefore, maintenance of essential HTT functions should be a goal in any therapeutic strategy targeting mHTT expression. An understanding of the role of individual protein domains in HTT's normal functions and their effect on mutant HTT's toxicity can contribute to this goal.

Previous work in the field has established roles for the each of the three HTT domains of interest (N17, polyQ, and PRR domains); however, much of this work was performed using over-expression and/or by expressing small N-terminal fragments of mHtt *in vitro*. Far less *in vivo* data with endogenous Htt expression levels, and with deletion mutations generated in the context of the full-length Htt protein exists. However, BACHD-ΔN17 mice, where the N17 domain has been deleted from the expanded *Htt* allele, have been generated and characterized [124]. In these mice, deletion of the N17 domain results in accelerated and worsened behavioral and neuropathological phenotypes

compared to control BACHD mice, demonstrating that the presence of the N17 domain reduces the toxicity of mHtt [124]. Ultimately, *in vivo* methods are needed to confirm the significant amount of *in vitro* evidence suggesting specific roles for the N17 and PRR domains in HTT function.

Chapter II: Materials and Methods

i. Generation of *Htt*$^{\Delta N17}$, *Htt*$^{\Delta QP}$, and *Htt*$^{\Delta NQP}$ mouse alleles

To delete amino acids (aa) 2-17 of the N17 domain from the endogenous *Htt* locus in mice (*Htt*$^{\Delta N17}$), two partially complementary oligonucleotides were annealed and filled in with the Klenow fragment of DNA polymerase I: 5′-CTT**CAGGGTCTG**TC CCATCGGGCAGGAAGCCGTCATGCAGCAGCAACAG-3′ and 5′–GGCGGCGCC TGCGGCGGTGGCTGCTGCTGCTGTTGCTGCTGCATGACGG–3′ (the *AlwN*I site is in bold and underlined, the *Nar*I site is underlined). The synthetic double-stranded DNA was then digested with *AlwN*I and *Nar*I to generate a DNA fragment incorporating the N17 deletion that was used to replace the wild type *AlwN*I – *Nar*I fragment in *Htt* exon 1. This DNA fragment was ligated into an *AlwN*I – *Nar*I digested pBSK+ vector containing 4,585 base pairs of the 5′ portion of *Htt* encompassing the Htt promoter, first exon, and a portion of the first intron (Fig. 3-2). A 5′ homologous sequence for gene targeting (that also contained a Neomycin resistance cassette) was digested with *Hin*dIII and *Not*I and subsequently ligated into the targeting vector. The targeting vector was linearized at a *Not*I restriction site adjacent to the 5′ homology sequence and electroporated into W9.5 embryonic stem (ES) cells (*129/Sv* strain background) (Fig. 3-2). G418-resistant ES cell colonies were first screened for the ΔN17 deletion by PCR genotyping (described below).

To confirm gene targeting in the ES clones that were PCR^{+}, Southern blot analyses were performed on *Nco*I digested genomic DNA fractionated on 0.7% agarose gels and transferred to nylon membranes. The blots were hybridized with a ^{32}P-labelled 3′ flanking probe located outside the 3′ homology arm of the targeting vector that recognizes a 10.0 kb WT allele fragment and an 11.9 kb fragment from the targeted

Htt$^{\Delta N17}$ allele (Fig. 3-2). The targeted allele is noticeably longer because of the insertion of the Neo cassette. Therefore, clones that were positive for homologous recombination had two bands, while negative clones only had one band (Fig. 3-3B). Southern^{+} ES cell clones were subsequently verified by western blot analysis of whole cell protein extracts using an antibody recognizing the Htt N17 domain (Biomol) together with an mTOR antibody (as a sample loading control) to detect a 50% decrease in the level of wild type Htt in the *Htt*$^{\Delta N17/+}$ ES cell protein extracts (Fig. 3-3C).

To delete both the polyQ stretch and the PRR from *Htt* exon 1 (*Htt*$^{\Delta QP}$), two partially complementary oligonucleotides were annealed and filled in with the Klenow fragment of DNA polymerase I. 5′-GAT**GAAGGCTTTC**GAGTCGCTCAAGTCGT TTCTGCCAGGTCCGG CAGAGGAACCGCTGCACCGACCGTGAGTCCGGTACC TCC-3′and 5′-GGAGGTACCGGACTCACGGT-3′ (the *Xmn*1site is in bold and underlined, the *Kpn*1 site is underlined). The synthetic double-stranded DNA was then digested with *Xmn*1 and *Kpn*1 to generate a DNA fragment that was used to replace the wild type *Xmn*1 – *Kpn*1 fragment in *Htt* exon 1 as described above. The 3xFLAG sequence was also synthesized using two oligonucleotides and Klenow enzyme and was ligated into the new vector immediately after the *Htt* start codon using the *Xmn*1-*AlwN*1 restriction sites located at the 5′end of *Htt* exon 1. The targeting vector was linearized and electroporated in ES cells as described, and G418-resistant ES clones were screened for the presence of the ΔQP deletion and 3xFLAG tag insertion by PCR genotyping (described below).

Confirmation of gene targeting in the PCR^{+}-ES cell clones was performed by Southern blot analysis as described above. Southern^{+}-ES cell clones were verified by western blot using MAB2166 (recognizing Htt aa181-810 in both 7Q-Htt and ΔQP-Htt,

and detecting a small shift in the migration of ΔQP-Htt in comparison to 7Q-Htt) and FLAGM2 antibodies (recognizing the 3xFLAG epitope tag in ΔQP-Htt) (Fig. 3-3C).

A third knock in mouse model was generated which expressed a version of Htt lacking aa 2-17, the polyQ stretch and the PRR ($Htt^{\Delta NQP}$) from endogenous mouse Htt. These mice were generated as described above using two synthetic oligomers that contained the desired ΔNQP deletion obtained from Alpha DNA, 5'-CTT**CAGGGT CTG**TCCCATCGGGCAGGAAGCCGTCATGCTGCCAGGTCCGGCAGAGGAAC CGCTGCACCGACCGTGAGTCC**GGTACC**TCC – 3' and 5'-GGA**GGTACC**GGACT CACGGT-3'. These two complimentary oligomers were annealed, and the missing base pairs were subsequently filled in using Klenow enzyme. The double stranded oligomer was then digested with *AlwN*1 and *Kpn*1 enzymes to generate a synthetic *AlwN*1-*Kpn*1 fragment that was ligated into an *AlwN*1 – *Kpn*1 digested pBSK+ vector containing 4,585 base pairs of the 5' portion of *Htt*. The targeting vector was linearized and electroporated in ES cells as described, and G418-resistant ES clones were then screened for the presence of the ΔNQP deletion by PCR genotyping (described below).

Confirmation of gene targeting in the PCR^{+}-ES cell clones was performed by Southern blot analysis and by western blot as described above using MAB2166 (recognizing Htt aa181-810 in both 7Q-Htt and ΔNQP-Htt, and detecting a shift in the migration of ΔNQP-Htt in comparison to 7Q-Htt) (Fig 3-3C).

The epitope tag insertion and all three exon 1 domain deletions were verified by DNA sequencing. Germ line transmitters were obtained from two independent ES clones for all three knock-in models, and there were no phenotypic differences observed between the progeny of both clones within each genotype.

ii. PCR genotyping

The following primers were used to detect modifications made in the *Htt* locus (Fig. 3-3A):

- For the ΔN17 mutation: HdEpi-1: 5'-GCGTAGTGCCAGTAGGCTCCAAG-3' and N2-17R2: 5'-GGCGGTGGCTGCTGCTGCTGT-3' (Htt^{+}: 135 bp; $Htt^{\Delta N17}$: 87 bp)

- For the ΔQP and ΔNQP mutation: HdEpi-1 and 140Reverse: 5′-GAAGGCACTGGAGTCGTGAC-3′ (Htt^{+} allele produces no product due to the high G/C content in the PRR region; $Htt^{\Delta QP}$: 347 bp, $Htt^{\Delta NQP}$: 233 bp)

- For the 3xFLAG epitope: HdEpi-1 and HdEpi-2: 5′-CTGAAACGACTTGAGCGACTC GAAAG-3′ (Htt^{+}: 112bp; $Htt^{\Delta QP}$: 178 bp).

- For detection of the 84 bp intronic deletion present in both $Htt^{\Delta N17}$, $Htt^{\Delta QP}$, and $Htt^{\Delta NQP}$: 140Forward: 5′-CTGCACCGACCGTGAGTCC-3′ and 140Reverse (Htt^{+}: 236 bp; $Htt^{\Delta N17}$, $Htt^{\Delta QP}$, and $Htt^{\Delta NQP}$: 152 bp)

iii. Mouse husbandry and behavioral analyses

Mice were maintained on a 12-hour light-dark schedule in humidity- and temperature-controlled rooms. Food and water were provided *ad libitum*. All experiments with the mice were approved by the ACUC at the University of Virginia. Mice were examined, weighed, and then subjected to accelerating rotarod, open field, and Morris water maze testing at 3, 6, 12, 18 and 24 months of age. Accelerating rotarod and open field tests were performed at the same time each day during the light phase of the circadian cycle. Morris water maze testing was performed 1 hour after the beginning of

the dark cycle. For all tests, mice were habituated for 30 min in the procedure rooms before testing began. Male progeny from F1 (129Sv X C57BL/6J) intercrosses were used in all behavioral tests to eliminate the potential effects of the estrus cycle on behavior (N=10-30/genotype, see Table 4-1, 5-1 for specific numbers used for each genotype at different ages).

Open Field Testing

Activity levels were assessed using the VersaMax Animal Activity Monitoring System (AccuScan Instruments). Each mouse was placed in the same starting location and movements were recorded for 5 min. The assessment box was cleaned between each test. Activity measurements (horizontal activity, vertical activity and total distance traveled) were generated using VersaMax software.

Rotarod

Mice were tested on an Economex accelerating rotarod (Columbus Instruments) to assess motor coordination and motor learning. Initial training included a 1-min stationary period to acclimate the mice to the apparatus. If a mouse could not complete this stationary phase task by remaining on the rod for 1 min, they were given 2 subsequent opportunities to complete this training phase. Once mice completed the stationary phase training, they were tested for their ability to stay for 1 min on the rod rotating at 2 rpm. Similar to the previous training phase, animals were given 2 subsequent opportunities to complete this training if they could not complete the task initially. Upon completion of these training tasks, mice were tested using constant

acceleration of the rod (0.1 rpm/s). This was repeated 2 additional times with 15-min breaks between runs on the first day of testing. Latency to fall was recorded for each test run and a daily average was calculated. This acceleration protocol (3 trials/day) was repeated on days 2 and 3 of testing. Because mice generally improve from day to day, their performance on consecutive days of testing were used as an assessment of motor learning.

Water maze

Morris water maze testing was performed to assess spatial learning and memory. The test was performed over 8 consecutive days and included a 4-day acquisition phase, a 1-day probe trial, a 2-day reversal task, and a final day of testing with a visible platform control. A circular pool (diameter 123 cm) was filled with water (22 ± 1° C) that was made opaque by the addition of non-toxic tempura paint. Water was filled so as to cover (by > 1 cm) a 10cm wide plexiglass escape platform. Three highly visible cues were placed around the procedure room, while the computer which controlled the tracking software and the tester were hidden behind a curtain hung in the room. All data was collected using EthoVision XT 5.0 software (Noldus Information Technology). For data collection, the pool was divided into 4 equally sized quadrants. The target quadrant contained the platform, and the exact location of the platform was designated as the platform zone.

Acquisition phase

During the acquisition phase, mice were gently placed in the water facing the tank wall immediately before initiation of the tracking software. Mice were given exactly 1 min to find the platform on their own before the task was terminated. If mice were able to find the platform, their time to the platform was recorded and they were given 20 additional seconds to remain on the platform and familiarize themselves with the cues in the room. If mice were not able to find the platform during the 1-min testing period, the tester placed the mouse on the platform and allowed them to stay on the platform for 20 seconds to familiarize themselves with the cues in the room, and a 60 second time to platform was recorded. Mice were then removed from the pool, gently dried with paper towels and returned to their home cage which was placed on a low-heat heating pad. Mice were given a minimum of 45 min rest between trials. Each mouse performed this task 4 times every day for 4 consecutive days.

Probe trial

On the fifth day of testing, during the probe trial, the platform was removed from the pool and each mouse was tested in a single 1-min trial. The amount of time that mice spent in the platform zone was measured. During this trial, mouse swim velocities were recorded to determine if there were any effects of swim speed on test performance.

Reversal phase

During the reversal phase, all spatial cues were kept the same, but the platform was placed back into the pool on the opposite side of its original location during the

acquisition phase. Each mouse completed four 1-min trials similar to the acquisition phase. Mice performed this task on 2 consecutive days.

Visible platform task

During the eighth and final day of testing, the platform was moved to a new area in the pool, and a glow stick with a red flag attached was placed on the platform for easy visibility. Mice were given a single 1-min trial to find the platform.

iv. Protein lysate preparation and subcellular fractionation

To initially confirm Htt expression in the F1 $Htt^{\Delta N17/\Delta N17}$, $Htt^{\Delta QP/\Delta QP}$, and $Htt^{\Delta NQP/\Delta NQP}$ mice (Fig. 3-4), whole brain lysates were prepared from 1-month-old homozygous mice. Brains were lysed in 50 mM Tris pH 8.8, 100 mM NaCl, 5 mM $MgCl_2$, 1 mM EDTA pH 8, 0.5% NP-40, 1 mM NaF, and Halt protease inhibitor (Thermo Scientific 78425). The lysates were centrifuged at 800xg for 20 min at 4˚C to obtain a crude cytoplasmic fraction (supernatant) for western analysis.

To examine autophagy markers and Htt's subcellular distribution, subcellular fractionation of whole brain lysates into enriched nuclear, microsomal, and cytosolic fractions was performed as described with minor modifications [125]. Briefly, brains from 6-month-old mice (all congenic in the C57BL/6J genetic background) were homogenized in 250 mM sucrose, 20 mM HEPES (pH7.3), 1 mM $MgCl_2$, 25 μg/ml spermine, 25 μg/ml spermidine, 1 mM DTT, 5 mM NaF and Halt protease inhibitor and centrifuged in an Eppendorf 5810R centrifuge, A-4-62 rotor at 800xg for 20 min at 4˚C. The pellet was resuspended in the same buffer and centrifuged again. The supernatants

from both centrifugations were combined and centrifuged for 75 min at 100,000xg in a Sorvall RC M120 centrifuge with an RP80AT-338 rotor at 4˚C to separate the supernatant (cytosolic fraction) from the pellet consisting of all remaining cytoplasmic organelles/vesicles. The pellet was resuspended in RIPA buffer with 1% SDS, 5 mM NaF, and Halt protease inhibitor, then centrifuged at 15,000xg for 15 min to obtain the microsomal fraction (supernatant).

The pellet of the 800xg spin was resuspended in 2 M sucrose, 20 mM HEPES (pH7.3), 1 mM $MgCl_2$, 25 μg/ml spermine, 25 μg/ml spermidine, 1 mM DTT, 5 mM NaF and Halt protease inhibitor and then layered over a cushion of the same buffer and centrifuged for 40 min at 80,000xg in a Beckman Coulter Avanti J-30I centrifuge with a JS-24.38 rotor at 4˚C to obtain purified nuclei. The nuclei were resuspended in RIPA buffer with 500 mM NaCl, 5 mM NaF, and Halt protease inhibitor, then sonicated for 5 min (with 10 seconds on/20 seconds off) using a Fisher Scientific Sonic Dismembrator (FB-505) with a cup horn attachment at 4˚C, followed by centrifugation for 15 min at 15,000xg to obtain the nuclear fraction (supernatant).

v. Western blotting

Protein concentrations were estimated using a Pierce BCA Protein Assay Kit (23227). Samples were incubated with ¼ volume 5X SDS-PAGE sample buffer (10% SDS, 20% glycerol, 0.2M Tris pH 6.8, 0.05% bromophenol blue, 0.1M β-mercaptoethanol) for 5 minutes at 95°C. To verify ΔN17-Htt, ΔQP-Htt, and ΔNQP-Htt expression (Fig. 3-4), 60 μg of the protein lysates were fractionated on 4.4% SDS-PAGE with a 3.75% stacking gel prepared from a 30% acrylamide solution containing 4.5%

N,N' diallyltartardiamide (DATD) cross-linker, and electrophoretically transferred onto 0.45 μm PVDF membranes (Millipore, Immobilon-P) at 30 V overnight. To verify the purity of the fractions from the subcellular fractionation, 40 μg of the protein lysates were fractionated on TGX stain-free 4-15% gradient gels and electrophoretically transferred onto Immobilon-P membranes using the Bio-Rad Transblot Turbo transfer system. Blots were incubated for 1 hour in a blocking solution containing 5% non-fat dry milk in TBST/0.05% Tween20 and 2% heat-inactivated goat serum. Blots were incubated overnight at 4˚C with the following antibodies: Calnexin (Abcam 22595; 1:1000), Lamin B1 (Cell Signaling 12586; 1:1000), LC3 (Novus NB100-2220; 1:1000), Htt-MAB2166 (Millipore; 1:3000), Htt-Biomol (Enzo PW0595; 1:1000), Htt-H7540 (Sigma-Aldrich; 1:3000), and FLAGM2 (Sigma-Aldrich F1804; 1:3000) diluted in 0.5% milk in TBS/0.05% Tween20. Blots were washed 6 times in TBST/0.1% Tween20 (5-7 min/wash). Blots were incubated in HRP-conjugated secondary antibody (Jackson ImmunoResearch, 715-036-151 and 111-036-003, 1:10,000) diluted in 0.5% milk in TBS/0.05% Tween20 for 1 hr at room temperature. Blots were washed as described, and SuperSignal WestDura chemiluminescent substrate (Pierce 34076) was used for detection in a ChemiDoc XRS+ imager (BioRad).

To evaluate autophagy and synaptic marker expression, 40 μg of the microsomal lysates were fractionated on Bio-Rad Mini-PROTEAN TGX stain-free 4-15% gradient gels (except for LC3-I and LC3-II lysates that were heated for 15 min at 37˚C and then fractionated on 15% SDS-PAGE), followed by electrophoretic transfer onto nitrocellulose membranes using a Bio-Rad Transblot Turbo transfer system. Blots were blocked in Odyssey TBS blocking buffer (LiCor 927-50000) for 1 hour, and then

incubated with primary antibody diluted in Odyssey blocking buffer at 4˚C overnight. Blots were washed as described above, incubated for 1 hr at room temperature in near-infrared emitting fluorophore-labeled secondary antibodies diluted in Odyssey blocking buffer, washed again and dried for at least 15 min.

Primary antibodies used were: LC3, p62 (American Research products 03-GP62-C; 1:1000), Actin (Cell Signaling 3700; 1:1000), Vglut1 (Millipore AB5905 1:3750), PSD-95 (Cell Signaling 3409; 1:800), and Vglut2 (Millipore AB2251; 1:5000). IRDye 800CW and IRDye 680RD conjugated secondary antibodies were purchased from Li-Cor (926-32212, 926-68073, 925-68070, 925-32211), and Alexa Fluor 680 conjugated secondary antibody was purchased from Jackson ImmunoResearch (706-625-148). Images were obtained with a Li-Cor Odyssey Fc imager and Image Studio software.

To quantify Htt levels, a salt active nuclease (SAN, ArcticZymes 70900) was added to the nuclear fraction at 6.425U/100 μg protein with 25 μg/ml spermine and spermadine, 2mM $MgCl_2$, and HALT protease inhibitor for 15 min at room temperature to remove DNA prior to SDS-PAGE. 50 μg protein from cytosolic and microsomal fractions and 100 μg protein from nuclear fractions were run on 4.4% SDS-PAGE with 3.75% stacking gel made from a 30% acrylamide solution containing 4.5% N,N' DATD and electrophoretically transferred onto 0.45 μm low-fluorescence PVDF membranes (Bio-Rad) at 30 V overnight. Blots were incubated with MAB2166 (Millipore; 1:1000), mTOR (Cell Signaling 2972; 1:1000) and Lamin B1 antibodies in Odyssey blocking buffer, and imaged as described above.

vi. Primary neuronal cultures and autophagic flux analysis

Primary cortical and striatal neuronal cultures were generated from postnatal day 5 (P5) pups as described [126] with modifications. Briefly, brains were removed from P5 pups and placed in a dish containing F12:DMEM (Gibco 11330-032) supplemented with gentamycin (Gibco 15710-064). The cortex and striatum were isolated and cut into 0.5 mm pieces in Hibernate-A media (Gibco 12475-01) with GlutaMAX (Gibco 35050-061) and gentamycin (HAG), and then digested with 40 units/ml pre-activated and filtered papain in HAG for 25 min at 30˚C with shaking at 40 rpm.

Following digestion, the tissues were rinsed twice with HAG containing B27 (Gibco 17504-001) (HABG), and then triturated gently with a flame polished, silicone-coated glass Pasteur pipette. The cell suspension was centrifuged for 4 min at 200xg, and the cell pellet was then resuspended in culture medium consisting of Neurobasal-A (Gibco 10888-022), B27, GlutaMAX, and gentamycin at 5.0 $x10^5$ cells/ml. 80 μl of cell suspension (4.0 x 10^4 cells) were plated on a poly-D-lysine coated glass coverslip (Carolina Biologicals 633009) and incubated at 37˚C in 5% CO_2. Coverslips were gently washed after 1 hr incubation and placed in a 24-well tissue culture plate containing 800 μl of pre-warmed culture medium/well; half of the medium was replaced on the third and seventh day *in vitro* (DIV).

On DIV8, chloroquine was diluted to 30 μM in conditioned medium removed from the cultures. Cells were then incubated in 300 μl/well of the chloroquine-conditioned medium for 4 or 8 hours before fixation and immunocytochemistry to assess autophagic flux.

vii. Immunohistochemistry and immunocytochemistry

For immunohistochemical analyses, 18-month-old mice were anesthetized and perfused with 10% sucrose in 0.1M phosphate buffer for 2 min (5 ml/min) using a peristaltic pump (Cole-Parmer Master flex L/S pump equipped with a model 77200-60 pump head), and their brains were then removed and frozen in O.C.T. compound (Tissue-Tek 4583). Frozen brains were sectioned at 20 μm using a Bright Instruments cryostat and stored -80˚C. Sections were fixed in 4% paraformaldehyde in 0.1M phosphate buffer for 10 min and then incubated for 5 min in 0.125M glycine in PBS before washing 3 times in PBS (5 min/wash). Sections were then incubated in blocking solution (5% donkey serum, 0.1% triton in PBS) for 30 min at room temperature. Sections were incubated in primary antibody diluted in blocking solution over night at 4˚C. Sections were washed 3 times (10 min/wash) in 1% donkey serum 0.1% triton, and then incubated for 1 hour in secondary antibody diluted in blocking solution. Sections were then washed 3 times (10 min/wash) with PBS, followed by a 5 minute 70% ethanol solution incubation. Sections were then incubated in auto fluorescence inhibitor for 5 minutes, washed 3 times with 70% ethanol, and washed 3 additional times with PBS. Sections were mounted in Vectashield mounting media.

For synapse quantification, 24-month-old mice were perfused with 10% sucrose in 0.1M phosphate buffer for 2 min, followed by 4% paraformaldehyde/10% sucrose in 0.1M phosphate buffer for 5 min, and then 10% sucrose in 0.1M phosphate buffer for 5 min. Brains were removed and processed as described above except the post-fixation step was eliminated. Progeny from F1 (129Sv X C57BL/6J) intercrosses were used in these studies.

For immunocytochemistry, cells on coverslips were fixed at 37˚C, washed, and then processed as described above, except the coverslips were mounted in Vectashield (Vector Laboratories, H-1000) immediately after PBS washes following the secondary antibody incubation without being treated with autofluorescence eliminator (Millipore, 2160).

Primary antibodies used are: p62 (American Research products 03-GP62-C; 1:200), LC3 (Cell signaling 12741; 1:100), Tuj1 (gift from A. Frankfurter, University of Virginia; 1:1000), Vglut1 (Millipore AB5905 1:3750), Vglut2 (Millipore AB2251; 1:5000), PSD-95 (Cell Signaling 3409; 1:800), GFAP (Millipore AB5804; 1:1000), and CD68 (Serotech FA-11; 1:400). Secondary antibodies were purchased from Jackson ImmunoResearch Laboratories (715-175-151, 706-166-148, 712-096-153, and 711-546-152). To-Pro-3 iodide (Invitrogen T3605; 1:1000) was used to stain nuclei.

viii. Image acquisition and image analyses

Images of brain sections and primary neuronal cultures were obtained using a Nikon C1 confocal system with a Nikon TE2000 inverted microscope. Confocal images were taken every 0.5 μm in the Z plane to generate an image stack for analysis. For immunocytochemistry, images of 30 neurons/dissection were taken from each quadrant of 2-3 coverslips. 3 dissections were performed per genotype. βIII tubulin immunostaining was used to identify healthy cells for imaging. 40 neurons/genotype were randomly selected for quantification. Image analysis and quantification were performed using NIS-Nikon Elements AR software. Maximum intensity projections were generated from the image stacks for image processing. To identify $LC3^{+}p62^{+}$

autophagosomes, thresholds were set for each marker and the pixel area of $LC3^+p62^+$ puncta was determined. To quantify $LC3^+p62^+$ autophagosomes in primary neuronal cell bodies, total $LC3^+p62^+$ pixel area in a cell body was divided by the pixel area of the entire cell body. To quantify $LC3^+p62^+$ autophagosomes in neurites, total $LC3^+p62^+$ pixel area in all neurites of the same neuron was divided by the total lengths of these neurites.

Images of brain sections for synaptic quantification (Vglut1/PSD-95, Vglut2/PSD-95) were obtained using a Zeiss LSM 880 confocal system and Zen software from bregma -0.555 mm to 1.245 mm (dorsal striatum) and bregma -1.155 mm to 1.245 mm (primary motor cortex layers I and II). To identify $PSD\text{-}95^+Vglut2^+$ synapses, thresholds were set for each marker and the pixel area of $PSD\text{-}95^+Vglut2^+$ puncta in an image was determined, then the total $PSD\text{-}95^+Vglut2^+$ pixel area was divided by the sum of the $PSD\text{-}95^+$ pixel area and the $Vglut2^+$ pixel area of the same image. $PSD\text{-}95^+Vglut1^+$ synapses were quantified in the same way.

ix. Statistical analyses

Data was analyzed using Prism 6 (Graphpad software), and statistical significance determined by ANOVA was set at $p < 0.05$. Post hoc tests used to compare groups to one another were Tukey's multiple comparison test for 2-way ANOVA, and Dunnett's multiple comparison test for 1-way ANOVA.

Chapter III: Generation of the mouse models expressing versions of Huntingtin with N-terminal domain deletions: *Htt*$^{\Delta N17}$, *Htt*$^{\Delta QP}$, and *Htt*$^{\Delta N17}$ mice

Chapters III and IV are modified and expanded from a published manuscript: Andre E.A., Braatz E.M., Liu J.P. and Zeitlin S.O. *Generation and Characterization of Knock-in Mouse Models Expressing Versions of Huntingtin with Either an N17 or a Combined PolyQ and Proline-Rich Region Deletion.* Journal of Huntington's Disease. 2017. (Epub ahead of print). PMID: 28211815. doi: 10.3233/JHD-160231.

i. Introduction

All three domains encoded by exon 1 have been thoroughly investigated in *in vitro* models, usually by over-expressing fragments of the Htt protein at non-physiological levels. While this approach has garnered important information concerning the possible functions of each of these domains [5, 7-9, 58, 127], there is a possibility that these proposed functions could be altered when the HTT N-terminal domains encoded by the first exon are analyzed in the context of the full-length protein, and at endogenous expression levels *in vivo*.

The Zeitlin laboratory has previously generated *Htt*$^{\Delta Q/\Delta Q}$, *Htt*$^{\Delta P/\Delta P}$, *Htt*$^{140Q/\Delta Q}$ and *Htt*$^{140Q\Delta P/+}$ knock-in mice, and their characterization, while still ongoing, has provided new insights into the functions of the PolyQ and PRR domains in Htt function [61, 109], and Jeh-Ping Liu, personal communication. Deletion of either the normal mouse polyQ or PRR domain is well tolerated throughout adulthood [61, 109]. These studies also suggest that deletion of the normal Htt polyQ stretch can modulate macroautophagy in *Htt*$^{140Q/\Delta Q}$ mice [110]. The PRR adjacent to an expanded polyQ stretch is hypothesized to help

stabilize the expanded polyQ stretch in a non-toxic conformation [50]; therefore, it was predicted that behavioral and neuropathological phenotypes in HD mouse models would be exacerbated in its absence. Although deletion of the PRR in the context of the normal 7Q stretch in mice did not result in robust phenotypes, when the PRR was deleted *in cis* to the expanded polyQ stretch in Q140 mice ($Htt^{140Q\Delta P/+}$ mice), some motor phenotypes were less severe in comparison to $Htt^{140Q/+}$ mice, and development of large 140QΔP-Htt aggregates was delayed [Liu et al in preparation]. These findings demonstrate the need for continued investigation of normal and mHtt function using knock-in mouse models to complement existing in vitro model systems.

I continued the laboratory's characterization of the functions of the Htt N-terminal domains by generating a new knock-in mouse model expressing full-length 7Q-Htt lacking amino acids 2-17 ($Htt^{\Delta N17}$), a model expressing a version of Htt lacking both the polyQ and PRR domains ($Htt^{\Delta QP}$), and a model expressing Htt lacking all 3 N-terminal domains ($Htt^{\Delta NQP}$). Homozygous domain deletion mutants were generated at normal Mendelian frequencies for all three models ($Htt^{\Delta N17/\Delta N17}$, $Htt^{\Delta QP/\Delta QP}$, $Htt^{\Delta NQP/\Delta NQP}$), suggesting that like the polyQ and PRR domains, the N17 domain is not essential for Htt's functions in embryonic development.

ii. Results

Generation of the $Htt^{\Delta N17}$, $Htt^{\Delta QP}$, and $Htt^{\Delta NQP}$ mice

The $Htt^{\Delta N17}$ knock-in mice, lacking amino acids 2-17, were generated by replacing the wild type *Htt* exon 1 sequence (Fig. 3-1A) with sequence containing the amino acid 2-17 deletion by gene targeting in ES cells (Fig. 3-1B, 3-2). The $Htt^{\Delta QP}$ knock-in mice were generated by replacing the wild type *Htt* exon 1 sequence with sequence encoding deletions of the 7Q and PRR domains. Sequence encoding a 3xFLAG epitope tag was also inserted into the $Htt^{\Delta QP}$ gene-targeting vector between the *Htt* exon 1 sequence encoding amino acids 1 and 2 (Fig. 3-1C and Methods). Similarly, the $Htt^{\Delta NQP}$ knock-in mice were generated by replacing the wild type *Htt* exon 1 sequence with sequence encoding deletion of amino acids 2-17, the PolyQ and PRR domains (Fig. 3-1D and Methods). Each gene targeting vector was verified by DNA sequencing.

Targeting vectors were electroporated into W9.5 ES cells and screened for homologous recombination by PCR, Southern blot and western blot analysis (Fig 3-3 and Methods). For western analysis of $Htt^{\Delta QP}$ clones, the 3xFLAG N-terminal epitope tag was detected with a FLAGM2 antibody, and the small decrease in size of ΔQP-Htt and ΔNQP-Htt compared to wild type Htt was detected with MAB2166, which recognizes all versions of Htt (Fig. 3-3C). Absence of the N17 domain in ΔN17-Htt was confirmed using an antibody recognizing amino acids 2-16 of the N17 domain, together with an mTOR antibody (as a sample loading control) to detect a 50% decrease in the level of wild type Htt in the $Htt^{\Delta N17/+}$ ES cell protein extracts in comparison to wild type extracts (Fig. 3-3C).

Targeted ES cell clones (3 per gene targeting construct) were injected into 3.5 day old C57BL/6J blastocysts to generate chimeric mice (Table 3-1) using standard procedures [109, 128]. Following ES cell injection, the embryos were transferred into pseudo-pregnant females 2.5 days after mating with vasectomized males. Approximately 17 days later, females gave birth to chimeric pups. Male chimeras were bred to female C57BL/6J mice to generate heterozygous F1 progeny. Western blot analyses of whole brain lysates obtained from 1-month-old mice were used to verify the expression of ΔN17-Htt, ΔQP-Htt and ΔNQP-Htt (Fig. 3-4 A,B,C).

Homozygous N-terminal domain deletions do not result in embryonic lethality or marked deficits in adult mice

Heterozygous intercrosses of F1 mice were used to generate cohorts of homozygous, heterozygous and wild type control mice for each domain deletion mutation ($Htt^{\Delta N17/\Delta N17}$, $Htt^{\Delta N17/+}$, $Htt^{\Delta QP/\Delta QP}$, $Htt^{\Delta QP/+}$, $Htt^{\Delta NQP/\Delta NQP}$, $Htt^{\Delta NQP/+}$, and $Htt^{+/+}$ mice). Of the 261 mice born from the $Htt^{\Delta QP/+}$ intercross, 74 (28.35%) were $Htt^{+/+}$, 113 (43.30%) were heterozygous ($Htt^{\Delta QP/+}$), and 74 (28.35%) were homozygous ($Htt^{\Delta QP/\Delta QP}$) (Table 3-2). This distribution is not significantly different from the expected Mendelian frequency (χ^2= 4.693, p=0.096, D_F=3). Among the 162 mice generated from the $Htt^{\Delta N17/+}$ intercross, 40 (24.69%) were $Htt^{+/+}$, 86 (53.09%) were heterozygous ($Htt^{\Delta N17/+}$), and 36 (22.22%) were homozygous ($Htt^{\Delta N17/\Delta N17}$) (Table 3-2). Despite the conservation of the N17 domain in all vertebrates, mice homozygous for the N17 deletion ($Htt^{\Delta N17/\Delta N17}$) were also born at the normal Mendelian frequency (χ^2=0.815, p=0.665, D_F=3), suggesting that, like the PRR and the polyQ stretch [61, 109], the N17 domain is not required for Htt's essential

functions during embryonic development. Among the 48 mice generated from the $Htt^{\Delta NQP/+}$ intercross, 12 (25.00%) were $Htt^{+/+}$, 16 (33.33%) were heterozygous ($Htt^{\Delta NQP/+}$), and 20 (41.67%) were homozygous ($Htt^{\Delta NQP/\Delta NQP}$) (Table 3-2). This distribution is significantly different from the expected Mendelian frequency (χ^2= 8.000, p=0.0183, D_F=3); however, the numbers of mice generated from this cross were relatively low, and when this heterozygous intercross was repeated with more progeny, mice were found to be born at the normal Mendelian frequency (data not shown).

$Htt^{\Delta QP/+}$ and $Htt^{\Delta N17/+}$ mice were also crossed with $Htt^{+/-}$ mice to determine if absence of normal *Htt* expression had any effect on the numbers of hemizygous $Htt^{\Delta QP/-}$ and $Htt^{\Delta N17/-}$ mice that were obtained. Both $Htt^{\Delta QP/-}$ and $Htt^{\Delta N17/-}$ mice were born at the normal Mendelian frequency ($Htt^{\Delta QP/-}$: χ^2=2.923, p=0.404, D_F=3) ($Htt^{\Delta N17/-}$: χ^2=2.800, p=0.424, D_F=3) (Table 1), suggesting that expression of ΔQP-Htt or ΔN17-Htt at 50% of the normal Htt level is sufficient for embryonic development. This finding is in agreement with previous work showing that when BAC transgenic mice expressing a full-length human HTT construct lacking the N17 domain (*BAC-Wt-*Δ*N17-*$Htt^{+/-}$ *tg* mice) were crossed with $Htt^{+/-}$ mice, *BAC-Wt-*Δ*N17-*$Htt^{-/-}$ mice were generated at the expected Mendelian frequency [124]. Additionally, the homozygous $Htt^{\Delta QP/\Delta QP}$ and $Htt^{\Delta N17/\Delta N17}$ mutants appeared normal and their weights were not significantly different from controls throughout their lifetime (data not shown).

Generation of the $Htt^{140Q/\Delta N17}$ and $Htt^{140Q/\Delta QP}$ mice

$Htt^{140Q/\Delta N17}$ and $Htt^{140Q/\Delta QP}$ knock-in mice were generated by crossing $Htt^{\Delta N17/\Delta N17}$ and $Htt^{\Delta QP/\Delta QP}$ knock-in mice to the $Htt^{140Q/+}$ knock-in mouse model for HD. Neither

Htt$^{140Q/\Delta N17}$ nor *Htt*$^{140Q/\Delta QP}$ mice exhibited embryonic lethality, reduced lifespan or reduced weights throughout their lives.

iii. Discussion

Homozygous and hemizygous domain deletion mice ($Htt^{\Delta N17/\Delta N17}$, $Htt^{\Delta N17/-}$, $Htt^{\Delta QP/\Delta QP}$, $Htt^{\Delta QP/-}$, and $Htt^{\Delta NQP/\Delta NQP}$) were born at normal Mendelian frequencies in agreement with previous studies, suggesting that the N17, polyQ, and PRR domains are not required for Htt's essential functions during embryonic development [48, 61, 109, 124]. Since prior work has shown that individual deletion of the polyQ or PRR domains does not result in embryonic lethality, it is not unexpected that a combined deletion of the polyQ and PRR domains also does not impact embryonic development [61, 109].

My observation that deletion of the Htt N17 domain in homozygosity does not affect embryogenesis is consistent with results obtained from the characterization of two Bacterial Artificial Chromosome (BAC) HD mouse models that over-express versions of full-length mHTT (BAC-HD-ΔN17) or full-length wild type HTT (BAC-WT-ΔN17) lacking the N17 domain [124]. To determine if BAC-HD-ΔN17 or BAC-WT-ΔN17 expression on a *Htt*-null genetic background was sufficient for normal embryonic development, the BAC transgenic models were crossed with $Htt^{+/-}$ mice, to generate BAC-HD-ΔN17-$Htt^{-/-}$ and BAC-WT-ΔN17-$Htt^{-/-}$ progeny and control littermates [124]. Similar to my findings, it was observed that both BAC-HD-ΔN17-$Htt^{-/-}$ and BAC-WT-ΔN17-$Htt^{-/-}$ mice were born at normal Mendelian frequencies [124]. Therefore, despite the conservation of this domain throughout vertebrate evolution, the N17 domain is not required for embryonic development.

As I was completing my thesis, a recent publication appeared that provided evidence suggesting that the entire N-terminus of Htt is dispensable for neuronal homeostasis and neurite extension [48]. When *Htt* expression is knocked-down in PC12

cells using shRNA, neurite extension was significantly reduced [48]. However, when a truncated version of Htt lacking its N-terminal 237 amino acids (a deletion including the first 5 exons and part of exon 6) was transfected into these PC12 cells lacking endogenous Htt expression, a rescue of the neurite extension phenotype could be observed [48].

These results, together with my observations, suggest that the entire N-terminus of vertebrate Htt does not contribute to its essential embryonic functions, and are consistent with the hypothesis that the N-terminus of HTT may have evolved to modulate HTT functions in the complex developing and/or adult nervous systems of vertebrates [4].

Clone	*# embryos implanted*	*# born*	*# chimeras*
ΔQP #19	26	6	0
ΔQP #40	24	13	7
ΔQP #60	12	5	2
ΔN17 #144	27	17	7
ΔN17 #167	19	13	10
ΔN17 #170	24	14	8
ΔNQP #128	11	3	0
ΔNQP #138	25	18	6
ΔNQP #144	38	13	6

Table 3-1. The number of embryos implanted, mice born, and chimeras generated for the various clones implanted.

Genetic Cross	*Genotype*	*# female*	*# male*	*Total*	*%*	χ^2
ΔQP/+ x ΔQP/+	+/+	45	29	74	28.35	4.693 *p*=0.096
	ΔQP/+	55	58	113	43.30	
	ΔQP/ΔQP	33	41	74	28.35	
ΔN17/+ x ΔN17/+	+/+	16	24	40	24.69	0.815 *p*=0.665
	ΔN17/+	40	46	86	53.09	
	ΔN17/ΔN17	17	19	36	22.22	
ΔNQP/+ x ΔNQP/+	+/+	4	8	12	25.00	8.000 **p*=0.0183
	ΔNQP/+	3	13	16	33.33	
	ΔNQP/ΔNQP	5	15	20	41.67	
ΔQP/+ x +/-	+/+	6	4	10	19.23	2.923 *p*=0.404
	+/-	6	11	17	32.69	
	ΔQP/+	6	4	10	19.23	
	ΔQP/-	10	5	15	28.85	
ΔN17/+ x +/-	+/+	5	4	9	30.00	2.800 *p*=0.424
	+/-	2	2	4	13.33	
	ΔN17/+	7	3	10	33.33	
	ΔN17/-	4	3	7	23.33	

Table 3-2. The number and percentage (by genotype and sex) of progeny born from the various crosses and the results of χ^2 analyses.

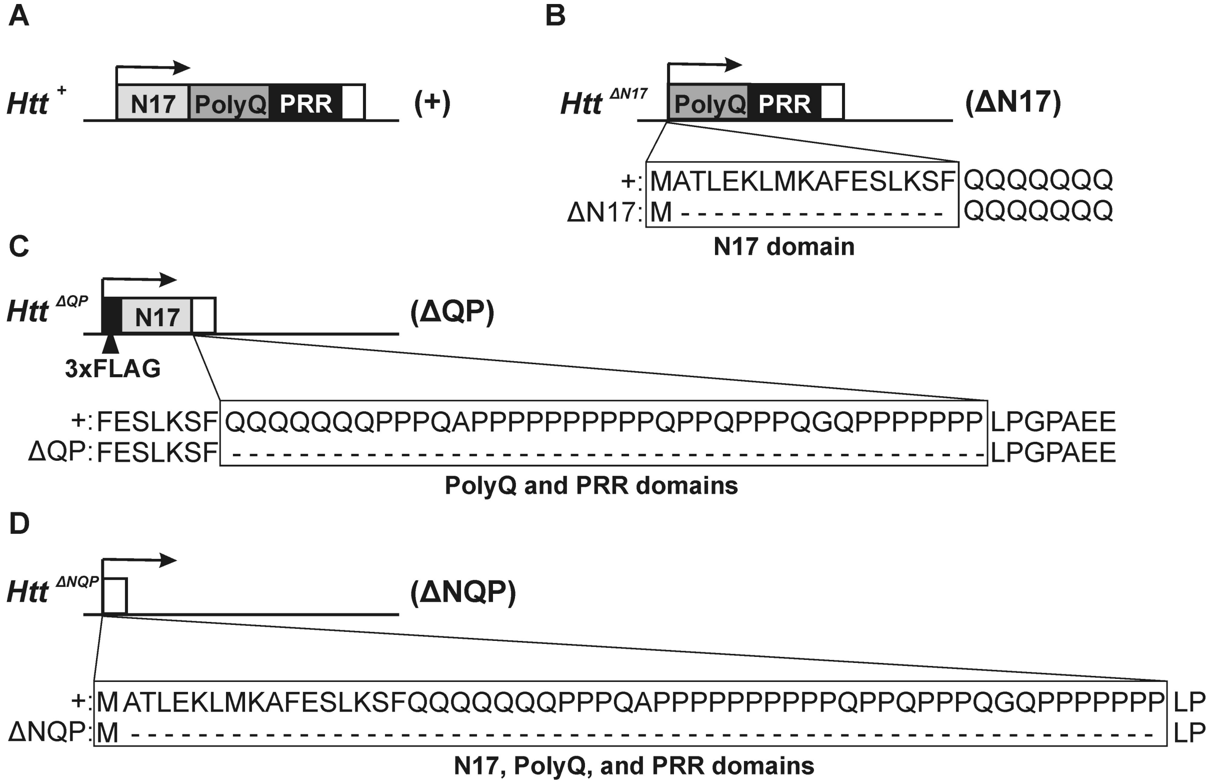

Figure 3-1. Illustration of the *Htt* N-terminal domain deletions. (A) Wild type *Htt* exon 1, (B) $Htt^{\Delta N17}$ (ΔN17), (C) $Htt^{\Delta QP}$ (ΔQP), and $Htt^{\Delta NQP}$ (ΔNQP) alleles. The N17 domain, polyQ stretch, and the mouse PRR are indicated. In the $Htt^{\Delta N17}$ allele, the first methionine was retained, while amino acids 2-17 were deleted.

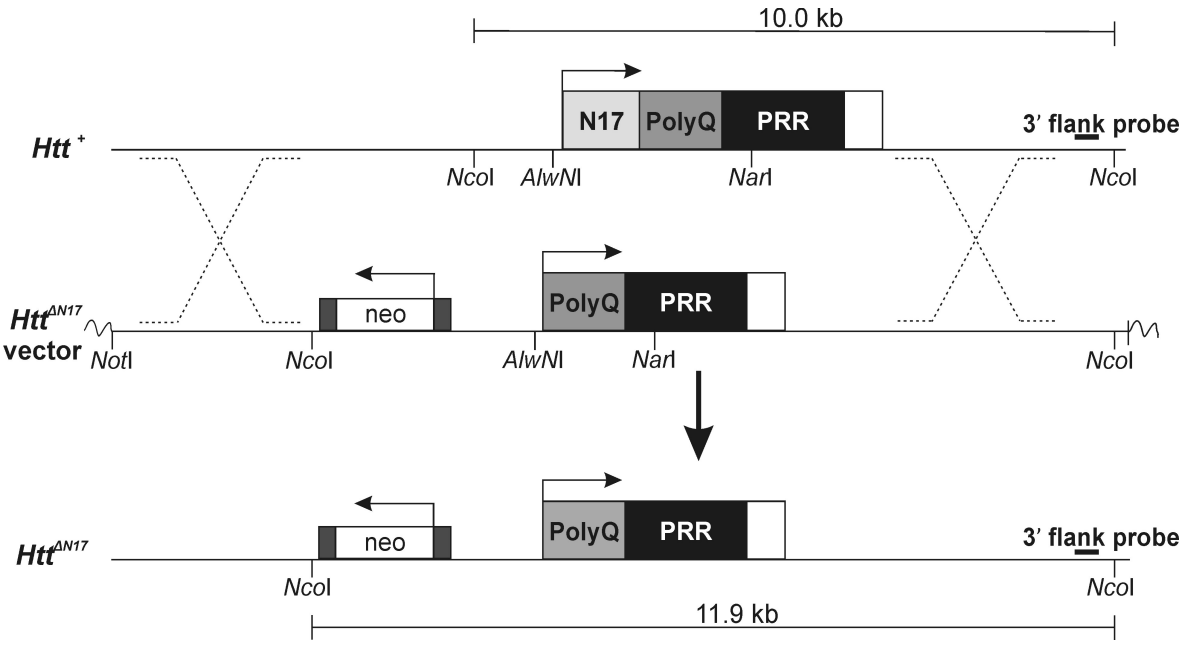

Figure 3-2. Gene targeting strategy for generating the $Htt^{\Delta N17/+}$ ES cells. A gene-targeting vector was constructed lacking sequence encoding amino acids 2-17 of *Htt* exon 1. Wild type exon 1 (Htt^{+}) is shown at the top, and the recombined locus is shown at the bottom. For positive selection of transfected ES cell clones, a neomycin phosphotransferase cassette (neo) flanked by loxP sites (black rectangles) was inserted 1.3 kb upstream of the transcriptional start site (arrows indicate the transcriptional direction of *Htt* and the neo cassette). The *AlwN*1 and *Nar*1 restriction sites that were used to generate the targeting vector are indicated. The sizes of diagnostic *Nco*I restriction fragments recognized by a 3′-flanking Southern blot probe are indicated above the wild type and below the recombined locus. A similar gene targeting strategy was used to generate the $Htt^{\Delta QP/+}$ and $Htt^{\Delta NQP/+}$ ES cell clones.

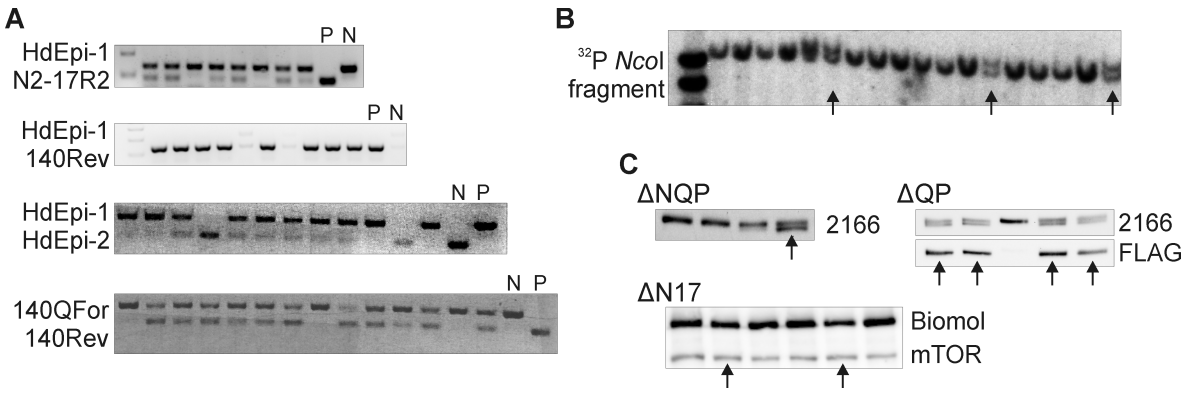

Figure 3-3. PCR (A), Southern blot (B), and western blot (C) analyses for detection of the targeted $Htt^{\Delta N17}$, $Htt^{\Delta QP}$, and $Htt^{\Delta NQP}$ alleles in ES clones. (A) Examples of PCR products run on agarose gels for each PCR primer pair (left) used to screen for recombination. Positive (P) and negative (N) controls for each PCR are indicated. (B) Southern blot analysis using a ^{32}P labeled 3′- flanking probe to detect the wild type (10.0 kb *Nco*I fragment) and recombined (11.9 kb *Nco*I fragment) alleles. Successfully gene targeted ES clones have an 11.9 kb/10.0 kb doublet as indicated by the arrows. (C) Western blot analysis of ES cell protein lysates. ΔQP-Htt and ΔNQP-Htt positive clones were identified by a small size shift compared to wild type Htt on SDS-PAGE western blots when probed with the MAB2166 antibody (arrows). ΔQP-Htt was also detected using the FLAGM2 antibody that recognizes the N-terminal 3xFLAG epitope tag. ΔN17-Htt-positive clones were validated using an antibody recognizing amino acids 2-16 (Biomol), and a sample loading control (mTOR) to detect a 50% decrease in wild type Htt levels in comparison to $Htt^{+/+}$ extracts (arrows).

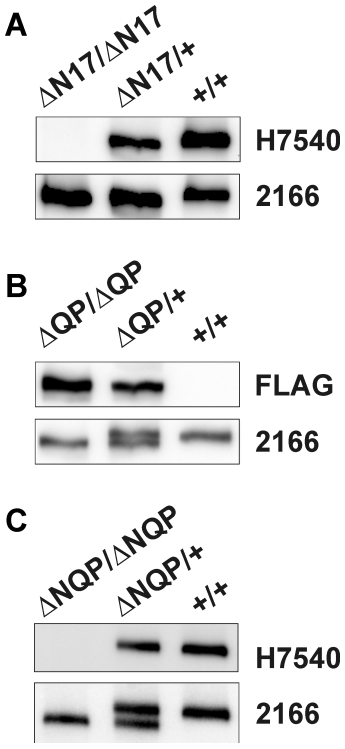

Figure 3-4. Whole brain lysates from 1-month-old mice were used to verify Htt expression in $Htt^{\Delta N17/\Delta N17}$, $Htt^{\Delta QP/\Delta QP}$, and $Htt^{\Delta NQP/\Delta NQP}$ mice. (A) $Htt^{+/+}$ (+/+), $Htt^{\Delta N17/+}$ (ΔN17/+), and $Htt^{\Delta N17/\Delta N17}$ (ΔN17/ΔN17) lysates probed with H7540 and MAB2166 antibodies. The N17-specific H7540 antibody detects wild type Htt in the +/+ and ΔN17/+ samples, but does not detect ΔN17-Htt in the ΔN17/ΔN17 sample, as expected. (B) $Htt^{+/+}$, $Htt^{\Delta QP/+}$ (ΔQP/+), and $Htt^{\Delta QP/\Delta QP}$ (ΔQP/ΔQP), lysates probed with FLAGM2 and MAB2166 antibodies. FLAGM2 antibody detects the N-terminal 3xFLAG epitope tag of ΔQP-Htt in the ΔQP/+ and ΔQP/ΔQP lanes. (C) The H7540 antibody detects wild type Htt in the +/+ and ΔNQP/+ lane, but does not detect ΔNQP-Htt in the ΔNQP/ΔNQP lane. MAB2166 detects wild type Htt, ΔN17-Htt, ΔQP-Htt and ΔNQP-Htt (A,B,C). Note that ΔQP-Htt and ΔNQP-Htt migrate slightly faster on SDS-PAGE resulting in an Htt doublet in the ΔQP/+ and ΔNQP/+ lanes probed with MAB2166.

Chapter IV: Characterization of knock-in $Htt^{\Delta N17}$ and $Htt^{\Delta QP}$ mice

i. Introduction

To investigate the contribution of the N17, polyQ, and PRR domains to wild type HTT function, the Zeitlin laboratory has pursued a strategy of generating domain deletion mutations in knock-in mouse models. Previous work has shown that the polyQ stretch itself does not contribute to essential Htt functions, as deletion of this stretch in mice does not perturb embryonic development or result in major neuropathological deficits in adults [109]. $Htt^{\Delta Q/\Delta Q}$ mice perform better on the accelerating rotarod and they have an extended lifespan when compared to $Htt^{+/+}$ controls; however, at 5 months of age they exhibit learning and memory deficits during a spatial learning and memory task [109, 110]. Additionally, the polyQ domain has a role in modulating neuronal autophagy [110]. Deletion of the PRR in Htt also has no impact on embryonic development; however, it does result in spatial learning and memory deficits in 18-month-old male mice [61]. Additionally, deletion of the PRR results in a reduction of phosphorylated Htt S13 indicating that the PRR may play a role in modulation of N17 post-translational modifications [61].

Data from several studies suggest that the N-terminus of Htt may play an important role in regulation of autophagic flux [9, 57, 110]. During autophagosome formation, LC3-I (diffusely localized in the cytosol) is conjugated to phosphatidylethanolamine (becoming LC3-II) and associates with the autophagosomal double membrane as it forms around its cargo [129-132]. p62 is an adaptor protein that has a C-terminal ubiquitin (Ub)-binding domain and a short LC3-interacting region [133, 134]. These two domains allow p62 to recognize and target ubiquitinated cargo for

degradation by selective macroautophagy [133-135]. Recent studies have suggested that the PB1 domain in p62 that allows for its self-aggregation may also influence the aggregation of ubiquitinated cargoes and subsequently serve as a nucleation point for autophagosome formation [135]. Because LC3-II and p62 are both degraded by autophagy, the number of autophagosomes and the steady-state levels of LC3-II and p62 can be affected by alterations in the autophagy pathway. For example, deletion of the Htt polyQ stretch results in increased steady-state levels of LC3-II in the striatum of 2-year-old mice, suggesting that autophagic flux may be increased in these mice [110].

Recent work has also shown that loss of *Htt* expression during CNS development results in significant synaptic deficits [95]. When *Htt* is conditionally knocked out in the forebrains of mice, both corticostriatal and thalamostriatal synapse numbers in the dorsal striatum are altered [95]. Additionally, Htt modulates clustering of PSD-95, which has been shown to modulate LTP and LTD and subsequently affect spatial learning and memory [40]. This interaction is dependent on the SH3-domain of PSD-95, and is therefore likely interacting with Htt's PRR [40]. Htt also directly interacts with three pre-synaptic proteins Bassoon, Piccolo, and Ahnak, and can modulate clathrin-coated vesicle endocytosis through its interaction with HIP1 [91, 94]. Therefore, there is evidence indicating that synapses could be affected due to the deletions of the Htt N-terminal domains.

In this chapter, I report the characterization of two knock-in mouse models $Htt^{\Delta N17}$ and $Htt^{\Delta QP}$. I have used several different behavioral and motor tests to characterize phenotypes that have been shown to be affected in HD mouse models, and that have close correlates to HD patient symptoms. Progressive motor and spatial learning and memory

deficits are present in both HD patients and in HD mouse models, and therefore, I have employed the accelerating rotarod (testing motor learning and coordination), automated activity cage (testing overall activity), and the Morris water maze (testing spatial learning and memory) as particularly relevant means to evaluate phenotypes in the N-terminal domain deletion knock-in mice [136, 137]. While only the $Htt^{\Delta QP/\Delta QP}$ mice exhibit changes in motor coordination, both $Htt^{\Delta N17/\Delta N17}$ and $Htt^{\Delta QP/\Delta QP}$ mice exhibit altered spatial learning and memory. Neither model displayed any changes in activity levels throughout their lifetime. While no changes in neuronal autophagy could be detected in either knock-in mouse model, I was able to determine that $Htt^{\Delta N17/\Delta N17}$ mice had changes in synaptic development and/or maintenance that resulted in decreased thalamostriatal synapses in 18-month-old mice.

ii. Results

Behavioral analyses of $Htt^{\Delta N17/\Delta N17}$ and $Htt^{\Delta QP/\Delta QP}$ mice

$Htt^{\Delta N17/\Delta N17}$ and $Htt^{\Delta QP/\Delta QP}$ mice were subjected to longitudinal behavioral testing at 3, 6, 12, 18, and 24 months of age to determine if the domain deletions affected activity levels, motor coordination, or spatial learning and memory. No differences in total horizontal movement, total vertical movement, or total distance traveled were observed between the mutants and controls at all ages examined (data not shown). However, $Htt^{\Delta QP/\Delta QP}$ mice consistently out-performed $Htt^{+/+}$ littermates on the accelerating rotarod as shown by their increased latency to fall at 3 (p<0.0001, F=13.61, D_F=2), 6 (p=0.0103, F=4.701, D_F=2), 12 (p=0.0079, F=4.974, D_F=2), 18 (p=0.0156, F=4.269, D_F=2), and 24 months of age (p=0.0077, F=5.052, D_F=2, 2-way ANOVA) (Fig. 4-1A). $Htt^{\Delta N17/\Delta N17}$ mice, in contrast, did not exhibit any consistent improvements on the rotarod when compared to controls (Fig. 4-1A).

In the Morris water maze, $Htt^{\Delta QP/\Delta QP}$ and $Htt^{\Delta N17/\Delta N17}$ mice were able to navigate to the hidden platform more quickly than controls during the initial acquisition (learning) phase of testing at 3 months of age (Fig. 4-1B; p=0.0003, F=8.194, D_F=2, 2-way ANOVA). $Htt^{\Delta QP/\Delta QP}$ mice were no different from controls at any other ages tested. $Htt^{\Delta N17/\Delta N17}$ mice were also able to find the platform more quickly than controls at 6 months of age (Fig. 4-1B; p<0.0001, F=22.44, D_F=2, 2-way ANOVA), but they took longer to find the platform during the acquisition phase in comparison to the controls by 12 months of age (Fig. 4-1B; p<0.0001, F=12.53, D_F=2, 2-way ANOVA) and at 24 months of age (Fig. 4-1B; p=0.0085, F=4.797, D_F=2, 2-way ANOVA). However, no significant differences from controls were detected in the ability of the homozygous

mutants to remember the position of the escape platform during the probe trials (Fig. 4-2B). Additionally, the ability of homozygous mutants to re-learn the platform location during the reversal trials was similar to controls (Fig. 4-2A), suggesting that neither memory recall nor memory extinction was affected by the QP or N17 deletions. No changes were seen during the visible platform trial (data not shown). To determine if the differences observed could be due to genotype-specific effects on swim speed, velocities recorded during the probe trial were compared. No significant differences were found between different genotypes at all the ages tested (Fig. 4-2C).

Subcellular localization of ΔQP-Htt or ΔN17-Htt is not significantly different from wild type Htt in the mouse brain

The N17 domain, in addition to having a membrane-association function, also contains a nuclear export signal. Therefore, ΔN17-Htt could exhibit altered subcellular localization in comparison to wild type Htt, ΔQ-Htt, or ΔQP-Htt [60, 127]. Whole brain protein lysates from 6-month-old mice (n=3-4/genotype) were separated into nuclear, cytosolic, and microsomal fractions. Western blotting was first performed to confirm the identity of the fractions using subcellular markers (Fig. 4-3), and then Htt levels in each fraction were quantified. Htt levels were first normalized to mTOR levels in the microsomal and cytosolic fractions and to Lamin B1 levels in the nuclear fractions. The Htt levels in the $Htt^{\Delta Q/\Delta Q}$, $Htt^{\Delta QP/\Delta QP}$, and $Htt^{\Delta N17/\Delta N17}$ samples were then compared to wild type Htt levels. There were no significant differences in nuclear Htt levels in the brains of $Htt^{\Delta N17/\Delta N17}$, $Htt^{\Delta QP/\Delta QP}$, and $Htt^{\Delta Q/\Delta Q}$ mice compared to the $Htt^{+/+}$ controls (Fig. 4-4; p=0.6421, F=0.5769, D_F=3, 1-way ANOVA). There were also no significant differences

in Htt levels in the cytosolic (Fig. 4-4; p=0.0781, F=3.310, D_F=3, 1-way ANOVA) or microsomal fractions (Fig. 4-4; p=0.1591, F=2.094, D_F=3, 1-way ANOVA).

Basal neuronal autophagy is not affected by the Htt N17 or QP deletion

To determine if neuronal autophagy was affected in the $Htt^{\Delta QP/\Delta QP}$ and $Htt^{\Delta N17/\Delta N17}$ mice, we first examined the steady-state levels of the autophagy markers LC3 and p62 in comparison to $Htt^{+/+}$and $Htt^{\Delta Q/\Delta Q}$ controls in the microsomal fractions (enriched in autophagosomes) obtained from 6-month-old $Htt^{+/+}$, $Htt^{\Delta QP/\Delta QP}$, $Htt^{\Delta N17/\Delta N17}$, and $Htt^{\Delta Q/\Delta Q}$ mice. No significant differences in the ratio of LC3-II to LC3-I in the microsomal fractions were detected between *Htt* homozygous deletion mutants and $Htt^{+/+}$ controls (Fig. 4-5A; p=0.6581, F=0.5568, D_F=3, n=3/genotype, 1-way ANOVA). p62 was also quantified in the cytosolic, microsomal, and nuclear fractions since it can be detected in all three fractions. No difference in p62 levels between the homozygous mutants and the controls was observed in any fraction (data not shown). Consistent with these results, we could not detect any changes in the number of $LC3^+p62^+$ autophagosomes or any differences in p62 immunostaining in the cortex or striatum of 18-month-old $Htt^{\Delta QP/\Delta QP}$ and $Htt^{\Delta N17/\Delta N17}$ mice compared to $Htt^{+/+}$ controls (n=3/genotype, data not shown.).

Because basal neuronal autophagy *in vivo* is very efficient, small changes in autophagy can be difficult to detect in the brain [138]. To better characterize autophagy in the deletion mutants, autophagic flux assays were performed in primary neuronal cultures generated from $Htt^{+/+}$, $Htt^{\Delta Q/\Delta Q}$, $Htt^{\Delta QP/\Delta QP}$ and $Htt^{\Delta N17/\Delta N17}$ mice. Primary cortical and striatal neurons were isolated from P5 pups and grown on Poly-D-lysine coated coverslips in serum-free medium for 8 DIV. To assess the formation of autophagosomes

within these neurons, cultures were treated with chloroquine. Chloroquine is a membrane-permeable compound that accumulates in acidic compartments within cells (e.g. lysosomes) and neutralizes their pH, thus inhibiting the degradation of autophagosomes [129, 139]. Therefore, an increase or decrease in autophagosome accumulation during the chloroquine treatment could reflect an increase or decrease in their formation. Neurons were fixed either without chloroquine treatment (no treatment), or after a 4- or 8-hour incubation in medium containing 30 μM chloroquine. Immunocytochemistry was then performed with LC3, p62 and βIII-tubulin antibodies to quantify cargo-containing autophagosomes ($LC3^+p62^+$ puncta) within neuronal cell bodies or processes ($\beta III\ tubulin^+$).

Incubation of neuronal cultures with 30 μM chloroquine resulted in an increase in total $LC3^+p62^+$ autophagosomes in the cell bodies of both striatal (Fig. 4-5B, C; $p<0.0001$, $F=235.1$, $D_F=2$, 2-way ANOVA) and cortical neurons (Fig. 4-6; $p<0.0001$, $F=200.1$, $D_F=2$, 2-way ANOVA) compared to cultures that did not receive chloroquine treatment. An increase in the amount of $LC3^+p62^+$ autophagosomes could also be observed in neurites (Fig. 4-5B, D; $p<0.0001$, $F=33.92$, $D_F=2$, 2-way ANOVA). However, in both striatal and cortical neuronal cultures, no differences in the amount of $LC3^+p62^+$ autophagosomes were detected between genotypes either in the cell bodies (Fig. 4-5C; $p=0.4350$, $F=0.9154$, $D_F=3$, 2-way ANOVA) (Fig. 4-6; $p=0.1063$, $F=2.071$, $D_F=3$, 2-way ANOVA) or in the neurites (Fig. 4-5D; $p=0.8792$, $F=0.2245$, $D_F=3$, 2-way ANOVA), with or without chloroquine treatment.

Lipofuscin is autofluorescent cell debris that predominantly consists of oxidized lipids and cross-linked proteins from organelles that are not fully digested by the

lysosome during autophagy [140, 141]. Oxidative stress and inefficient autophagy both lead to an increase in lipofuscin accumulation in post-mitotic cells, and several studies have reported increased lipofuscin in HD mouse models [110, 142]. We therefore investigated whether lipofuscin accumulation in $Htt^{\Delta QP/\Delta QP}$ and $Htt^{\Delta N17/\Delta N17}$ mice was enhanced in comparison to controls. No significant differences in lipofuscin accumulation were found in the brains of 18-month-old $Htt^{\Delta QP/\Delta QP}$, $Htt^{\Delta N17/\Delta N17}$, and $Htt^{+/+}$mice (data not shown). We also did not detect any differences in reactive astrocytes ($GFAP^+$) or activated microglia ($CD68^+$) in brain sections from 18-month-old $Htt^{\Delta QP/\Delta QP}$, $Htt^{\Delta N17/\Delta N17}$, and $Htt^{+/+}$ mice (data not shown).

Thalamostriatal synapses are reduced in $Htt^{\Delta N17/\Delta N17}$ mice

The dorsal striatum is innervated by projections from the cortex and several different thalamic nuclei [143]. These cortical and thalamic projections account for a majority of the excitatory synaptic input into the striatum [143]. To determine if changes in synapse numbers could be detected in the $Htt^{\Delta QP/\Delta QP}$ and $Htt^{\Delta N17/\Delta N17}$ mice in comparison to $Htt^{+/+}$ controls, brain sections from 24-month-old mice were stained with a post-synaptic marker (PSD-95) and pre-synaptic markers to label either cortical axon terminals (Vglut1, Fig. 4-8) or thalamic axon terminals (Vglut2, Fig. 4-7) in the dorsal striatum and in the motor cortex. No changes in the number of $Vglut1^+PSD\text{-}95^+$ puncta representing corticostriatal synapses in the dorsal striatum (Fig. 4-8A; p=0.6467, F=0.4380, D_F=2, 1-way ANOVA) or in the number of $Vglut1^+PSD\text{-}95^+$ puncta representing cortico-cortical synapses in the primary motor cortex (Fig. 4-8B; p=0.1129,

F=2.231, D_F=2, 1-way ANOVA) were observed in deletion mutants compared to controls.

In contrast, a significant reduction in the number of Vglut2$^+$PSD-95$^+$ puncta representing thalamostriatal synapses in the dorsal striatum of *Htt*$^{\Delta N17/\Delta N17}$ mice was observed in comparison to controls (Fig. 4-7A, D; p=0.0013, F=7.294, D_F=2, 1-way ANOVA). Additionally, we observed a significant decrease in the number of Vglut2$^+$PSD-95$^+$ puncta in the primary motor cortex (thalamocortical synapses) in *Htt*$^{\Delta N17/\Delta N17}$ mice compared to *Htt*$^{\Delta QP/\Delta QP}$ mice (Fig. 4-7B, E; p=0.0324, F=3.602, D_F=2, 1-way ANOVA), and a trend towards a decrease in *Htt*$^{\Delta N17/\Delta N17}$ mice in comparison to controls.

Vglut1 and Vglut2 are expressed widely throughout the brain in largely complementary expression patterns, and together they account for nearly all excitatory synaptic inputs [143-145]. To determine if there was a change in Vglut1, Vglut2, or PSD-95 expression in the *Htt*$^{\Delta Q/\Delta Q}$, *Htt*$^{\Delta QP/\Delta QP}$, *Htt*$^{\Delta N17/\Delta N17}$, and *Htt*$^{+/+}$ mice, we quantified their levels by western blotting of whole brain microsomal fractions (containing synaptosomes) isolated from 6-month-old mice (n=3/genotype). No changes in the amount of total PSD-95 or total Vglut1 were detected in a comparison of the deletion mutants and controls (Fig. 4-9). However, we did observe a small but significant increase in the level of Vglut2 in both *Htt*$^{\Delta QP/\Delta QP}$ and *Htt*$^{\Delta N17/\Delta N17}$ mice compared to controls (Fig. 4-9; p=0.008, F=6.655, D_F=3, 1-way ANOVA).

iii. Discussion

Several previous studies have proposed a role for HTT in selective macroautophagy [57, 65, 75, 81]. The C-terminal portion of HTT (with structural similarity to Atg11) interacts with both LC3 and p62, and thus, may be essential for HTT's role in selective macroautophagy. Additionally, Htt interacts with Bassoon, a pre-synaptic protein that in addition to its role in modulating endo- and exocytosis can also modulate autophagy within the pre-synaptic terminal [94, 146]. Prior work from the Zeitlin laboratory has shown that deletion of the Htt polyQ stretch enhances autophagy *in vitro* and extends lifespan in mice [110]. Despite these observations, I did not detect any changes in autophagic flux in primary neuronal cultures or in steady-state LC3-II levels in whole brain microsomal fractions obtained from 6-month-old $Htt^{+/+}$, $Htt^{\Delta Q/\Delta Q}$, $Htt^{\Delta QP/\Delta QP}$, and $Htt^{\Delta N17/\Delta N17}$ mice. I note that a recent study investigating the consequence of *Htt* inactivation in the brains of adult mice also did not detect significant changes in LC3 or p62 protein levels [147]. Because stress can induce selective macroautophagy [57], and recent *in vitro* studies have identified N17 domain-dependent roles for HTT in cellular stress and DNA damage responses [60, 82, 114, 116], it is possible that the contribution of the HTT N-terminus in these pathways may not be apparent until homeostasis is perturbed, such as under chronic stress. For example, the expression of 140Q-Htt was needed to elicit more robust autophagy phenotypes in $Htt^{140Q/\Delta Q}$ mice [110]. Therefore, similar studies in $Htt^{140Q/\Delta QP}$ and $Htt^{140Q/\Delta N17}$ mice may be required to evaluate the potential contributions of the Htt N17 or QP domains to these cellular mechanisms *in vivo*.

I did not detect a significant change in the steady-state subcellular localization of ΔN17-Htt in the cytosolic, microsomal, or nuclear fractions. This may be due to the presence of an additional nuclear export signal in the C-terminus of Htt and a second membrane association domain located at Htt amino acids 229-246 that could compensate for the loss of the N17 domain [70, 148]. However, my results do not exclude the possibility that small changes in ΔN17-Htt subcellular localization that cannot be detected reliably by western blotting do occur in the brains of $Htt^{\Delta N17/\Delta N17}$ mice.

No differences between the homozygous mutants and controls were observed in activity levels, but $Htt^{\Delta QP/\Delta QP}$ mice exhibited a consistent improvement in motor coordination on the accelerating rotarod throughout their lifespan, a result that is similar to the improved motor coordination phenotype exhibited by $Htt^{\Delta Q/\Delta Q}$ mice [109]. In contrast, neither $Htt^{\Delta P/\Delta P}$ [61] nor $Htt^{\Delta N17/\Delta N17}$ mice exhibit any differences on the rotarod in comparison to controls. $Htt^{\Delta N17/\Delta N17}$ mice displayed an improvement in the acquisition (learning) phase of the Morris water maze test in comparison to controls at 3 and 6 months of age, but began to exhibit deficits as they aged. $Htt^{\Delta QP/\Delta QP}$ mice also exhibited an initial improvement in the acquisition phase of the Morris water maze at 3 months of age, but no differences were detected in comparison to the controls at older ages. Male $Htt^{\Delta P/\Delta P}$ mice exhibited significant deficits in the Morris water maze at 18 months of age during the acquisition phase, the probe trial, and the reversal phase, but behaved similar to controls at younger ages [61]. Although $Htt^{\Delta Q/\Delta Q}$ mice have not been tested in the Morris water maze, they have been tested in the analogous Barnes maze, and they exhibited deficits during this task at 5 months of age [109]. The differences in learning and memory phenotypes between these mice suggest that the polyQ and the PRR could

potentially modulate each other's effects on spatial learning and memory. Further characterization of the $Htt^{\Delta NQP}$ mice with a deletion of all three domains encoded by Htt's exon 1 may be needed to further evaluate their interactions.

Although the cause of the behavioral phenotypes in the homozygous Htt N-terminal domain deletion mice has yet to be identified, we did observe a significant decrease in thalamostriatal synapses in 24-month-old $Htt^{\Delta N17/\Delta N17}$ mice. $Htt^{\Delta N17/\Delta N17}$ mice had fewer Vglut2^{+}PSD-95^{+} thalamostriatal synapses in the dorsal striatum and a trend towards decreased Vglut2^{+}PSD-95^{+} thalamocortical synapses in the primary motor cortex. Previous studies have identified a role for normal Htt in the development and maintenance of corticostriatal and thalamostriatal synapses in mice, and have also shown an effect of mHtt expression on age-related synapse loss in HD mouse models [42, 43, 95]. Conditional loss of Htt expression using *Emx1-Cre* in the developing CNS results in an initial increase in corticostriatal and thalamostriatal synapses [95]. However, synapse numbers in older *Htt* conditional knock-out brains were not examined; therefore, it is not known if early increases in synaptogenesis could result in later age-related phenotypes.

The behavioral impact of decreased thalamic innervation of the striatum is difficult to determine because the striatum receives input from several different thalamic nuclei [143]. Nevertheless, thalamic volumetric decline is associated with more severe cognitive symptoms in HD patients [149, 150]. My observations that $Htt^{\Delta N17/\Delta N17}$ and $Htt^{\Delta QP/\Delta QP}$ mice exhibited an increase in whole-brain Vglut2 levels at 6 months of age together with a decrease in Vglut2^{+}PSD-95^{+} puncta in the dorsal striatum of $Htt^{\Delta N17/\Delta N17}$ mice at 24 months of age, suggests that synaptogenesis and/or synapse maintenance could be altered in these mice. Future studies will be needed to determine if the synaptic

phenotypes we observe are due to a developmental defect, or if they appear as mice age. Nevertheless, the effect of the N17 domain deletion on thalamostriatal synapses lends support to the hypothesis that during evolution, the N-terminus of HTT may have evolved to contribute to specific neuronal functions in vertebrates in addition to its other cellular functions.

	+/+	ΔQP/ΔQP	ΔN17/ΔN17
3 months	30	15	15
6 months	30	14	15
12 months	29	14	15
18 months	27	13	12
24 months	23	12	10

Table 4-1. The numbers of $Htt^{+/+}$, $Htt^{\Delta QP/\Delta QP}$, and $Htt^{\Delta N17/\Delta N17}$ mice used for behavioral testing at each age.

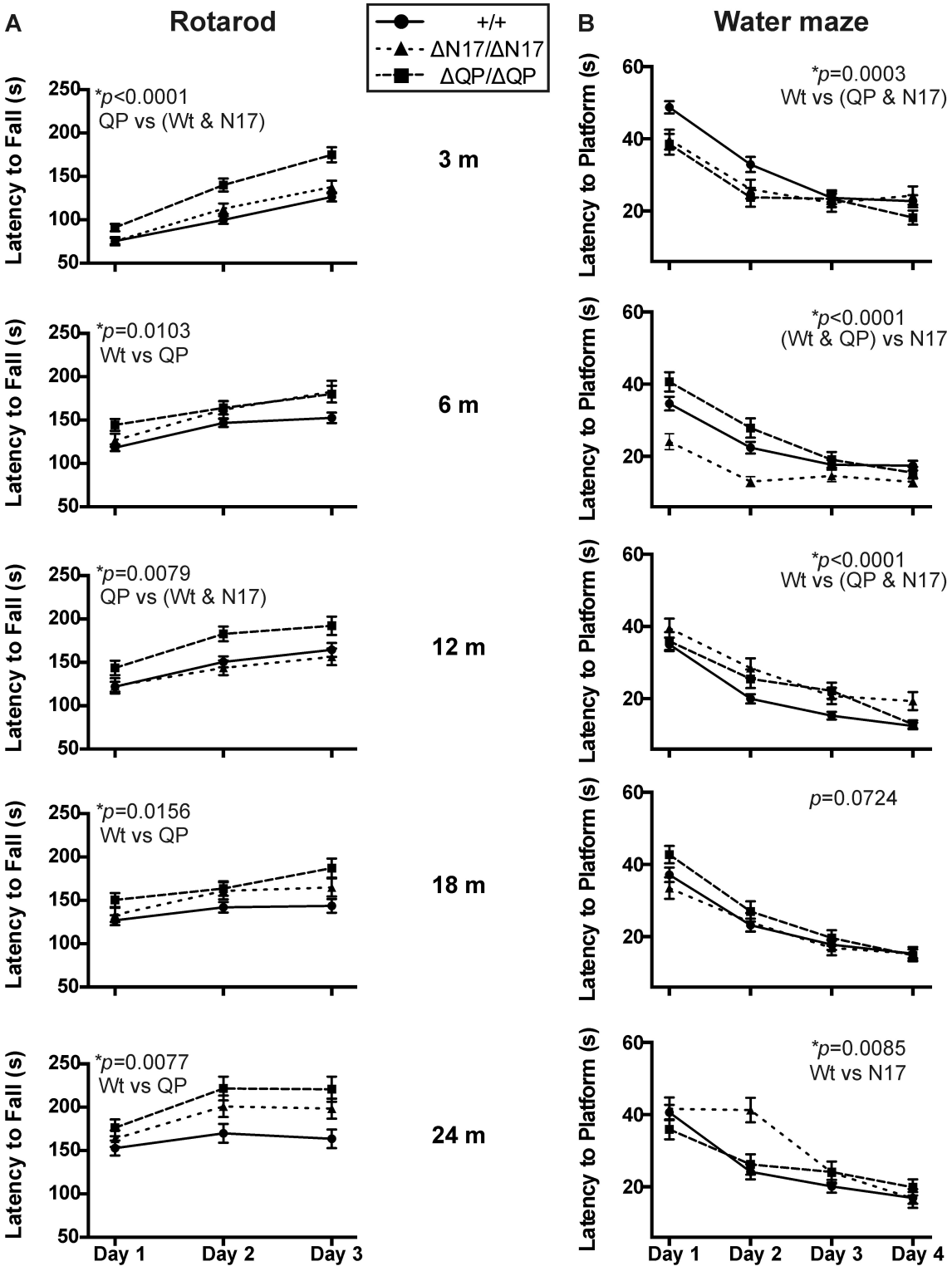

Figure 4-1. Behavioral analyses of the homozygous domain deletion mice. (A) $Htt^{\Delta QP/\Delta QP}$ (ΔQP/ΔQP) mice consistently out-performed $Htt^{+/+}$ (+/+) littermates on the accelerating

rotarod at 3 (p<0.0001), 6 (p=0.0103), 12 (p=0.0079), 18 (p=0.0156), and 24 months of age (p=0.0077, 2-way ANOVA). (B) In the acquisition phase of the Morris water maze test, both $Htt^{\Delta QP/\Delta QP}$ and $Htt^{\Delta N17/\Delta N17}$ (ΔN17/ΔN17) mice were able to navigate to the platform more quickly than controls at 3 months of age (p=0.0003, 2-way ANOVA). $Htt^{\Delta N17/\Delta N17}$ mice continued to find the platform more quickly than controls at 6 months (p<0.0001, 2-way ANOVA), but by 12 months (p<0.0001, 2-way ANOVA) and 24 months of age (p=0.0085, 2-way ANOVA) they were slower to learn the location of the platform during the acquisition phase. The numbers of mice tested for each genotype at each specific age are listed in Table 4-1.

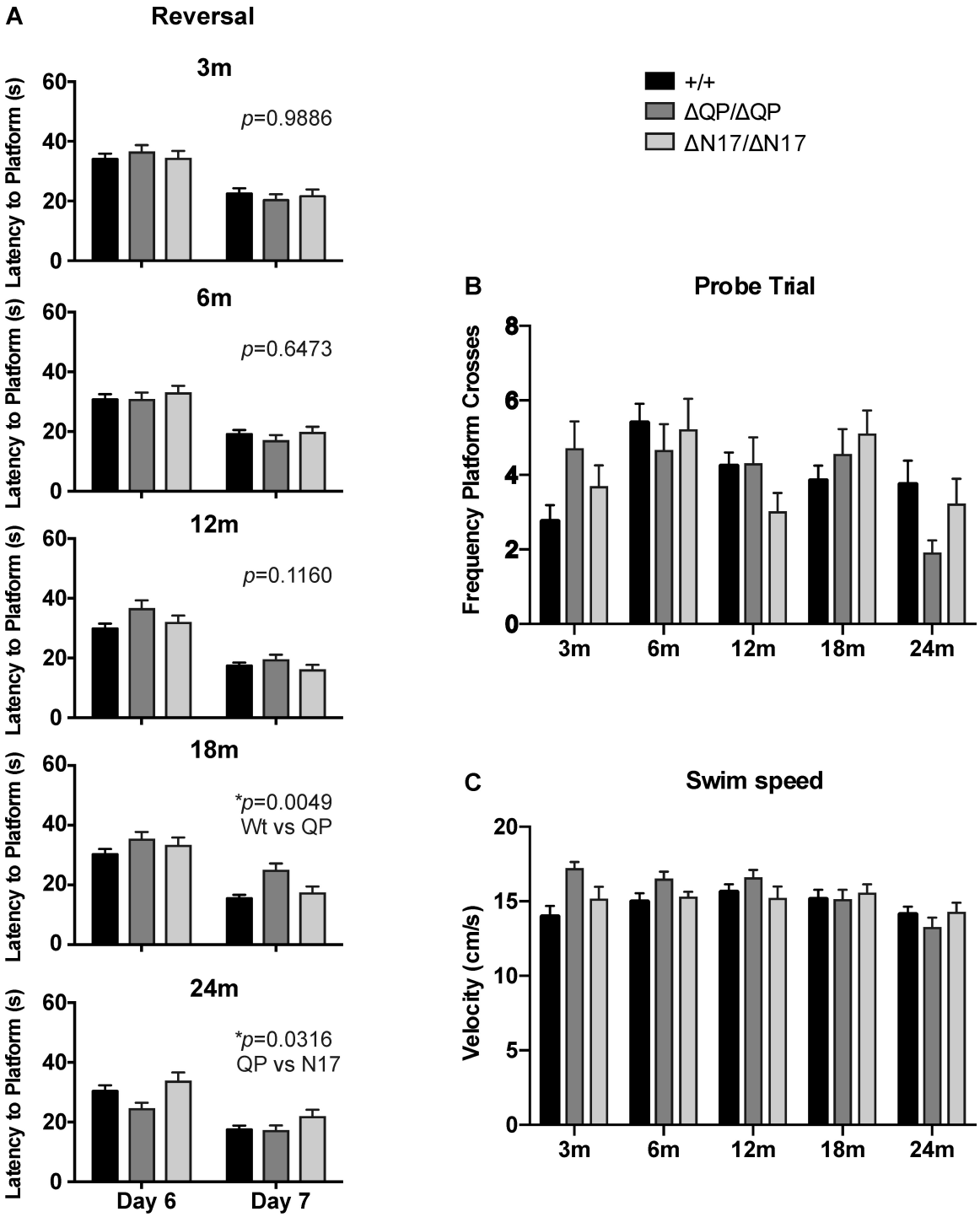

Figure 4-2. Morris water maze additional analyses. (A) No significant differences were observed during the reversal task between $Htt^{\Delta QP/\Delta QP}$ (ΔQP/ΔQP), $Htt^{\Delta N17/\Delta N17}$ (ΔN17/ΔN17), and $Htt^{+/+}$ (+/+) mice except for a decreased latency to the platform for $Htt^{\Delta QP/\Delta QP}$ mice compared to controls (p=0.0049) at 18 months of age. Additionally, at 24

months of age, $Htt^{\Delta QP/\Delta QP}$ and $Htt^{\Delta N17/\Delta N17}$ mice were significantly different from one another (p=0.0316, 2-way ANOVA), but were not different from controls. (B) No differences were observed in the frequency of platform crosses during the probe trial between genotypes at 3 (p=0.0581), 6 (p=0.7238), 12 (p=0.1638), 18 (p=0.2633), and 24 (p=0.1334) months of age (1-way ANOVA). (C) Swim velocities of each mouse were determined during the probe trials. No significant differences were observed between genotypes at all ages tested (2-way ANOVA).

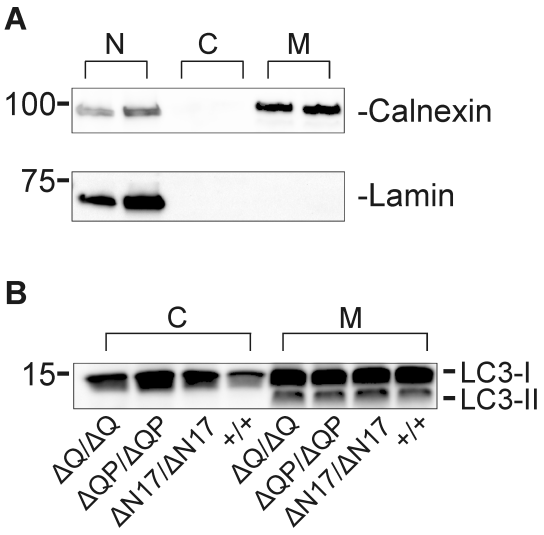

Figure 4-3. Western blots of marker proteins in the nuclear (N), cytosolic (C), and microsomal (M) fractions isolated from the brains of $Htt^{+/+}$, $Htt^{\Delta Q/\Delta Q}$, $Htt^{\Delta QP/\Delta QP}$, and $Htt^{\Delta N17/\Delta N17}$ mice. (A) Calnexin is located in the endoplasmic reticulum and on the nuclear envelope. Thus, it is detected in both the nuclear and microsomal fractions, but is absent from the cytosolic fraction. Lamin B1 is associated with the nuclear membrane and is only detected in the nuclear fraction. (B) LC3-I is detected in both cytosolic and microsomal fractions, but LC3-II, which is associated with autophagosomes, can only be detected in the microsomal fraction.

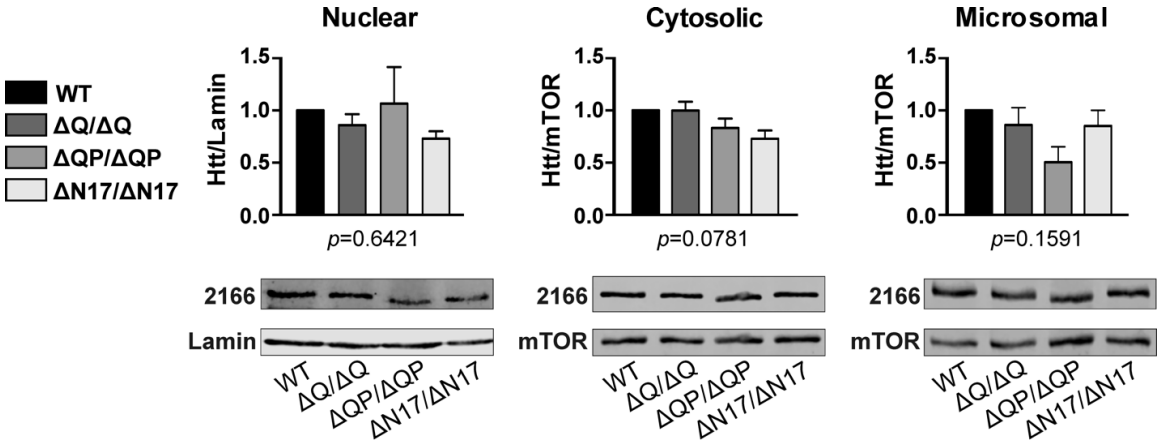

Figure 4-4. Htt levels in subcellular fractions. Whole brain lysates from 6-month-old $Htt^{+/+}$ (+/+), $Htt^{\Delta Q/\Delta Q}$ (ΔQ/ΔQ), $Htt^{\Delta QP/\Delta QP}$ (ΔQP/ΔQP), and $Htt^{\Delta N17/\Delta N17}$ (ΔN17/ΔN17) mice were separated into nuclear, cytosolic, and microsomal fractions. No significant differences in Htt protein levels were observed between the homozygous mutants and wild type controls in any of these fractions. For quantification, Htt (MAB2166) levels were first normalized to mTOR levels in the microsomal and cytosolic fractions, and to Lamin B1 levels in the nuclear fractions. The normalized Htt levels in the $Htt^{\Delta Q/\Delta Q}$, $Htt^{\Delta QP/\Delta QP}$, and $Htt^{\Delta N17/\Delta N17}$ samples were then compared to normalized wild type Htt levels. Nuclear fraction: $Htt^{\Delta Q/\Delta Q}$: 1.062 ± 0.459, $Htt^{\Delta QP/\Delta QP}$: 0.669 ± 0.198, $Htt^{\Delta N17/\Delta N17}$: 0.616 ± 0.208; p=0.6421. Cytosolic fraction: $Htt^{\Delta Q/\Delta Q}$: 0.999 ± 0.085, $Htt^{\Delta QP/\Delta QP}$: 0.832 ± 0.090, $Htt^{\Delta N17/\Delta N17}$: 0.730 ± 0.078; p=0.0781. Microsomal fraction: $Htt^{\Delta Q/\Delta Q}$: 0.861 ± 0.166, $Htt^{\Delta QP/\Delta QP}$: 0.505 ± 0.148, $Htt^{\Delta N17/\Delta N17}$: 0.851 ± 0.150; p=0.1591. (mean ± SEM, 1-way ANOVA, n=3-4/genotype)

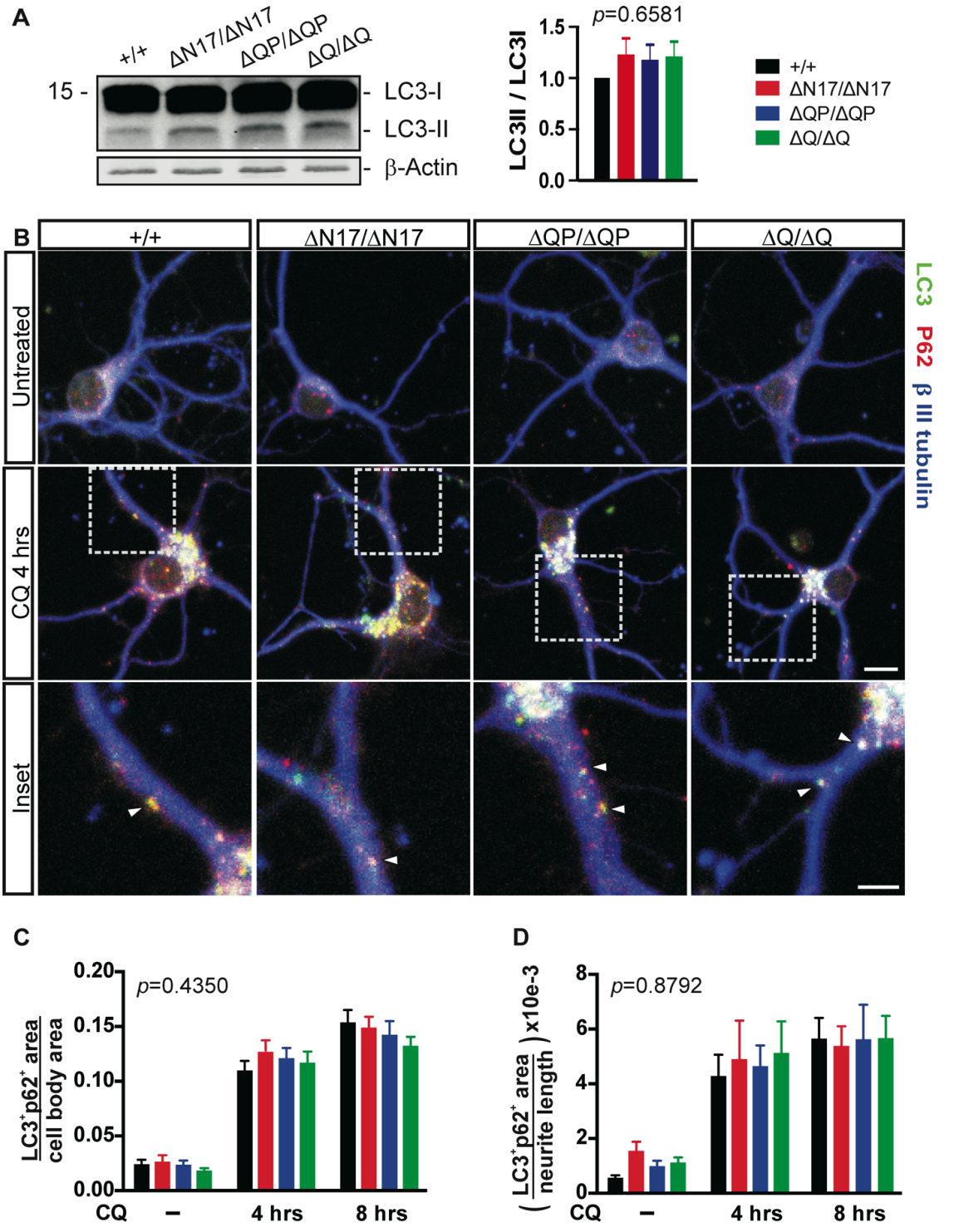

Figure 4-5. Autophagy analyses. (A) Western blot analysis of LC3 levels in the microsomal fractions from 6-month-old $Htt^{+/+}$ (+/+), $Htt^{\Delta Q/\Delta Q}$ (ΔQ/ΔQ), $Htt^{\Delta QP/\Delta QP}$ (ΔQP/ΔQP), and $Htt^{\Delta N17/\Delta N17}$ (ΔN17/ΔN17) mice. No significant differences were

detected in the ratio of LC3-II to LC3-I between different genotypes ($Htt^{\Delta N17/\Delta N17}$: 1.222 ± 0.167, $Htt^{\Delta QP/\Delta QP}$: 1.172 ± 0.154, $Htt^{\Delta Q/\Delta Q}$: 1.204 ± 0.152, mean ± SEM, n=3/genotype; p=0.6581, 1-way ANOVA). (B-D) Primary striatal neurons isolated from the brains of postnatal day 5 $Htt^{+/+}$, $Htt^{\Delta Q/\Delta Q}$, $Htt^{\Delta QP/\Delta QP}$, and $Htt^{\Delta N17/\Delta N17}$ mice were grown in serum free media for 8 DIV before treating with 30 μM chloroquine (CQ) to assess autophagic flux. (B) Fixed cells were immunostained with antibodies recognizing LC3 (green), p62 (red) and βIII tubulin (blue). Scale bar = 10 μm for top 8 panels. Arrowheads in the insets indicate $LC3^{+}p62^{+}$ cargo-containing autophagosomes within neurites. Scale bar = 5 μm for 4 inset panels. (C) Quantification of the $LC3^{+}p62^{+}$ area within the cell bodies of striatal neurons (p=0.4350, F=0.9154, D_F=3, 2-way ANOVA). (D) Quantification of the $LC3^{+}p62^{+}$ area per μm of neurite in the striatal neurons (p=0.8792, F=0.2245, D_F=3, 2-way ANOVA). No significant differences were observed between the $Htt^{+/+}$ controls and all three domain deletion mutants (n=40 cells/genotype from 3 different dissections/genotype).

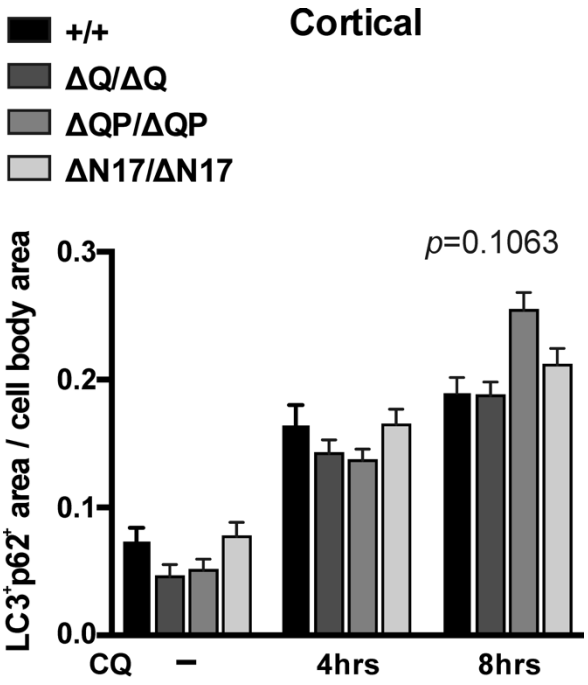

Figure 4-6. Autophagic flux analyses of cortical neurons. Primary cortical neurons from the brains of P5 $Htt^{+/+}$ (+/+), $Htt^{\Delta Q/\Delta Q}$ (ΔQ/ΔQ), $Htt^{\Delta QP/\Delta QP}$ (ΔQP/ΔQP), and $Htt^{\Delta N17/\Delta N17}$ (ΔN17/ΔN17) mice were grown for 8 DIV, and then treated with 30 μM CQ for 4 or 8 hours before immunostaining with antibodies recognizing LC3, p62 and βIII tubulin. There was an increase in $LC3^{+}p62^{+}$ cargo-containing autophagosomes in neurons treated with CQ compared to neurons that were not treated (p<0.0001, F=200.1, D_F=2, 2-way ANOVA). However, there were no significant differences between genotypes either with or without CQ treatment (p=0.1063, F=2.071, D_F=3, 2-way ANOVA).

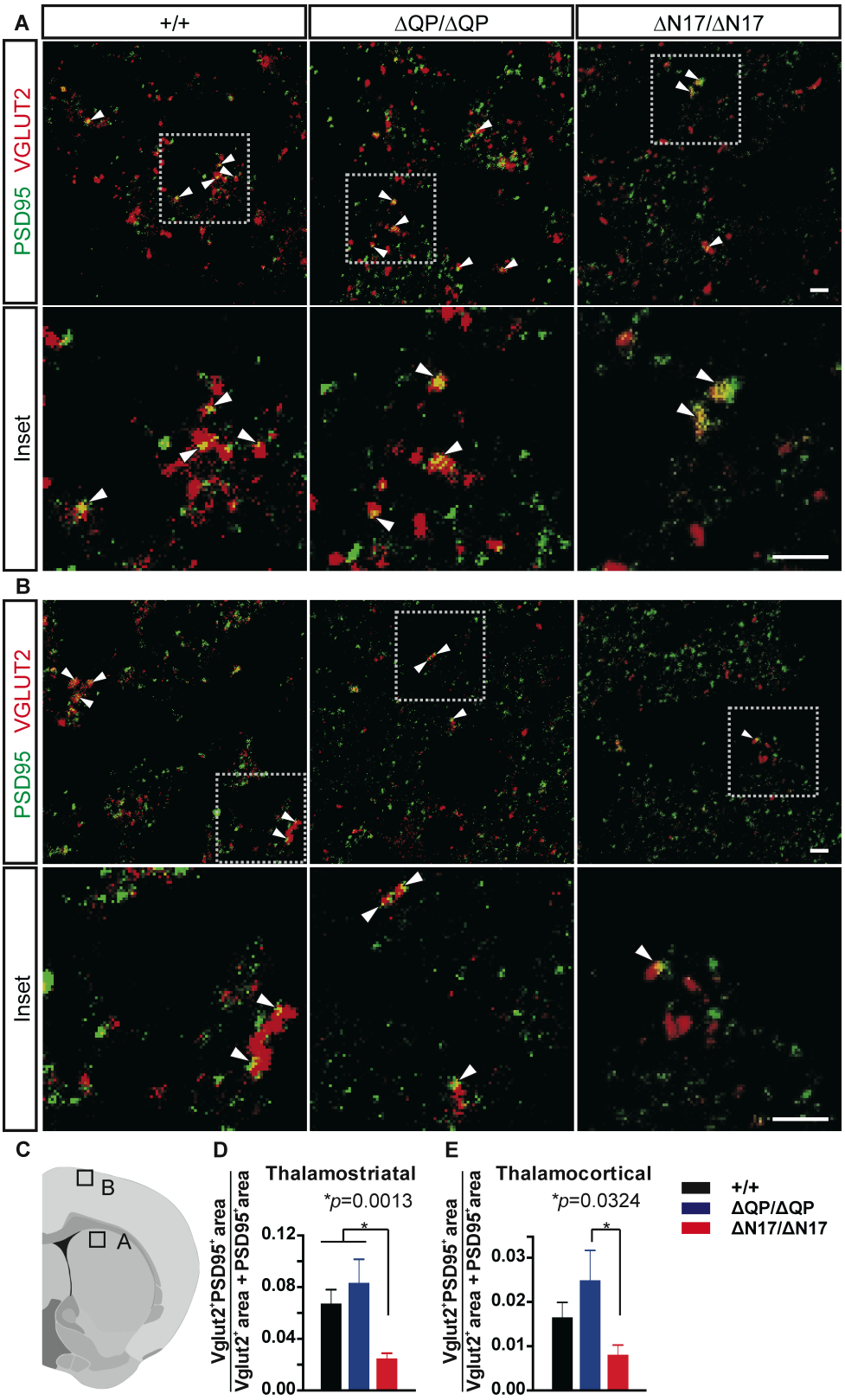
A
+/+
ΔQP/ΔQP
ΔN17/ΔN17
PSD95 VGLUT2
Inset
B
PSD95 VGLUT2
Inset
C
B
A
D
Thalamostriatal
*p=0.0013
Vglut2+PSD95+ area
Vglut2+ area + PSD95+ area
0.12
0.08
0.04
0.00
E
Thalamocortical
*p=0.0324
0.03
0.02
0.01
0.00
+/+
ΔQP/ΔQP
ΔN17/ΔN17

Figure 4-7. Synapse quantification in the brains of 24-month-old $Htt^{+/+}$ (+/+), $Htt^{\Delta QP/\Delta QP}$ (ΔQP/ΔQP), and $Htt^{\Delta N17/\Delta N17}$ (ΔN17/ΔN17) mice. (A, B) Representative images from brain sections immunostained with PSD-95 (green) and Vglut2 (red). (A) Dorsal striatum. Arrowheads indicate co-localized PSD-95 and Vglut2 (yellow), which represent thalamostriatal synapses. Scale bar = 2 μm. (B) Primary motor cortex (layers I/II). Arrowheads indicate co-localized PSD-95 and Vglut2, which represent thalamocortical synapses. Scale bar = 2 μm. (C) Diagram illustrating the two brain regions imaged in (A, B). (D, E) Quantification of PSD-95/Vglut2 co-localization in the dorsal striatum (D) and primary motor cortex (E). $Htt^{\Delta N17/\Delta N17}$ mice had reduced PSD-95^{+}Vglut2^{+} synapses in the striatum compared to $Htt^{+/+}$ controls ($Htt^{+/+}$: 0.05887 ± 0.00683, $Htt^{\Delta QP/\Delta QP}$: 0.07323 ± 0.01249, $Htt^{\Delta N17/\Delta N17}$: 0.02940 ± 0.00391, p=0.0013). $Htt^{\Delta N17/\Delta N17}$ mice also exhibited a trend toward reduced PSD-95^{+}Vglut2^{+} synapses in the primary motor cortex compared to $Htt^{+/+}$ controls and a significant reduction compared to $Htt^{\Delta QP/\Delta QP}$ mice ($Htt^{+/+}$: 0.01652 ± 0.0034, $Htt^{\Delta QP/\Delta QP}$: 0.02490 ± 0.00676, $Htt^{\Delta N17/\Delta N17}$: 0.008080 ± 0.00219, p=0.0324) (mean ± SEM, n= 23-25 images from 3 mice/genotype, 1-way ANOVA).

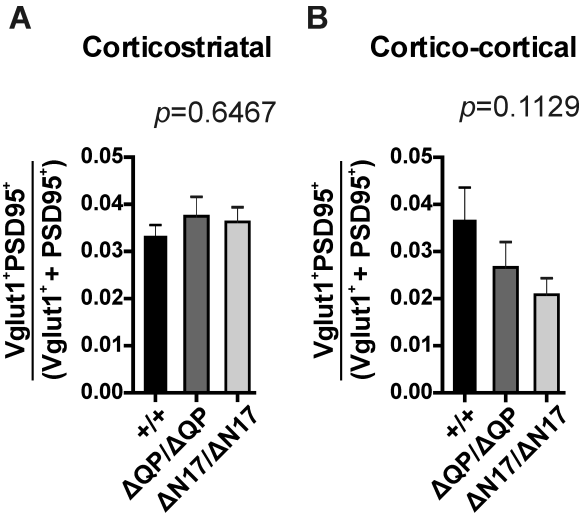

Figure 4-8. Quantification of Vglut1^{+}PSD-95^{+} synapses in the brains of 24-month-old mice. (A) No differences in the number of corticostriatal synapses were detected between *Htt*$^{\Delta QP/\Delta QP}$ (ΔQP/ΔQP), *Htt*$^{\Delta N17/\Delta N17}$ (ΔN17/ΔN17) mice and *Htt*$^{+/+}$ controls (+/+) in the dorsal striatum (p=0.6467, F=0.4380, D_F=2, 1-way ANOVA). (B) There was also no significant difference in the number of cortico-cortical synapses in the primary motor cortex between genotypes (p=0.1129, F=2.231, D_F=2, 1-way ANOVA).

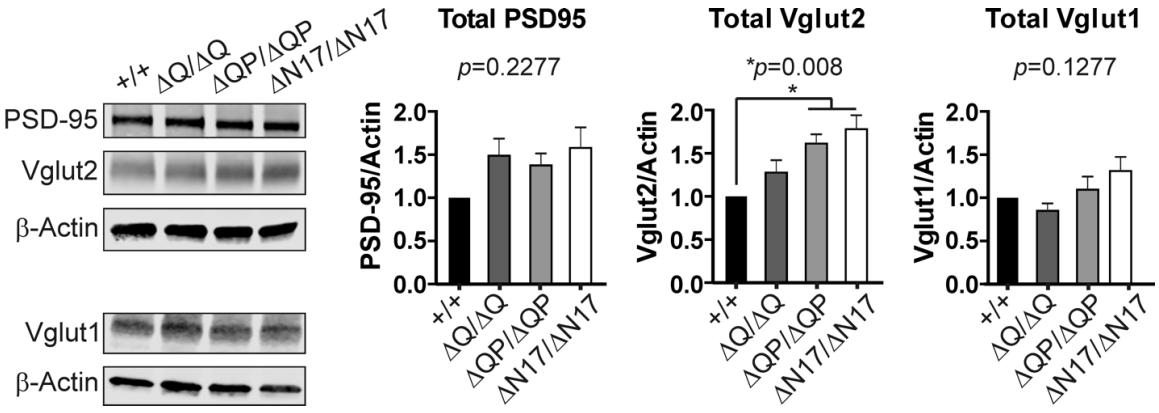

Figure 4-9. Western blots of whole brain microsomal fractions from 6-month-old mice. $Htt^{\Delta QP/\Delta QP}$ (ΔQP/ΔQP) and $Htt^{\Delta N17/\Delta N17}$ (ΔN17/ΔN17) mice had significantly more Vglut2 expression in comparison to controls ($Htt^{\Delta Q/\Delta Q}$: 1.276 ± 0.146, $Htt^{\Delta QP/\Delta QP}$: 1.612 ± 0.106, $Htt^{\Delta N17/\Delta N17}$: 1.780 ± 0.161, p=0.008). PSD-95 and Vglut1 levels were not significantly different between genotypes (PSD-95: $Htt^{\Delta Q/\Delta Q}$: 1.487 ± 0.198, $Htt^{\Delta QP/\Delta QP}$: 1.375 ± 0.139, $Htt^{\Delta N17/\Delta N17}$: 1.578 ± 0.238, p=0.2277), (Vglut1: $Htt^{\Delta Q/\Delta Q}$: 0.8487 ± 0.0878, $Htt^{\Delta QP/\Delta QP}$: 1.094 ± 0.1512, $Htt^{\Delta N17/\Delta N17}$: 1.310 ± 0.164, p=0.1277) (mean ± SEM, n=3 mice /genotype, 1-way ANOVA).

Chapter V: Characterization of *Htt*$^{140Q/\Delta N17}$ and *Htt*$^{140Q/\Delta QP}$ mice

i. Introduction

Expansion of the polyQ domain within the HTT protein causes significant neuronal dysfunction that eventually results in substantial neuronal death and severe motor, cognitive and psychiatric symptoms in HD patients. The generation of mHTT toxic N-terminal fragments, oligomers, fibrils, and aggregates causes deficits in protein-protein interactions, mitochondrial bioenergetics, fast axonal transport, excitotoxicity, and altered transcriptional regulation in HD [28, 29, 31, 34, 41, 56].

Defects in cellular clearance mechanisms result in the inefficient degradation of proteins and organelles, including mHTT, and can exacerbate the deficits observed in other cellular functions in HD. mHTT causes significant changes in macroautophagic flux and efficiency in HD patients and mouse models [30-32, 151]. An increased number of autophagosomes within neurons, and increased mRNA levels of key autophagy pathway proteins LC3A, ULK1, and LAMP2A in the brains of HD patients and HD mouse models has been described, suggesting that autophagy is upregulated in response to mHTT expression [17, 152-154]. This increase in autophagy may be due, in part, to the fact that mTOR, which is a negative regulator of autophagy, is frequently found to be sequestered into mHTT aggregates. Thus, decreased levels of functional mTOR could subsequently lead to autophagy induction in HD tissues [151].

Despite the observation that autophagy is increased in HD, the clearance of mHTT and other cellular waste is decreased due to a cargo recognition failure that occurs in the presence of mHTT, leading to the generation of empty autophagosomes [30]. Additionally, while wild type HTT promotes retrograde transport of autophagosomes,

mHTT expression impairs the efficiency of autophagosomal transport [31]. This is particularly harmful in neurons, since maturation and acidification of autophagosomes that are generated in the distal tips of axons occurs during retrograde transport, and eventual fusion with lysosomes occurs in the soma [33]. It is therefore not surprising that a mHTT-mediated transport defect can result in an accumulation of autophagosomes and reduced clearance of cellular waste [31]. In addition to changes in autophagosome generation and transport, HD mouse models also have altered lysosomal subcellular positioning, which can significantly alter autophagosome-lysosome fusion dynamics [32].

Previous work characterizing Htt N-terminal domain deletions in vivo has shown that the deletion of the polyQ domain in $Htt^{140Q/\Delta Q}$ mice results in the amelioration of motor phenotypes, worsening of cognitive phenotypes, and an increase in neuronal autophagy when compared to $Htt^{140Q/+}$ mice [110]. An *in trans* deletion of the PRR in $Htt^{140Q/\Delta P}$ mice resulted in less severe horizontal activity and grip strength deficits, while deletion of the PRR in the mutant allele of Q140 mice ($Htt^{140Q\Delta P/+}$ mice) resulted in improvements in grip strength, and a delay in the appearance of large neuronal aggregates [Liu et al *in preparation*]. Deletion of the N17 domain *in cis* to the expanded polyQ stretch in BACHD-ΔN17 mice significantly exacerbates motor phenotypes, weight loss, and striatal volumetric decline in comparison to BACHD mice without the N17 domain deletion [124].

In this chapter, I report the characterization of $Htt^{140Q/\Delta N17}$ and $Htt^{140Q/\Delta QP}$ mice using longitudinal behavioral analyses, and by assessing neuronal macroautophagy. Interestingly, $Htt^{140Q/\Delta N17}$ and $Htt^{140Q/\Delta QP}$ mice exhibit improvements during cognitive testing in comparison to $Htt^{140Q/+}$ mice, but both genotypes displayed deficits during

motor testing. Moreover, autophagy deficits were observed in primary striatal neurons derived from *Htt*$^{140Q/\Delta N17}$ and *Htt*$^{140Q/\Delta QP}$ mice, but not in primary cortical neurons derived from these same mice. These results suggest that expression of ΔN17-Htt, or ΔQP-Htt *in trans* with 140Q-Htt, can cause neuronal cell type-specific deficits in macroautophagy.

ii. Results

Behavioral analyses of *Htt*$^{140Q/\Delta N17}$ and *Htt*$^{140Q/\Delta QP}$ mice

Htt$^{+/+}$, *Htt*$^{140Q/+}$, *Htt*$^{140Q/\Delta N17}$ and *Htt*$^{140Q/\Delta QP}$ mice were subjected to longitudinal behavioral testing at 3, 6, 12, and 18 months of age to determine if the expression of either of the domain deletion mutations *in trans* to an expanded *Htt* allele could affect HD mouse model behavioral phenotypes. Beginning at 12 months of age, both *Htt*$^{140Q/\Delta N17}$ and *Htt*$^{140Q/\Delta QP}$ mice exhibited reduced activity levels. Both *Htt*$^{140Q/\Delta N17}$ and *Htt*$^{140Q/\Delta QP}$ mice demonstrated reduced total distance traveled compared to *Htt*$^{+/+}$ mice (Fig. 5-1C, p=0.0043, 1-way ANOVA, F=3, D_F=4.913). Additionally, *Htt*$^{140Q/\Delta N17}$ mice had reduced vertical activity compared to *Htt*$^{140Q/+}$ and *Htt*$^{+/+}$ mice (Fig. 5-1A, p=0.0035, 1-way ANOVA, F=3, D_F=5.099), and *Htt*$^{140Q/\Delta QP}$ mice had reduced horizontal activity levels compared to *Htt*$^{+/+}$ mice (Fig. 5-1B, p=0.0070, 1-way ANOVA, F=3, D_F=4.478). This decrease in activity levels observed in *Htt*$^{140Q/\Delta N17}$ and *Htt*$^{140Q/\Delta QP}$ mice occurred before any significant decrease in *Htt*$^{140Q/+}$ mice could be observed in comparison to *Htt*$^{+/+}$ controls. At 18 months of age both *Htt*$^{140Q/\Delta N17}$ and *Htt*$^{140Q/\Delta QP}$ mice demonstrate decreased vertical (Fig 5-1A, p=0.0001, 1-way ANOVA, F=3, D_F=8.245) and horizontal (Fig 5-1B, p=0.0005, 1-way ANOVA, F=3, D_F=7.007) activity levels compared to controls. Additionally, *Htt*$^{140Q/\Delta N17}$, *Htt*$^{140Q/\Delta QP}$, and *Htt*$^{140Q/+}$ mice all exhibited decreased total distance traveled at 18 months of age in comparison to *Htt*$^{+/+}$ controls (Fig 5-1C, p<0.0001, 1-way ANOVA, F=3, D_F=8.601).

Htt$^{140Q/\Delta N17}$ and *Htt*$^{140Q/\Delta QP}$ mice also demonstrated a similar worsening of *Htt*$^{140Q/+}$ behavioral phenotypes in the rotarod task. At 6 months of age, *Htt*$^{140Q/\Delta N17}$ mice performed worse than *Htt*$^{140Q/+}$ and *Htt*$^{+/+}$ controls, and *Htt*$^{140Q/\Delta QP}$ mice performed worse

compared to $Htt^{140Q/+}$ mice (Fig. 5-2A, $p<0.0001$, 2-way ANOVA, F=10.46, D_F=3). Similar to the differences seen during activity cage testing, the decline in rotarod performance of the $Htt^{140Q/\Delta N17}$ and $Htt^{140Q/\Delta QP}$ mice occurred before there were any detectable differences between $Htt^{140Q/+}$ mice and $Htt^{+/+}$ controls. At 18 months of age, both the $Htt^{140Q/\Delta N17}$ and $Htt^{140Q/\Delta QP}$ mice exhibited a decrease in rotarod performance compared to $Htt^{+/+}$ controls, and the $Htt^{140Q/\Delta N17}$ mice also performed worse compared to the $Htt^{140Q/+}$ mice (Fig. 5-2A, $p<0.0001$, 2-way ANOVA, F=12.68, D_F=3). 18 months is also the age that the $Htt^{140Q/+}$ mice first performed worse compared to controls. Grip strength testing was also performed on these mice at 18 months of age; $Htt^{140Q/\Delta N17}$, $Htt^{140Q/\Delta QP}$, and $Htt^{140Q/+}$ mice all displayed weakened grip strength compared to controls (Fig. 5-2C, $p<0.0001$, 1-way ANOVA, F=11.42, D_F=3).

Interestingly, the general trend for enhanced or an earlier onset of behavioral phenotypes in the $Htt^{140Q/\Delta N17}$ and $Htt^{140Q/\Delta QP}$ mice compared to the $Htt^{140Q/+}$ mice was not observed during Morris water maze testing. At 3 months of age, the $Htt^{140Q/\Delta N17}$ and $Htt^{140Q/\Delta QP}$ mice learned the location of the hidden platform during the acquisition phase of the test more quickly in comparison to the $Htt^{140Q/+}$ mice (Fig. 5-2B, p=0.0051, F=4.366, D_F=3). At 6 months of age, the $Htt^{140Q/\Delta N17}$ mice performed better when compared to $Htt^{140Q/\Delta QP}$ mice and $Htt^{+/+}$ controls (Fig. 5-2B, p=0.0190, F=3.383, D_F=3). At 12 months of age, the $Htt^{140Q/\Delta N17}$ mice again found the platform more quickly compared to $Htt^{140Q/+}$ mice (Fig. 5-2B, p=0.0010, F=5.623, D_F=3). Deficits in the $Htt^{140Q/+}$ mice in comparison to the $Htt^{+/+}$ controls during the acquisition phase were not observed until 18 months of age, when the $Htt^{140Q/+}$ mice took longer to find the platform

compared to the $Htt^{140Q/\Delta N17}$, $Htt^{140Q/\Delta QP}$ mice, and $Htt^{+/+}$ controls (Fig. 5-2B, p=0.0005, F=6.084, D_F=3).

No significant differences between any of the genotypes were observed during the reversal task at 3 (Fig. 5-3A, p=0.7292, F=0.4335, D_F=3), 6 (p=0.3038, F=1.218, D_F=3), 12 (p=0.3653, F=1.064, D_F=3), and 18 months of age (p=0.4405, F=0.903, D_F=3, 2-way ANOVA). Additionally, no differences were observed between the genotypes in the frequency of platform crosses during the probe trial at 3 (Fig. 5-3B, p=0.4480, F=0.898, D_F=3), 6 (p=0.6157, F=0.6031, D_F=3), 12 (p=0.4119, F=.9738, D_F=3), and 18 (p=0.2177, F=1.53, D_F=3, 1-way ANOVA) months of age. These two findings suggest that memory extinction and memory recall were not different amongst the genotypes tested. To determine if motor deficits observed during the rotarod task could have an impact on water maze performance, swim velocities for each mouse were determined during the probe trial. No significant differences were observed between genotypes at 3 (Fig. 5-3C, p=0.5525, F=0.7059, D_F=3), 6 (p=0.5851, F=0.6523, D_F=3), 12 (p=0.2307, F=1.477, D_F=3), and 18 months of age (p=0.7286, F=0.4353, D_F=3, 2-way ANOVA).

Autophagic flux is affected in $Htt^{140Q/\Delta N17}$ and $Htt^{140Q/\Delta QP}$ primary neuronal cultures

Previous studies have shown that neuronal autophagy is significantly affected in HD patients and HD animal models. To investigate the potential of the Htt N-terminal domain deletion mutations to affect neuronal macroautophagy *in trans*, primary striatal and cortical neuronal cultures were generated from P5 $Htt^{140Q/+}$, $Htt^{140Q/\Delta Q}$, $Htt^{140Q/\Delta N17}$, and $Htt^{140Q/\Delta QP}$ pups. Primary cultures were treated with chloroquine on the 8th DIV for 4 or 8 hrs, and fixed neurons were subsequently immunostained with LC3, p62 and βIII-

tubulin antibodies to quantify the accumulation of cargo-containing autophagosomes ($LC3^+p62^+$ puncta) within neuronal cell bodies or processes (βIII $tubulin^+$) as described in chapter IV.

Similar to my prior analyses of autophagic flux in $Htt^{\Delta QP/\Delta QP}$ and $Htt^{\Delta N17/\Delta N17}$ primary neurons, I observed an increase in $LC3^+p62^+$ autophagosomes in both the cell bodies (Fig. 5-4A,B; $p<0.0001$, $F=54.52$, $D_F=2$) and in the neurites (Fig. 5-4A,C; $p<0.0001$, $F=12.22$, $D_F=2$) of striatal neurons, and in the cell bodies (Fig. 5-5A,B; $p<0.0001$, $F=73.50$, $D_F=2$) and neurites (Fig. 5-5A,C; $p<0.0001$, $F=10.42$, $D_F=2$) of cortical neurons after chloroquine treatment. Additionally, I was able to detect a decrease in the amount of $LC3^+p62^+$ autophagosomes in the cell bodies of $Htt^{140Q/\Delta N17}$ and $Htt^{140Q/\Delta QP}$ striatal neurons in comparison to $Htt^{140Q/+}$ and $Htt^{140Q/\Delta Q}$ neurons after chloroquine treatment (Fig. 5-4A,B; $p<0.0001$, $F=11.11$, $D_F=3$). In the neurites of striatal neurons, the amount of $LC3^+p62^+$ autophagosomes was comparable in the $Htt^{140Q/+}$, $Htt^{140Q/\Delta N17}$, and $Htt^{140Q/\Delta QP}$ neurons; however, the $Htt^{140Q/\Delta Q}$ striatal neurons exhibited increased $LC3^+p62^+$ autophagosomes in their neurites in comparison to the $Htt^{140Q/\Delta N17}$ and $Htt^{140Q/\Delta QP}$ neurons after 8 hrs of chloroquine treatment (Fig. 5-4A,C; $p=0.0492$, $F=2.712$, $D_F=3$).

Interestingly, I did not observe these same phenotypes in cortical neurons, suggesting that neuronal autophagy may be differentially regulated in different neuronal subtypes. No differences were observed in the amount of $LC3^+p62^+$ autophagosomes in the $Htt^{140Q/+}$, $Htt^{140Q/\Delta N17}$, and $Htt^{140Q/\Delta QP}$ cortical neurons in either their cell bodies or in their neurites. I did observe, however, an increase in the amount of $LC3^+p62^+$ autophagosomes in the cell bodies of the $Htt^{140Q/\Delta Q}$ neurons in comparison to the

Htt$^{140Q/\Delta N17}$ neurons after chloroquine treatment (Fig. 5-5A,B; p=0.0416, F=2.848, D_F=3). Additionally I observed an increase in the amount of $LC3^+p62^+$ autophagosomes after 4 hrs chloroquine treatment in the neurites of the *Htt*$^{140Q/\Delta Q}$ neurons compared to *Htt*$^{140Q/+}$ and *Htt*$^{140Q/\Delta N17}$ neurons (Fig. 5-5A,C; p=0.0315, F=3.071, D_F=3).

In addition to the changes I observed in the amount of autophagosomes during the autophagic flux experiments, I also observed a significant increase in the levels of p62 immunostaining in primary neurons derived from the *Htt*$^{140Q/\Delta N17}$ mice. Both striatal and cortical *Htt*$^{140Q/\Delta N17}$ primary neurons exhibited a range of increased p62 immunostaining, with some cells exhibiting a diffuse but high level of p62 staining throughout the cell body, nucleus and neurites, while others exhibited elevated p62 staining predominantly in the cell body and neurites, but not in the nucleus. p62 levels in the cell bodies of these neurons were quantified, and we found that *Htt*$^{140Q/\Delta N17}$ striatal (Fig. 5-6A,B; p<0.0001, F=39.11, D_F=3) and cortical (Fig. 5-6C; p<0.0001, F=19.11, D_F=3) neurons demonstrated significantly elevated p62 immunostaining in comparison to the *Htt*$^{140Q/+}$, *Htt*$^{140Q/\Delta Q}$, and *Htt*$^{140Q/\Delta QP}$ neurons, with or without chloroquine treatment.

iii. Discussion

Htt$^{140Q/\Delta N17}$ and *Htt*$^{140Q/\Delta QP}$ mice were initially very similar to *Htt*$^{140Q/+}$ and *Htt*$^{+/+}$ mice in weight, motor performance, and activity cage performance suggesting that the *in trans* N17 and polyQ-PRR domain deletions did not result in any gross developmental phenotypes in Q140 mice. I did, however, observe decreased performance of *Htt*$^{140Q/\Delta N17}$ and *Htt*$^{140Q/\Delta QP}$ mice on the rotarod task beginning at 6 months of age, and a decline in activity levels beginning at 12 months of age in comparison to *Htt*$^{140Q/+}$ and *Htt*$^{+/+}$ controls. The decreased performance observed during both tasks was surprising because it preceded any deficits observed between the *Htt*$^{140Q/+}$ mice and *Htt*$^{+/+}$ controls, which did not occur until 18 months of age. At this age, during both activity cage and rotarod testing, *Htt*$^{140Q/\Delta N17}$ and *Htt*$^{140Q/\Delta QP}$ mice continued to perform poorly while the *Htt*$^{140Q/+}$ mice exhibited a modest decline when compared *Htt*$^{+/+}$ controls for the first time.

We have previously reported that the polyQ domain deletion in *Htt*$^{140Q/\Delta Q}$ mice results in improved motor performance and a rescue of activity cage deficits in comparison to *Htt*$^{140Q/+}$ mice [110]. In addition, homozygous deletion of the polyQ stretch in *Htt*$^{\Delta Q/\Delta Q}$ or *Htt*$^{\Delta QP/\Delta QP}$ mice resulted in sustained improvements in motor coordination [109]. *Htt*$^{\Delta P/\Delta P}$ mice, did not exhibit any improvements or deficits in motor coordination or activity levels, but *Htt*$^{140Q/\Delta P}$ mice exhibited a decrease in the severity of horizontal activity cage and grip strength deficits observed in *Htt*$^{140Q/+}$ mice [61]. It was therefore unexpected, not only that *Htt*$^{140Q/\Delta QP}$ mice did not exhibit an improvement during rotarod testing similar to *Htt*$^{140Q/\Delta Q}$ mice, but that these mice exhibited more severe motor phenotypes compared to *Htt*$^{140Q/+}$ mice. One hypothesis that could explain these results would be that the deletion of such a large portion of the Htt N-terminus is

likely to result in conformational changes that could affect Htt's ability to respond normally to the chronic stress elicited by 140Q-Htt expression in $Htt^{140Q/\Delta QP}$ neurons.

Despite the absence of any changes in rotarod performance or in activity levels in $Htt^{\Delta N17/\Delta N17}$ mice, I hypothesized that $Htt^{140Q/\Delta N17}$ mice would exhibit behavioral deficits due to the loss of the N17 domain's proposed functions in neuronal stress response from ΔN17-Htt, in combination with the chronic stress provided by 140Q-Htt expression [82, 114, 116].

Interestingly, while deficits were observed during motor coordination and activity cage testing in the $Htt^{140Q/\Delta N17}$ and $Htt^{140Q/\Delta QP}$ mice, improvements were observed during the acquisition phase of the water maze learning and memory task. During the initial acquisition phase of this task, $Htt^{140Q/+}$ mice performed poorly compared to $Htt^{140Q/\Delta N17}$ and $Htt^{140Q/\Delta QP}$ mice, which were indistinguishable from $Htt^{+/+}$ controls. $Htt^{140Q/\Delta N17}$ mice again outperformed $Htt^{140Q/+}$ mice at 12 months of age, and all three genotypes, $Htt^{140Q/\Delta N17}$, $Htt^{140Q/\Delta QP}$, and $Htt^{+/+}$ mice, performed better compared to $Htt^{140Q/+}$ mice at 18 months of age. Both $Htt^{\Delta QP/\Delta QP}$ and $Htt^{\Delta N17/\Delta N17}$ mice performed better than controls during the initial acquisition phase of the water maze task, so it is perhaps not surprising that $Htt^{140Q/\Delta N17}$ and $Htt^{140Q/\Delta QP}$ mice displayed an initial improvement in this test in comparison to the $Htt^{140Q/+}$ mice. However, as the mice aged, $Htt^{\Delta QP/\Delta QP}$ mice performed similar to controls, and $Htt^{\Delta N17/\Delta N17}$ mice exhibited a deficit compared to controls, making the improvement in performance of the 18-month-old $Htt^{140Q/\Delta N17}$ mice in comparison to the $Htt^{140Q/+}$ mice very unexpected. These changes are potentially interesting considering that the $Htt^{\Delta Q/\Delta Q}$ mice exhibited early deficits compared to controls in the Barnes maze, a

similar learning and memory task, while the $Htt^{140Q/\Delta Q}$ mice performed better in this test in comparison to the $Htt^{140Q/+}$ mice [109, 110].

My analysis of autophagic flux in primary cortical and striatal neuronal cultures obtained from the $Htt^{140Q/\Delta N17}$ and $Htt^{140Q/\Delta QP}$ mice revealed several interesting differences in comparison to $Htt^{140Q/+}$ cultures. Since $Htt^{140Q/\Delta Q}$ mice were reported to have elevated numbers of autophagosomes [110], we had previously hypothesized that autophagic flux in $Htt^{140Q/\Delta QP}$ mice would also be increased, or that it would be similar to controls. However, primary striatal neurons derived from both $Htt^{140Q/\Delta N17}$ and $Htt^{140Q/\Delta QP}$ mice exhibited a deficit in amount of autophagosomes accumulating in the cell body when the cultures were treated with chloroquine. Importantly, I was not able to observe this deficit in autophagosome accumulation in primary cortical neurons generated from the same mice. This suggests that Htt's proposed function in neuronal macroautophagy may not be the same in different neuronal subtypes.

The most striking autophagy phenotype that I observed was an increase in p62 immunostaining in $Htt^{140Q/\Delta N17}$ primary neurons in comparison to all other genotypes tested. As is apparent in figure 5-6, there was some variability in the level of p62 immunostaining detected in individual neurons; some cells exhibited an increase in the amount of p62 puncta, others exhibited an increase in diffuse cytoplasmic p62 staining, and some exhibited both increased nuclear and cytoplasmic p62 immunostaining. Very few neurons generated from $Htt^{140Q/+}$, $Htt^{140Q/\Delta Q}$, and $Htt^{140Q/\Delta QP}$ mice demonstrated a similar increase in p62 immunostaining, while nearly all the $Htt^{140Q/\Delta N17}$ neurons exhibited high levels of p62 immunostaining. Quantification of this phenotype revealed that both $Htt^{140Q/\Delta N17}$ primary cortical and striatal neurons exhibited a significant increase

in p62 immunostaining in comparison to $Htt^{140Q/+}$, $Htt^{140Q/\Delta Q}$, and $Htt^{140Q/\Delta QP}$ under conditions of basal autophagy and after chloroquine treatment.

Further characterization of the $Htt^{140Q/\Delta N17}$ and $Htt^{140Q/\Delta QP}$ mice is ongoing. Of particular interest is aggregate formation kinetics including time of appearance, number, size, and localization of aggregates in each model. Additionally, $Htt^{140Q/\Delta N17}$ and $Htt^{140Q/\Delta QP}$ mice will be examined for changes in synapse development and maintenance.

	+/+	140Q/+	140Q/ΔQP	140Q/ΔN17
3 months	15	15	15	15
6 months	15	15	15	14
12 months	15	15	15	14
18 months	13	14	15	14

Table 5-1. The numbers of $Htt^{+/+}$, $Htt^{140Q/+}$, $Htt^{140Q/\Delta QP}$, and $Htt^{140Q/\Delta N17}$ mice used for behavioral testing at each age.

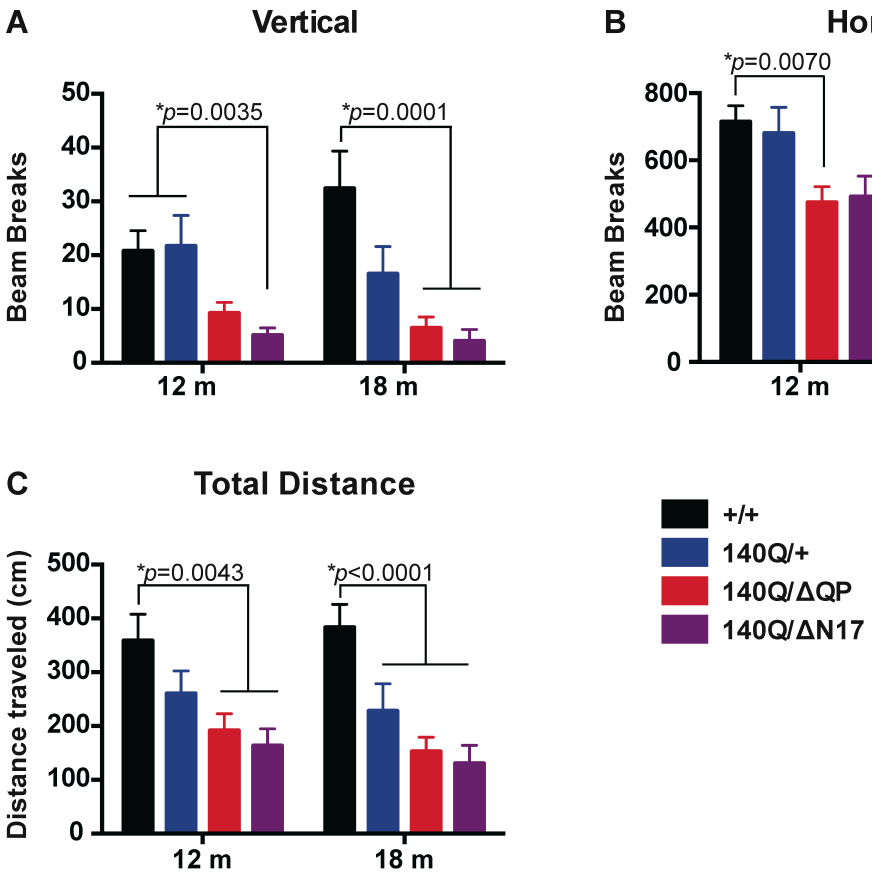

Figure 5-1. Activity levels in $Htt^{+/+}$, $Htt^{140Q/+}$, $Htt^{140Q/\Delta N17}$ and $Htt^{140Q/\Delta QP}$ mice. Beginning at 12 months of age, $Htt^{140Q/\Delta N17}$ mice began to exhibit decreased vertical (A, p=0.0035) activity levels, and decreased total distance traveled (C, p=0.0043) during a 5 min activity assessment compared to $Htt^{+/+}$ controls. Additionally, $Htt^{140Q/\Delta QP}$ mice demonstrated decreased horizontal activity (B, p=0.0070) and decreased total distance traveled (C, p=0.0043) compared to controls. At 18 months of age, both $Htt^{140Q/\Delta N17}$ and $Htt^{140Q/\Delta QP}$ mice demonstrated decreased vertical (A, p=0.0001) and horizontal activity levels (B, p=0.0005) compared to controls. Additionally $Htt^{140Q/+}$, $Htt^{140Q/\Delta N17}$ and $Htt^{140Q/\Delta QP}$ mice all exhibited decreased total distance traveled at 18 months of age (C, p<0.0001, 1-way ANOVA).

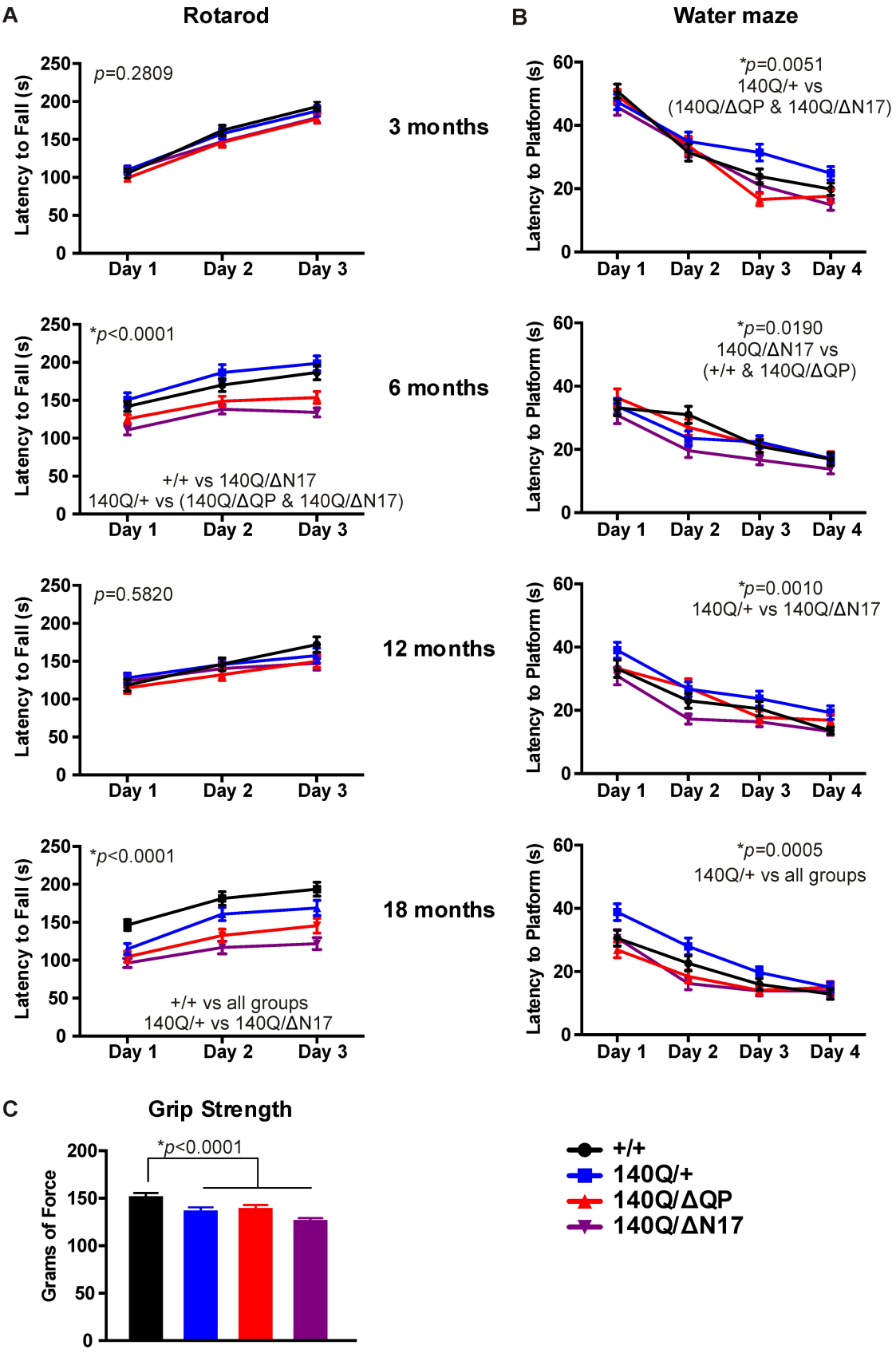
A
Rotarod
B
Water maze
Latency to Fall (s)
Latency to Platform (s)
Day 1
Day 2
Day 3
Day 4
p=0.2809
3 months
*p=0.0051
140Q/+ vs
(140Q/ΔQP & 140Q/ΔN17)
*p<0.0001
6 months
+/+ vs 140Q/ΔN17
140Q/+ vs (140Q/ΔQP & 140Q/ΔN17)
*p=0.0190
140Q/ΔN17 vs
(+/+ & 140Q/ΔQP)
p=0.5820
12 months
*p=0.0010
140Q/+ vs 140Q/ΔN17
*p<0.0001
18 months
+/+ vs all groups
140Q/+ vs 140Q/ΔN17
*p=0.0005
140Q/+ vs all groups
C
Grip Strength
*p<0.0001
Grams of Force
+/+
140Q/+
140Q/ΔQP
140Q/ΔN17

Figure 5-2. Motor coordination and spatial learning and memory testing of $Htt^{+/+}$, $Htt^{140Q/+}$, $Htt^{140Q/\Delta N17}$ and $Htt^{140Q/\Delta QP}$ mice. (A) $Htt^{140Q/\Delta N17}$ and $Htt^{140Q/\Delta QP}$ mice exhibited a decrease in their latency to fall from the rotarod compared to $Htt^{+/+}$ and $Htt^{140Q/+}$ mice at 6 months of age (p<0.0001, 2-way ANOVA). At 18 months of age, $Htt^{140Q/+}$, $Htt^{140Q/\Delta N17}$ and $Htt^{140Q/\Delta QP}$ mice all performed worse on the rotarod compared to $Htt^{+/+}$ mice, and $Htt^{140Q/\Delta N17}$ mice were also worse compared to $Htt^{140Q/+}$ mice (p<0.0001, 2-way ANOVA). (B) In the acquisition phase of the Morris water maze test, $Htt^{140Q/+}$ mice demonstrated a deficit in spatial learning compared to $Htt^{140Q/\Delta N17}$ and $Htt^{140Q/\Delta QP}$ mice at 3 months of age (p=0.0051), to $Htt^{140Q/\Delta N17}$ mice at 12 months of age (p=0.0010), and to $Htt^{+/+}$, $Htt^{140Q/\Delta N17}$ and $Htt^{140Q/\Delta QP}$ mice at 18 months of age (p=0.0005, 2-way ANOVA). The numbers of mice tested for each genotype at each specific age are listed in Table 5-1.

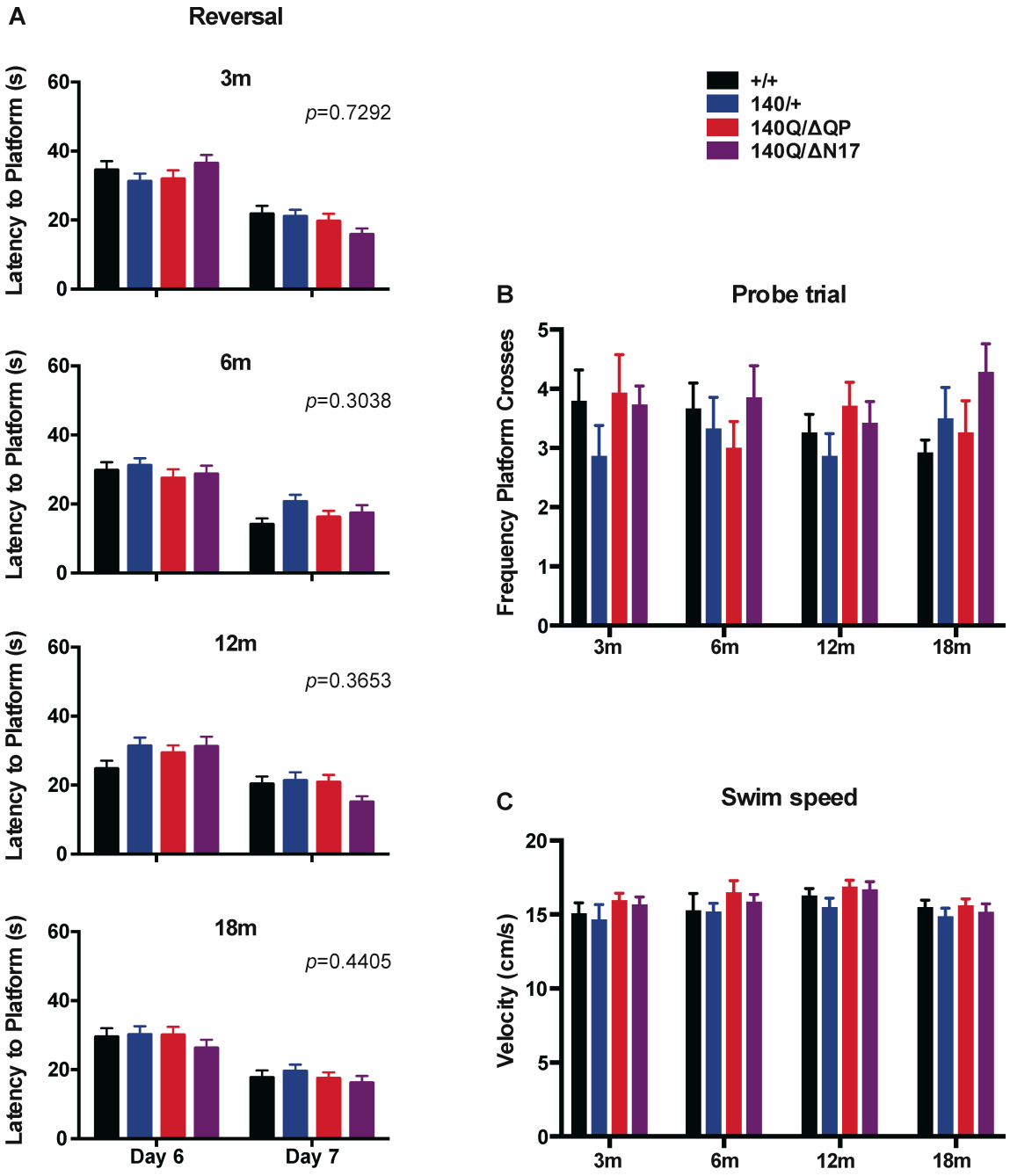

Figure 5-3. Morris water maze additional testing. (A) No significant differences were observed between the $Htt^{+/+}$, $Htt^{140Q/+}$, $Htt^{140QP/\Delta QP}$, and $Htt^{140Q/\Delta N17}$ mice during the reversal task at 3 (p=0.7292), 6 (p=0.3038), 12 (p=0.3653), and 18 months of age (p=0.4405, 2-way ANOVA). (B) No differences were observed between genotypes in the frequency of platform crosses during the probe trial at 3 (p=0.4480), 6 (p=0.6157), 12

(p=0.4119), and 18 (p=0.2177) months of age (1-way ANOVA). (C) Swim velocities for each mouse were determined during the probe trial. No significant differences between genotypes were observed at 3 (p=0.5525), 6 (p=0.5851), 12 (p=0.2307), and 18 months of age (p=0.7286, 2-way ANOVA).

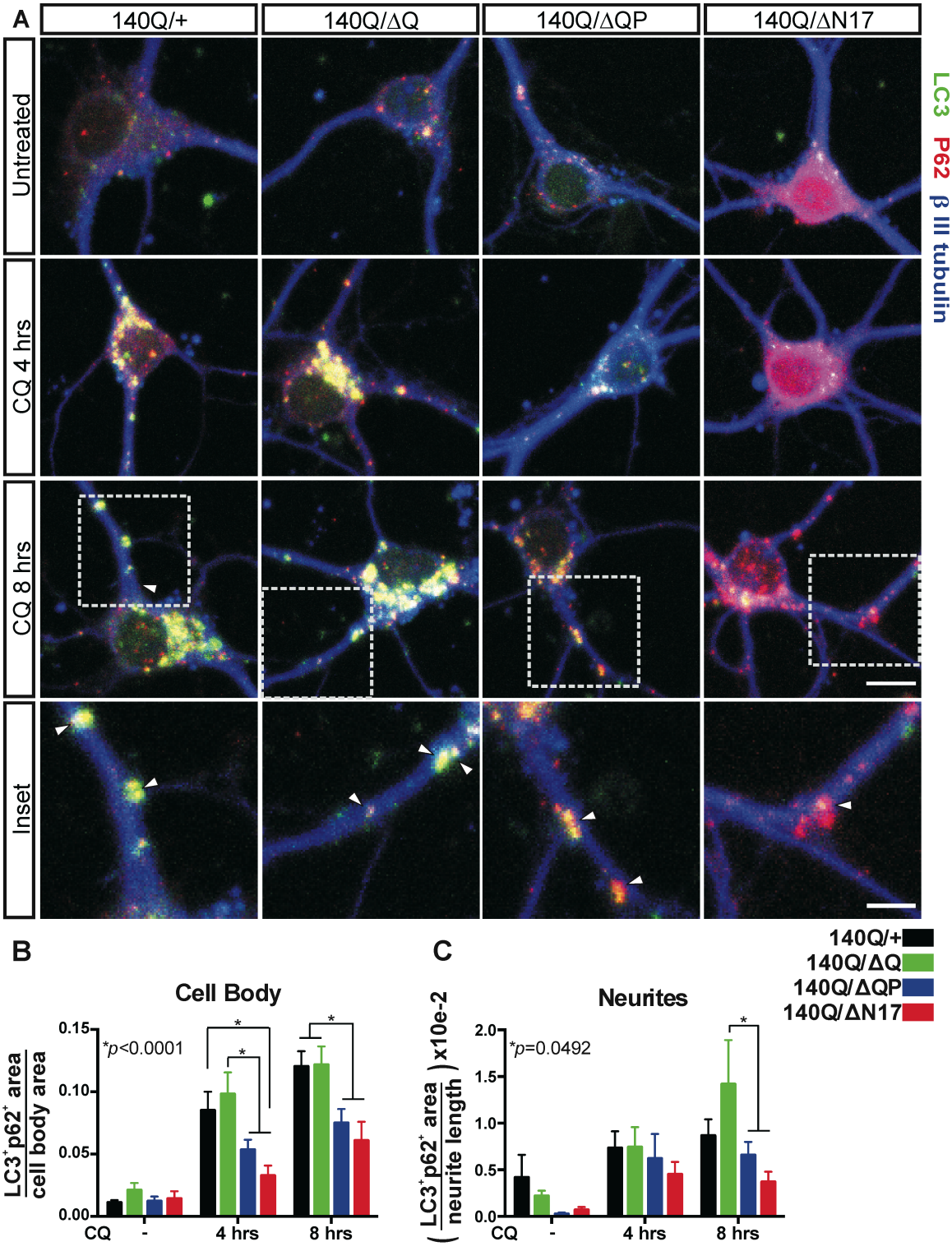

Figure 5-4. Autophagic flux analyses in striatal neurons. (A) Primary striatal neurons isolated from the brains of postnatal day 5 $Htt^{140Q/+}$, $Htt^{140Q/\Delta Q}$, $Htt^{140Q/\Delta QP}$, and

Htt$^{140Q/\Delta N17}$ mice were grown in serum free media for 8 DIV before treating with 30 μM chloroquine (CQ) to assess autophagic flux. Fixed cells were immunostained with antibodies recognizing LC3 (green), p62 (red) and βIII tubulin (blue). Scale bar = 10 μm for the top 12 panels, 5 μm for the 4 inset panels. Arrowheads in the inset panels indicate $LC3^{+}p62^{+}$ cargo-containing autophagosomes within neuronal processes. (B) Quantification of the $LC3^{+}p62^{+}$ area within the cell bodies of striatal neurons ($p<0.0001$, $F=11.11$, $D_F=3$, 2-way ANOVA). (C) Quantification of the $LC3^{+}p62^{+}$ area per μm of neuronal process in the striatal neurons ($p=0.0492$, $F=2.712$, $D_F=3$, 2-way ANOVA). (n=25 cells/genotype from 3 different dissections/genotype).

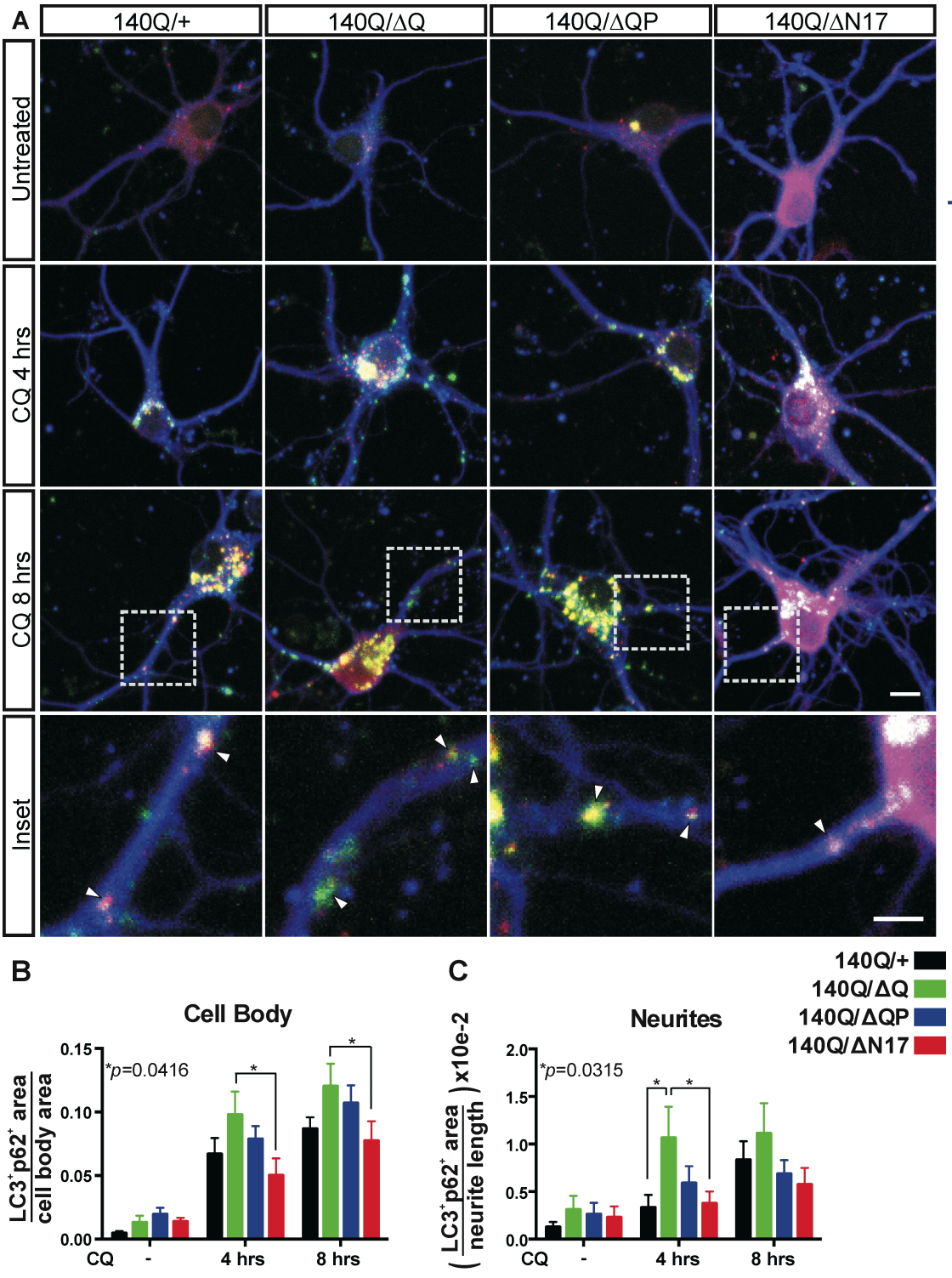

Figure 5-5. Autophagic flux analyses in cortical neurons. (A) Primary cortical neurons isolated from the brains of postnatal day 5 $Htt^{140Q/+}$, $Htt^{140Q/\Delta Q}$, $Htt^{140Q/\Delta QP}$, and $Htt^{140Q/\Delta N17}$ mice were grown for 8 DIV before treating with 30 μM CQ and

immunostained as described in Fig 5-4. Scale bar = 10 μm for the top 12 panels, 5 μm for the 4 inset panels. Arrowheads in the inset panels indicate $LC3^{+}p62^{+}$ cargo-containing autophagosomes within the neuronal processes. (B) Quantification of the $LC3^{+}p62^{+}$ area within the cell bodies of cortical neurons (p=0.0416, F=2.848, D_F=3, 2-way ANOVA). (C) Quantification of the $LC3^{+}p62^{+}$ area per μm of neuronal process in the cortical neurons (p=0.0315, F=3.071, D_F=3, 2-way ANOVA). (n=25 cells/genotype from 3 different dissections/genotype).

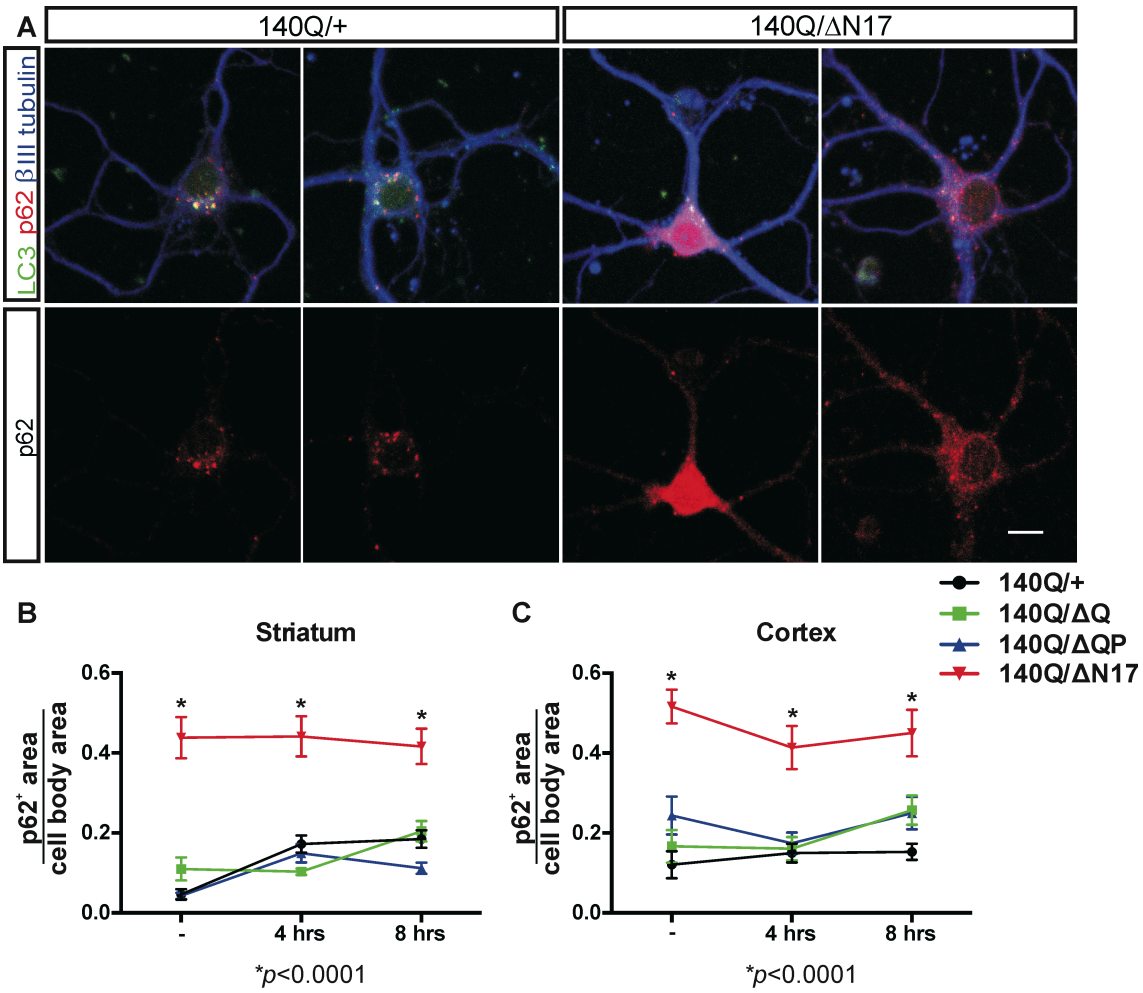

Figure 5-6. p62 immunostaining is elevated in *Htt*$^{140Q/\Delta N17}$ primary striatal and cortical neurons. (A) Primary striatal neurons isolated from the brains of postnatal day 5 *Htt*$^{140Q/+}$ and *Htt*$^{140Q/\Delta N17}$ mice were grown for 8 DIV and immunostained as described in Fig 5-4. Images in (A) were not treated with CQ. Multiple images are shown for each genotype to illustrate the range of p62 immunostaining observed. Scale bar = 10 µm. (B) Quantification of the p62^{+} area within the cell bodies of striatal neurons (p<0.0001, F=39.11, D_F=3, 2-way ANOVA). (C) Quantification of the p62^{+} area within the cell bodies of cortical neurons (p<0.0001, F=19.11, D_F=3, 2-way ANOVA). (n=25 cells/genotype from 3 different dissections/genotype).

Chapter VI: Conclusions and future directions

The results of the experiments described in this thesis have provided new information about the contribution of Htt's N-terminal domains to its normal function. Due to the strict conservation of the N17 domain throughout nearly all vertebrates, I originally hypothesized that the N17 domain deletion mice would have extensive deficits that might manifest as a change in the number of $Htt^{\Delta N17/\Delta N17}$ mice born, or as more severe behavioral and neuropathological deficits in $Htt^{\Delta N17/\Delta N17}$ mice. However, the experiments presented in the previous chapters have shown that the Htt N17 domain is not required for Htt's essential functions in embryonic development, and its deletion results in modest behavioral phenotypes that are not observed until ~12 months of age. Indeed, deletion of all three Htt N-terminal domains encoded by *Htt* exon 1 does not result in embryonic lethality or alterations in Mendelian frequency. Thus, the contribution of these domains to normal Htt function is more likely to be modulatory rather than necessary for normal Htt function.

	$Htt^{\Delta Q/\Delta Q}$	$Htt^{\Delta P/\Delta P}$	$Htt^{\Delta QP/\Delta QP}$	$Htt^{\Delta N17/\Delta N17}$
Activity Cage	nc	nc	nc	nc
Rotarod	+	nc	++	nc
Learning and memory	-	- late	+	+ early - late
Investigator:	E. Clabough	M. Neveklovska	E. Andre	E. Andre

Table 6-1. A summary of the homozygous N-terminal domain deletion mice generated by myself and others in the Zeitlin lab and the results of their behavioral characterizations in comparison to controls. Learning and memory testing was performed using the Barnes maze with the $Htt^{\Delta Q/\Delta Q}$ mice and using the Morris water maze with the $Htt^{\Delta P/\Delta P}$, $Htt^{\Delta QP/\Delta QP}$, and $Htt^{\Delta N17/\Delta N17}$ mice. (nc=no change).

Based on the results of my longitudinal behavioral analyses, I have confirmed a contribution of the polyQ stretch to Htt functions in motor learning and coordination on

the accelerating rotarod. Interestingly, despite previous observations that deletion of the polyQ stretch or PRR results in learning and memory deficits, their combined deletion results in initial improvements in spatial learning and memory, but has no effect later in life (Table 6-1).

I have also established a role for the Htt N17 domain in spatial learning and memory, dependent on age of testing. Additionally, I have described a role for this domain in either the development or maintenance of thalamostriatal synapses. Learning and memory in mammals is dependent on a complicated network of brain regions; however, there is evidence suggesting that the decreased performance of $Htt^{\Delta N17/\Delta N17}$ mice during the acquisition phase of the Morris water maze test at 12 and 24 months of age could be related to the decrease in thalamostriatal synapses observed in 24-month-old mice. In studies that have correlated HD patient symptoms with structural changes characterized by MRI imaging, thalamic volumetric decline correlated with decreased performance on cognitive tests, but did not correlate with other HD patient symptoms (*i.e*. motor symptoms) [149, 150]. Specifically, thalamic nuclei that project to the striatum and to the prefrontal cortex were shown to exhibit volumetric decline in patients with discernable cognitive deterioration lending support to a potential correlation between the behavioral and neuropathological phenotypes I observed in $Htt^{\Delta N17/\Delta N17}$ mice [150].

In order to clarify the effect of the N17 domain deletion on synaptic development/homeostasis and the potential link to cognitive function, I propose several future studies. First, immunohistochemical (IHC) characterization of brains from younger $Htt^{\Delta N17/\Delta N17}$ mice must be performed to determine if the change in thalamostriatal

synapses is a result of changes in synaptic development, or if the change is a result of an age-related loss of synapses specific to $Htt^{\Delta N17/\Delta N17}$ mice. These analyses can be compared to the water maze phenotypes that were observed in younger mice. Additionally, co-cultures of cortical and thalamic primary neurons can be used to assess synaptic development at multiple different time points *in vitro*.

	$Htt^{140Q/\Delta Q}$	$Htt^{140Q/\Delta QP}$	$Htt^{140Q/\Delta N17}$
Activity Cage	++	-	-
Rotarod	++	-	--
Learning and memory	+	+	+
Investigator:	E. Clabough	E. Andre	E. Andre

Table 6-2. Summary of behavioral data from HD mouse model mice crossed with N-terminal domain deletion mice in comparison to $Htt^{140Q/+}$ controls generated by myself and others in the Zeitlin lab. Learning and memory testing was performed with the Barnes maze in $Htt^{140Q/\Delta Q}$ mice, and with the Morris water maze for both the $Htt^{140Q/\Delta QP}$ and $Htt^{140Q/\Delta N17}$ mice.

I additionally observed unexpected phenotypes in my characterization of the $Htt^{140Q/\Delta N17}$ and $Htt^{140Q/\Delta QP}$ mice. Given the improvement in motor and cognitive tests observed in $Htt^{140Q/\Delta Q}$ mice compared to $Htt^{140Q/+}$ controls, I had hypothesized that $Htt^{140Q/\Delta QP}$ mice would either perform better than or at least similar to $Htt^{140Q/+}$ controls. Therefore, the deficits I observed on the accelerating rotarod and in the activity cage testing of the $Htt^{140Q/\Delta QP}$ mice were particularly unexpected (Table 6-2). These phenotypes suggest that deletion of both the Htt polyQ stretch and PRR domains in combination not only negate any benefit when either of these domains is deleted separately, but result in exacerbated HD mouse model phenotypes. I had hypothesized that deletion of the N17 domain would be detrimental especially in the presence of the expanded mHtt allele which can act as a chronic stressor in neurons. Therefore, the

improvement I observed during spatial learning and memory testing in $Htt^{140Q/\Delta N17}$ mice compared to $Htt^{140Q/+}$ controls was also unforeseen.

Because increased autophagosome generation can be observed in $Htt^{140Q/\Delta Q}$ mice, I hypothesized that a similar change would be observed in $Htt^{140Q/\Delta QP}$ mice. Instead, I observed that autophagic flux was decreased in $Htt^{140Q/\Delta QP}$ primary neuronal cultures. Perhaps the most striking phenotype that I observed in my autophagic flux experiments was the significant increase in p62 immunostaining during basal autophagy and after autophagy induction in both striatal and cortical neurons derived from $Htt^{140Q/\Delta N17}$ mice. As I was not able to observe this phenotype in $Htt^{\Delta N17/\Delta N17}$ mice, the N17 domain may be of particular importance for Htt's functions in selective macroautophagy during periods of chronic stress.

Future directions include additional immunohistochemical analyses of the $Htt^{140Q/\Delta N17}$ and $Htt^{140Q/\Delta QP}$ mice. For example, any potential changes in the onset or severity of DARPP-32 loss in the striatum, mHtt aggregation, gliosis, and lipofuscin accumulation should be investigated in longitudinal analyses to determine if potential phenotypes could simply be due to a delay or an advance in the onset of pathogenesis. Additionally, the effect of the N17 domain deletion on Htt's function in the modulation of cellular stress responses and involvement in the base excision repair of damaged DNA should be examined.

Lastly, the $Htt^{\Delta NQP}$ mice require further characterization. $Htt^{\Delta NQP/\Delta NQP}$, $Htt^{\Delta NQP/+}$, and $Htt^{\Delta NQP/-}$ mice have been generated and are currently being evaluated for motor coordination, activity, and spatial learning/memory phenotypes. Additionally, $Htt^{140Q/\Delta NQP}$ mice are being generated for future behavioral and neuropathological

analyses to determine the consequences of deleting all three of Htt's N-terminal domains on HD mouse model pathogenesis. Characterization of these mice will supplement my investigations presented in this thesis and provide further insight into the role of Htt's N-terminal domains in modulating Htt functions in the CNS.

References

[1] Zuccato C, Valenza M, Cattaneo E. Molecular mechanisms and potential therapeutical targets in Huntington's disease. Physiol Rev. 2010;90(3):905-81. doi: 10.1152/physrev.00041.2009.

[2] Lakhani VV, Ding F, Dokholyan NV. Polyglutamine induced misfolding of huntingtin exon1 is modulated by the flanking sequences. PLoS Comput Biol. 2010;6(4):e1000772. doi: 10.1371/journal.pcbi.1000772.

[3] Candiani S, Pestarino M, Cattaneo E, Tartari M. Characterization, developmental expression and evolutionary features of the huntingtin gene in the amphioxus Branchiostoma floridae. BMC Dev Biol. 2007;7:127. doi: 10.1186/1471-213X-7-127.

[4] Tartari M, Gissi C, Lo Sardo V, Zuccato C, Picardi E, Pesole G, et al. Phylogenetic comparison of huntingtin homologues reveals the appearance of a primitive polyQ in sea urchin. Mol Biol Evol. 2008;25(2):330-8. doi: 10.1093/molbev/msm258.

[5] Passani LA, Bedford MT, Faber PW, McGinnis KM, Sharp AH, Gusella JF, et al. Huntingtin's WW domain partners in Huntington's disease post-mortem brain fulfill genetic criteria for direct involvement in Huntington's disease pathogenesis. Hum Mol Genet. 2000;9(14):2175-82. doi: 10.1093/hmg/9.14.2175.

[6] Liu YF, Deth RC, Devys D. SH3 domain-dependent association of huntingtin with epidermal growth factor receptor signaling complexes. J Biol Chem. 1997;272(13):8121-4. doi: 10.1074/jbc.272.13.8121.

[7] Gao YG, Yan XZ, Song AX, Chang YG, Gao XC, Jiang N, et al. Structural insights into the specific binding of huntingtin proline-rich region with the SH3 and WW domains. Structure. 2006;14(12):1755-65. doi: 10.1016/j.str.2006.09.014.

[8] Rockabrand E, Slepko N, Pantalone A, Nukala VN, Kazantsev A, Marsh JL, et al. The first 17 amino acids of Huntingtin modulate its sub-cellular localization, aggregation and effects on calcium homeostasis. Hum Mol Genet. 2007;16(1):61-77. doi: 10.1093/hmg/ddl440.

[9] Atwal RS, Xia J, Pinchev D, Taylor J, Epand RM, Truant R. Huntingtin has a membrane association signal that can modulate huntingtin aggregation, nuclear entry and toxicity. Hum Mol Genet. 2007;16(21):2600-15. doi: 10.1093/hmg/ddm217.

[10] A novel gene containing a trinucleotide repeat that is expanded and unstable on Huntington's disease chromosomes. The Huntington's Disease Collaborative Research Group. Cell. 1993;72(6):971-83.

[11] Adam Rosenblatt NGR, Martha A. Nance, Jane S. Paulson. A Physician's Guide to the Management of Huntington's Disease. 2nd ed. New York: Huntington's Disease Society of America; 1999. 92 p.

[12] Ross CA, Tabrizi SJ. Huntington's disease: from molecular pathogenesis to clinical treatment. Lancet Neurol.10(1):83-98. doi: 10.1016/S1474-4422(10)70245-3.

[13] Mielcarek M. Huntington's disease is a multi-system disorder. Rare diseases (Austin, Tex). 2015;3(1):1058464. doi: 10.1080/21675511.2015.1058464.

[14] Cisbani G, Cicchetti F. An in vitro perspective on the molecular mechanisms underlying mutant huntingtin protein toxicity. Cell death & disease. 2012;3:382. doi: 10.1038/cddis.2012.121.

[15] Johnson CD, Davidson BL. Huntington's disease: progress toward effective disease-modifying treatments and a cure. Hum Mol Genet. 2010;19(R1):R98-r102. doi: 10.1093/hmg/ddq148.

[16] Tsvetkov AS, Arrasate M, Barmada S, Ando DM, Sharma P, Shaby BA, et al. Proteostasis of polyglutamine varies among neurons and predicts neurodegeneration. Nat Chem Biol. 2013;9(9):586-92. doi: 10.1038/nchembio.1308.

[17] Davies SW, Turmaine M, Cozens BA, DiFiglia M, Sharp AH, Ross CA, et al. Formation of neuronal intranuclear inclusions underlies the neurological dysfunction in mice transgenic for the HD mutation. Cell. 1997;90(3):537-48. doi: 10.1016/S0092-8674(00)80513-9.

[18] Cooper JK, Schilling G, Peters MF, Herring WJ, Sharp AH, Kaminsky Z, et al. Truncated N-terminal fragments of huntingtin with expanded glutamine repeats form nuclear and cytoplasmic aggregates in cell culture. Hum Mol Genet. 1998;7(5):783-90. doi: 10.1093/hmg/7.5.783

[19] Filimonenko M, Isakson P, Finley KD, Anderson M, Jeong H, Melia TJ, et al. The selective macroautophagic degradation of aggregated proteins requires the PI3P-binding protein Alfy. Mol Cell. 2010;38(2):265-79. doi: 10.1016/j.molcel.2010.04.007.

[20] Jansen AH, van Hal M, Op den Kelder IC, Meier RT, de Ruiter AA, Schut MH, et al. Frequency of nuclear mutant huntingtin inclusion formation in neurons and glia is cell-type-specific. Glia. 2017;65(1):50-61. doi: 10.1002/glia.23050.

[21] Graham RK, Deng Y, Slow EJ, Haigh B, Bissada N, Lu G, et al. Cleavage at the caspase-6 site is required for neuronal dysfunction and degeneration due to mutant huntingtin. Cell. 2006;125(6):1179-91. doi: 10.1016/j.cell.2006.04.026.

[22] Goldberg YP, Nicholson DW, Rasper DM, Kalchman MA, Koide HB, Graham RK, et al. Cleavage of huntingtin by apopain, a proapoptotic cysteine protease, is modulated by the polyglutamine tract. Nat Genet. 1996;13(4):442-9. doi: 10.1038/ng0896-442 [doi].

[23] Kim YJ, Yi Y, Sapp E, Wang Y, Cuiffo B, Kegel KB, et al. Caspase 3-cleaved N-terminal fragments of wild-type and mutant huntingtin are present in normal and Huntington's disease brains, associate with membranes, and undergo calpain-dependent proteolysis. Proc Natl Acad Sci U S A. 2001;98(22):12784-9. doi: 10.1073/pnas.221451398.

[24] Lunkes A, Lindenberg KS, Ben-Haiem L, Weber C, Devys D, Landwehrmeyer GB, et al. Proteases acting on mutant huntingtin generate cleaved products that differentially build up cytoplasmic and nuclear inclusions. Mol Cell. 2002;10(2):259-69. doi: 10.1016/S1097-2765(02)00602-0.

[25] Banez-Coronel M, Ayhan F, Tarabochia AD, Zu T, Perez BA, Tusi SK, et al. RAN Translation in Huntington Disease. Neuron. 2015;88(4):667-77. doi: 10.1016/j.neuron.2015.10.038.

[26] Sathasivam K, Neueder A, Gipson TA, Landles C, Benjamin AC, Bondulich MK, et al. Aberrant splicing of HTT generates the pathogenic exon 1 protein in Huntington disease. Proc Natl Acad Sci U S A. 2013;110(6):2366-70. doi: 10.1073/pnas.1221891110.

[27] Kuemmerle S, Gutekunst CA, Klein AM, Li XJ, Li SH, Beal MF, et al. Huntington aggregates may not predict neuronal death in Huntington's disease. Ann Neurol. 1999;46(6):842-9. doi: 10.1002/1531-8249(199912)46:6<842::AID-ANA6>3.0.CO;2-O.

[28] Nucifora FC, Jr., Sasaki M, Peters MF, Huang H, Cooper JK, Yamada M, et al. Interference by huntingtin and atrophin-1 with cbp-mediated transcription leading to cellular toxicity. Science. 2001;291(5512):2423-8. doi: 10.1126/science.1056784.

[29] Trushina E, Dyer RB, Badger JD, Ure D, Eide L, Tran DD, et al. Mutant Huntingtin Impairs Axonal Trafficking in Mammalian Neurons In Vivo and In Vitro. Mol Cell Biol. 2004;24(18):8195-209. doi: 10.1128/mcb.24.18.8195-8209.2004.

[30] Martinez–Vicente M, Talloczy Z, Wong E, Tang G, Koga H, Kaushik S, et al. Cargo recognition failure is responsible for inefficient autophagy in Huntington's disease. Nat Neurosci. 2010;13(5):567-76. doi: 10.1038/nn.2528.

[31] Wong YC, Holzbaur EL. The regulation of autophagosome dynamics by huntingtin and HAP1 is disrupted by expression of mutant huntingtin, leading to defective cargo degradation. J Neurosci. 2014;34(4):1293-305. doi: 10.1523/jneurosci.1870-13.2014.

[32] Erie C, Sacino M, Houle L, Lu ML, Wei J. Altered lysosomal positioning affects lysosomal functions in a cellular model of Huntington's disease. The European journal of neuroscience. 2015;42(3):1941-51. doi: 10.1111/ejn.12957.

[33] Maday S, Wallace KE, Holzbaur EL. Autophagosomes initiate distally and mature during transport toward the cell soma in primary neurons. J Cell Biol. 2012;196(4):407-17. doi: 10.1083/jcb.201106120.

[34] Kuwert T, Lange HW, Langen KJ, Herzog H, Aulich A, Feinendegen LE. Cortical and subcortical glucose consumption measured by PET in patients with Huntington's disease. Brain. 1990;113 (Pt 5):1405-23. doi: 10.1016/j.brainresbull.2009.07.010.

[35] Song W, Chen J, Petrilli A, Liot G, Klinglmayr E, Zhou Y, et al. Mutant huntingtin binds the mitochondrial fission GTPase dynamin-related protein-1 and increases its enzymatic activity. Nat Med.17(3):377-82. doi: 10.1038/nm.2313.

[36] Napoli E, Wong S, Hung C, Ross-Inta C, Bomdica P, Giulivi C. Defective mitochondrial disulfide relay system, altered mitochondrial morphology and function in Huntington's disease. Hum Mol Genet. 2013;22(5):989-1004. doi: 10.1093/hmg/dds503.

[37] Browne SE, Bowling AC, MacGarvey U, Baik MJ, Berger SC, Muqit MM, et al. Oxidative damage and metabolic dysfunction in Huntington's disease: selective vulnerability of the basal ganglia. Ann Neurol. 1997;41(5):646-53. doi: 10.1002/ana.410410514.

[38] Gu M, Gash MT, Mann VM, Javoy-Agid F, Cooper JM, Schapira AH. Mitochondrial defect in Huntington's disease caudate nucleus. Ann Neurol. 1996;39(3):385-9. doi: 10.1002/ana.410390317.

[39] Martin WR, Clark C, Ammann W, Stoessl AJ, Shtybel W, Hayden MR. Cortical glucose metabolism in Huntington's disease. Neurology. 1992;42(1):223-9. doi: 10.1002/cam4.1016

[40] Sun Y, Savanenin A, Reddy PH, Liu YF. Polyglutamine-expanded huntingtin promotes sensitization of N-methyl-D-aspartate receptors via post-synaptic density 95. J Biol Chem. 2001;276(27):24713-8. doi: 10.1074/jbc.M103501200.

[41] Arzberger T, Krampfl K, Leimgruber S, Weindl A. Changes of NMDA receptor subunit (NR1, NR2B) and glutamate transporter (GLT1) mRNA expression in Huntington's disease--an in situ hybridization study. Journal of neuropathology and experimental neurology. 1997;56(4):440-54.

[42] Deng YP, Wong T, Bricker-Anthony C, Deng B, Reiner A. Loss of corticostriatal and thalamostriatal synaptic terminals precedes striatal projection neuron pathology in heterozygous Q140 Huntington's disease mice. Neurobiology of disease. 2013;60:89-107. doi: 10.1016/j.nbd.2013.08.009.

[43] Deng YP, Wong T, Wan JY, Reiner A. Differential loss of thalamostriatal and corticostriatal input to striatal projection neuron types prior to overt motor symptoms in the Q140 knock-in mouse model of Huntington's disease. Frontiers in systems neuroscience. 2014;8:198. doi: 10.3389/fnsys.2014.00198.

[44] Rocher AB, Gubellini P, Merienne N, Boussicault L, Petit F, Gipchtein P, et al. Synaptic scaling up in medium spiny neurons of aged BACHD mice: A slow-progression model of Huntington's disease. Neurobiology of disease. 2016;86:131-9. doi: 10.1016/j.nbd.2015.10.016.

[45] Zuccato C, Marullo M, Conforti P, MacDonald ME, Tartari M, Cattaneo E. Systematic assessment of BDNF and its receptor levels in human cortices affected by Huntington's disease. Brain pathology (Zurich, Switzerland). 2008;18(2):225-38. doi: 10.1111/j.1750-3639.2007.00111.x.

[46] Tang TS, Slow E, Lupu V, Stavrovskaya IG, Sugimori M, Llinas R, et al. Disturbed Ca2+ signaling and apoptosis of medium spiny neurons in Huntington's disease. Proc Natl Acad Sci U S A. 2005;102(7):2602-7. doi: 10.1073/pnas.0409402102.

[47] Tang TS, Tu H, Chan EY, Maximov A, Wang Z, Wellington CL, et al. Huntingtin and huntingtin-associated protein 1 influence neuronal calcium signaling mediated by inositol-(1,4,5) triphosphate receptor type 1. Neuron. 2003;39(2):227-39. doi: 10.1016/S0896-6273(03)00366-0.

[48] Liu X, Wang CE, Hong Y, Zhao T, Wang G, Gaertig MA, et al. N-terminal Huntingtin Knock-In Mice: Implications of Removing the N-terminal Region of Huntingtin for Therapy. PLoS Genet. 2016;12(5). doi: 10.1371/journal.pgen.1006083.

[49] Fusco FR, Chen Q, Lamoreaux WJ, Figueredo-Cardenas G, Jiao Y, Coffman JA, et al. Cellular localization of huntingtin in striatal and cortical neurons in rats: lack of correlation with neuronal vulnerability in Huntington's disease. J Neurosci. 1999;19(4):1189-202.

[50] Kim MW, Chelliah Y, Kim SW, Otwinowski Z, Bezprozvanny I. Secondary structure of Huntingtin amino-terminal region. Structure. 2009;17(9):1205-12. doi: 10.1016/j.str.2009.08.002.

[51] Bhattacharyya A, Thakur AK, Chellgren VM, Thiagarajan G, Williams AD, Chellgren BW, et al. Oligoproline effects on polyglutamine conformation and aggregation. J Mol Biol. 2006;355(3):524-35. doi: 10.1016/j.jmb.2005.10.053.

[52] Darnell G, Orgel JP, Pahl R, Meredith SC. Flanking polyproline sequences inhibit beta-sheet structure in polyglutamine segments by inducing PPII-like helix structure. J Mol Biol. 2007;374(3):688-704. doi: 10.1016/j.jmb.2007.09.023.

[53] Reumers J, Maurer-Stroh S, Schymkowitz J, Rousseau F. Protein sequences encode safeguards against aggregation. Human mutation. 2009;30(3):431-7. doi: 10.1002/humu.20905.

[54] Miller J, Rutenber E, Muchowski PJ. Polyglutamine dances the conformational cha-cha-cha. Structure. 2009;17(9):1151-3. doi: 10.1016/j.str.2009.08.004.

[55] Perutz MF, Johnson T, Suzuki M, Finch JT. Glutamine repeats as polar zippers: their possible role in inherited neurodegenerative diseases. Proc Natl Acad Sci U S A. 1994;91(12):5355-8.

[56] Zuccato C, Tartari M, Crotti A, Goffredo D, Valenza M, Conti L, et al. Huntingtin interacts with REST/NRSF to modulate the transcription of NRSE-controlled neuronal genes. Nat Genet. 2003;35(1):76-83. doi: 10.1038/ng1219.

[57] Atwal RS, Truant R. A stress sensitive ER membrane-association domain in Huntingtin protein defines a potential role for Huntingtin in the regulation of autophagy. Autophagy. 2008;4(1):91-3. doi: 10.4161/auto.5201.

[58] Atwal RS, Desmond CR, Caron N, Maiuri T, Xia J, Sipione S, et al. Kinase inhibitors modulate huntingtin cell localization and toxicity. Nat Chem Biol. 2011;7(7):453-60. doi: 10.1038/nchembio.582.

[59] Burke KA, Kauffman KJ, Umbaugh CS, Frey SL, Legleiter J. The interaction of polyglutamine peptides with lipid membranes is regulated by flanking sequences associated with huntingtin. J Biol Chem. 2013;288(21):14993-5005. doi: 10.1074/jbc.M112.446237.

[60] Maiuri T, Woloshansky T, Xia J, Truant R. The huntingtin N17 domain is a multifunctional CRM1 and Ran-dependent nuclear and cilial export signal. Hum Mol Genet. 2013;22(7):1383-94. doi: 10.1093/hmg/dds554.

[61] Neveklovska M, Clabough, E.B.D., Steffan, J.S., Zeitlin, S.O. Deletion of the huntingtin proline-rich region does not significantly affect normal huntingtin function in mice. Journal of Huntington's Disease. 2012;1:71-87. doi: 10.3233/JHD-2012-120016.

[62] Faber PW, Barnes GT, Srinidhi J, Chen J, Gusella JF, MacDonald ME. Huntingtin interacts with a family of WW domain proteins. Hum Mol Genet. 1998;7(9):1463-74. doi: 10.1093/hmg/7.9.1463.

[63] Dlugosz M, Trylska J. Secondary structures of native and pathogenic huntingtin N-terminal fragments. J Phys Chem B. 2011;115(40):11597-608. doi: 10.1021/jp206373g.

[64] Caron NS, Desmond CR, Xia J, Truant R. Polyglutamine domain flexibility mediates the proximity between flanking sequences in huntingtin. Proc Natl Acad Sci U S A. 2013;110(36):14610-5. doi: 10.1073/pnas.1301342110.

[65] Ochaba J, Lukacsovich T, Csikos G, Zheng S, Margulis J, Salazar L, et al. Potential function for the Huntingtin protein as a scaffold for selective autophagy. Proc Natl Acad Sci U S A. 2014;111(47):16889-94. doi: 10.1073/pnas.1420103111.

[66] Palidwor GA, Shcherbinin S, Huska MR, Rasko T, Stelzl U, Arumughan A, et al. Detection of alpha-rod protein repeats using a neural network and application to huntingtin. PLoS Comput Biol. 2009;5(3):e1000304. doi: 10.1371/journal.pcbi.1000304.

[67] Shirasaki DI, Greiner ER, Al-Ramahi I, Gray M, Boontheung P, Geschwind DH, et al. Network organization of the huntingtin proteomic interactome in mammalian brain. Neuron. 2012;75(1):41-57. doi: 10.1016/j.neuron.2012.05.024.

[68] Andrade MA, Petosa C, O'Donoghue SI, Muller CW, Bork P. Comparison of ARM and HEAT protein repeats. J Mol Biol. 2001;309(1):1-18. doi: 10.1006/jmbi.2001.4624.

[69] Takano H, Gusella JF. The predominantly HEAT-like motif structure of huntingtin and its association and coincident nuclear entry with dorsal, an NF-kB/Rel/dorsal family transcription factor. BMC Neuroscience. 2002;3:15. doi: 10.1186/1471-2202-3-15.

[70] Xia J, Lee DH, Taylor J, Vandelft M, Truant R. Huntingtin contains a highly conserved nuclear export signal. Hum Mol Genet. 2003;12(12):1393-403. doi: 10.1093/hmg/ddg156.

[71] Gu X, Greiner ER, Mishra R, Kodali R, Osmand A, Finkbeiner S, et al. Serines 13 and 16 are critical determinants of full-length human mutant huntingtin induced disease pathogenesis in HD mice. Neuron. 2009;64(6):828-40. doi: 10.1016/j.neuron.2009.11.020.

[72] Thompson LM, Aiken CT, Kaltenbach LS, Agrawal N, Illes K, Khoshnan A, et al. IKK phosphorylates Huntingtin and targets it for degradation by the proteasome and lysosome. J Cell Biol. 2009;187(7):1083-99. doi: 10.1083/jcb.200909067.

[73] Luo S, Vacher C, Davies JE, Rubinsztein DC. Cdk5 phosphorylation of huntingtin reduces its cleavage by caspases: implications for mutant huntingtin toxicity. J Cell Biol. 2005;169(4):647-56. doi: 10.1083/jcb.200412071.

[74] Colin E, Zala D, Liot G, Rangone H, Borrell-Pagès M, Li XJ, et al. Huntingtin phosphorylation acts as a molecular switch for anterograde/retrograde transport in neurons. Embo j. 2008;27(15):2124-34. doi: 10.1038/emboj.2008.133.

[75] Steffan JS. Does Huntingtin play a role in selective macroautophagy? Cell Cycle. 2010;9(17):3401-13. doi: 10.4161/cc.9.17.12671.

[76] Steffan JS, Agrawal N, Pallos J, Rockabrand E, Trotman LC, Slepko N, et al. SUMO modification of Huntingtin and Huntington's disease pathology. Science. 2004;304(5667):100-4. doi: 10.1126/science.1092194.

[77] Ochaba J, Monteys AM, O'Rourke JG, Reidling JC, Steffan JS, Davidson BL, et al. PIAS1 Regulates Mutant Huntingtin Accumulation and Huntington's Disease-Associated Phenotypes In Vivo. Neuron. 2016;90(3):507-20. doi: 10.1016/j.neuron.2016.03.016.

[78] Yanai A, Huang K, Kang R, Singaraja RR, Arstikaitis P, Gan L, et al. Palmitoylation of huntingtin by HIP14 is essential for its trafficking and function. Nat Neurosci. 2006;9(6):824-31. doi: 10.1038/nn1702.

[79] Juenemann K, Weisse C, Reichmann D, Kaether C, Calkhoven CF, Schilling G. Modulation of mutant huntingtin N-terminal cleavage and its effect on aggregation and cell death. Neurotox Res.20(2):120-33. doi: 10.1007/s12640-010-9227-6.

[80] Burguillos MA, Deierborg T, Kavanagh E, Persson A, Hajji N, Garcia-Quintanilla A, et al. Caspase signalling controls microglia activation and neurotoxicity. Nature.472(7343):319-24. doi: 10.1038/nature09788.

[81] Rui YN, Xu Z, Patel B, Chen Z, Chen D, Tito A, et al. Huntingtin functions as a scaffold for selective macroautophagy. Nat Cell Biol. 2015;17(3):262-75. doi: 10.1038/ncb3101.

[82] Maiuri T, Mocle AJ, Hung CL, Xia J, van Roon-Mom WM, Truant R. Huntingtin is a scaffolding protein in the ATM oxidative DNA damage response complex. Hum Mol Genet. 2016 Dec 25 (Epub ahead of print). doi: 10.1093/hmg/ddw395.

[83] Duyao MP, Auerbach AB, Ryan A, Persichetti F, Barnes GT, McNeil SM, et al. Inactivation of the mouse Huntington's disease gene homolog Hdh. Science. 1995;269(5222):407-10. doi: 10.1126/science.7618107

[84] Nasir J, Floresco SB, O'Kusky JR, Diewert VM, Richman JM, Zeisler J, et al. Targeted disruption of the Huntington's disease gene results in embryonic lethality and behavioral and morphological changes in heterozygotes. Cell. 1995;81(5):811-23. doi: 10.1016/0092-8674(95)90542-1.

[85] Zeitlin S, Liu JP, Chapman DL, Papaioannou VE, Efstratiadis A. Increased apoptosis and early embryonic lethality in mice nullizygous for the Huntington's disease gene homologue. Nat Genet. 1995;11(2):155-63. doi: 10.1038/ng1095-155.

[86] White JK, Auerbach W, Duyao MP, Vonsattel JP, Gusella JF, Joyner AL, et al. Huntingtin is required for neurogenesis and is not impaired by the Huntington's disease CAG expansion. Nat Genet. 1997;17(4):404-10. doi: 10.1038/ng1297-404.

[87] Henshall TL, Tucker B, Lumsden AL, Nornes S, Lardelli MT, Richards RI. Selective neuronal requirement for huntingtin in the developing zebrafish. Hum Mol Genet. 2009;18(24):4830-42. doi: 10.1093/hmg/ddp455.

[88] Auerbach W, Hurlbert MS, Hilditch-Maguire P, Wadghiri YZ, Wheeler VC, Cohen SI, et al. The HD mutation causes progressive lethal neurological disease in mice expressing reduced levels of huntingtin. Hum Mol Genet. 2001;10(22):2515-23.

[89] Reiner A, Del Mar N, Meade CA, Yang H, Dragatsis I, Zeitlin S, et al. Neurons lacking huntingtin differentially colonize brain and survive in chimeric mice. J Neurosci. 2001;21(19):7608-19.

[90] Nopoulos P JB, E Axelson, A Conrad, A Mahmood,, J Paulsen VM. Abnormal brain structure in children at risk for Huntington's disease: Evidence for abnormal brain development. Clin Genet. 2009;76 Suppl 1:1-127. doi: 10.1111/j.1399-0004.2009.01266.x.

[91] Parker JA, Metzler M, Georgiou J, Mage M, Roder JC, Rose AM, et al. Huntingtin-interacting protein 1 influences worm and mouse presynaptic function and protects Caenorhabditis elegans neurons against mutant polyglutamine toxicity. J Neurosci. 2007;27(41):11056-64. doi: 10.1523/JNEUROSCI.1941-07.2007.

[92] Smith R, Brundin P, Li JY. Synaptic dysfunction in Huntington's disease: a new perspective. Cell Mol Life Sci. 2005;62(17):1901-12. doi: 10.1007/s00018-005-5084-5.

[93] Modregger J, DiProspero NA, Charles V, Tagle DA, Plomann M. PACSIN 1 interacts with huntingtin and is absent from synaptic varicosities in presymptomatic Huntington's disease brains. Hum Mol Genet. 2002;11(21):2547-58. doi: 10.1093/hmg/11.21.2547.

[94] Yao J, Ong SE, Bajjalieh S. Huntingtin is associated with cytomatrix proteins at the presynaptic terminal. Molecular and cellular neurosciences. 2014;63:96-100. doi: 10.1016/j.mcn.2014.10.003.

[95] McKinstry SU, Karadeniz YB, Worthington AK, Hayrapetyan VY, Ozlu MI, Serafin-Molina K, et al. Huntingtin is required for normal excitatory synapse development in cortical and striatal circuits. J Neurosci. 2014;34(28):9455-72. doi: 10.1523/jneurosci.4699-13.2014.

[96] Jung CH, Jun CB, Ro SH, Kim YM, Otto NM, Cao J, et al. ULK-Atg13-FIP200 complexes mediate mTOR signaling to the autophagy machinery. Mol Biol Cell. 2009;20(7):1992-2003. doi: 10.1091/mbc.E08-12-1249.

[97] Kim J, Kundu M, Viollet B, Guan KL. AMPK and mTOR regulate autophagy through direct phosphorylation of Ulk1. Nat Cell Biol. 2011;13(2):132-41. doi: 10.1038/ncb2152.

[98] Ganley IG, Lam du H, Wang J, Ding X, Chen S, Jiang X. ULK1-ATG13-FIP200 complex mediates mTOR signaling and is essential for autophagy. J Biol Chem. 2009;284(18):12297-305. doi: 10.1074/jbc.M900573200.

[99] Wold MS, Lim J, Lachance V, Deng Z, Yue Z. ULK1-mediated phosphorylation of ATG14 promotes autophagy and is impaired in Huntington's disease models. Mol Neurodegener. 2016;11(1):76. doi: 10.1186/s13024-016-0141-0.

[100] Caviston JP, Ross JL, Antony SM, Tokito M, Holzbaur EL. Huntingtin facilitates dynein/dynactin-mediated vesicle transport. Proc Natl Acad Sci U S A. 2007;104(24):10045-50. doi: 10.1073/pnas.0610628104.

[101] Caviston JP, Zajac AL, Tokito M, Holzbaur EL. Huntingtin coordinates the dynein-mediated dynamic positioning of endosomes and lysosomes. Mol Biol Cell.22(4):478-92. doi: 10.1091/mbc.E10-03-0233.

[102] Zala D, Hinckelmann MV, Yu H, Lyra da Cunha MM, Liot G, Cordelieres FP, et al. Vesicular glycolysis provides on-board energy for fast axonal transport. Cell. 2013;152(3):479-91. doi: 10.1016/j.cell.2012.12.029.

[103] Adachi N, Numakawa T, Nakajima S, Fukuoka M, Odaka H, Katanuma Y, et al. Glucocorticoid affects dendritic transport of BDNF-containing vesicles. Scientific reports. 2015;5. doi: 10.1038/srep12684.

[104] Gunawardena S, Her LS, Brusch RG, Laymon RA, Niesman IR, Gordesky-Gold B, et al. Disruption of axonal transport by loss of huntingtin or expression of pathogenic polyQ proteins in Drosophila. Neuron. 2003;40(1):25-40. doi: 10.1016/S0896-6273(03)00594-4.

[105] Gauthier LR, Charrin BC, Borrell-Pages M, Dompierre JP, Rangone H, Cordelieres FP, et al. Huntingtin controls neurotrophic support and survival of neurons by enhancing BDNF vesicular transport along microtubules. Cell. 2004;118(1):127-38. doi: 10.1016/j.cell.2004.06.018.

[106] Gines S, Paoletti P, Alberch J. Impaired TrkB-mediated ERK1/2 activation in huntington disease knock-in striatal cells involves reduced p52/p46 Shc expression. J Biol Chem.285(28):21537-48. doi: 10.1074/jbc.M109.084202.

[107] Keryer G, Pineda JR, Liot G, Kim J, Dietrich P, Benstaali C, et al. Ciliogenesis is regulated by a huntingtin-HAP1-PCM1 pathway and is altered in Huntington disease. The Journal of Clinical Investigation. 2011;121(11):4372-82. doi: 10.1172/jci57552.

[108] Godin JD, Colombo K, Molina-Calavita M, Keryer G, Zala D, Charrin BC, et al. Huntingtin is required for mitotic spindle orientation and mammalian neurogenesis. Neuron.67(3):392-406. doi: 10.1016/j.neuron.2010.06.027.

[109] Clabough EB, Zeitlin SO. Deletion of the triplet repeat encoding polyglutamine within the mouse Huntington's disease gene results in subtle behavioral/motor phenotypes in vivo and elevated levels of ATP with cellular senescence in vitro. Hum Mol Genet. 2006;15(4):607-23. doi: 10.1093/hmg/ddi477.

[110] Zheng S, Clabough EB, Sarkar S, Futter M, Rubinsztein DC, Zeitlin SO. Deletion of the huntingtin polyglutamine stretch enhances neuronal autophagy and longevity in mice. PLoS Genet. 2010;6(2):e1000838. doi: 10.1371/journal.pgen.1000838.

[111] Hotamisligil GS. Endoplasmic reticulum stress and the inflammatory basis of metabolic disease. Cell.140(6):900-17. doi: 10.1016/j.cell.2010.02.034.

[112] Ogata M, Hino S, Saito A, Morikawa K, Kondo S, Kanemoto S, et al. Autophagy is activated for cell survival after endoplasmic reticulum stress. Mol Cell Biol. 2006;26(24):9220-31. doi: 10.1128/MCB.01453-06.

[113] Tao T, Tartakoff AM. Nuclear relocation of normal huntingtin. Traffic. 2001;2(6):385-94. doi: 10.1034/j.1600-0854.2001.002006385.x.

[114] Munsie L, Caron N, Atwal RS, Marsden I, Wild EJ, Bamburg JR, et al. Mutant huntingtin causes defective actin remodeling during stress: defining a new role for transglutaminase 2 in neurodegenerative disease. Hum Mol Genet. 2011;20(10):1937-51. doi: 10.1093/hmg/ddr075.

[115] Munsie LN, Desmond CR, Truant R. Cofilin Nuclear-Cytoplasmic Shuttling Affects Cofilin-Actin Rod Formation During Stress. J Cell Sci. doi: 10.1242/jcs.097667.

[116] Nath S, Munsie LN, Truant R. A huntingtin-mediated fast stress response halting endosomal trafficking is defective in Huntington's disease. Hum Mol Genet. 2015;24(2):450-62. doi: 10.1093/hmg/ddu460.

[117] DiGiovanni LF, Mocle AJ, Xia J, Truant R. Huntingtin N17 domain is a reactive oxygen species sensor regulating huntingtin phosphorylation and localization. Hum Mol Genet. 2016;25(18):3937-45. doi: 10.1093/hmg/ddw234.

[118] Choudhury KR, Bhattacharyya NP. Chaperone protein HYPK interacts with the first 17 amino acid region of Huntingtin and modulates mutant HTT-mediated aggregation and cytotoxicity. Biochemical and biophysical research communications. 2015;456(1):66-73. doi: 10.1016/j.bbrc.2014.11.035.

[119] Crick SL, Ruff KM, Garai K, Frieden C, Pappu RV. Unmasking the roles of N- and C-terminal flanking sequences from exon 1 of huntingtin as modulators of polyglutamine aggregation. Proc Natl Acad Sci U S A. 2013;110(50):20075-80. doi: 10.1073/pnas.1320626110.

[120] Tam S, Geller R, Spiess C, Frydman J. The chaperonin TRiC controls polyglutamine aggregation and toxicity through subunit-specific interactions. Nat Cell Biol. 2006;8(10):1155-62. doi: 10.1038/ncb1477.

[121] Chaibva M, Jawahery S, Pilkington AWt, Arndt JR, Sarver O, Valentine S, et al. Acetylation within the First 17 Residues of Huntingtin Exon 1 Alters Aggregation and Lipid Binding. Biophysical journal. 2016;111(2):349-62. doi: 10.1016/j.bpj.2016.06.018.

[122] Baias M, Smith PE, Shen K, Joachimiak LA, Zerko S, Kozminski W, et al. Structure and Dynamics of the Huntingtin Exon-1 N-Terminus: A Solution NMR Perspective. Journal of the American Chemical Society. 2017;139(3):1168-76. doi: 10.1021/jacs.6b10893.

[123] Van Raamsdonk JM, Pearson J, Rogers DA, Bissada N, Vogl AW, Hayden MR, et al. Loss of wild-type huntingtin influences motor dysfunction and survival in the YAC128 mouse model of Huntington disease. Hum Mol Genet. 2005;14(10):1379-92. doi: 10.1093/hmg/ddi147.

[124] Gu X, Cantle JP, Greiner ER, Lee CY, Barth AM, Gao F, et al. N17 Modifies mutant Huntingtin nuclear pathogenesis and severity of disease in HD BAC transgenic mice. Neuron. 2015;85(4):726-41. doi: 10.1016/j.neuron.2015.01.008.

[125] Cox B, Emili A. Tissue subcellular fractionation and protein extraction for use in mass-spectrometry-based proteomics. Nat Protoc. 2006;1(4):1872-8. doi: 10.1038/nprot.2006.273.

[126] Brewer GJ, Torricelli JR. Isolation and culture of adult neurons and neurospheres. Nat Protoc. 2007;2(6):1490-8. doi: 10.1038/nprot.2007.207.

[127] Zheng Z, Li A, Holmes BB, Marasa JC, Diamond MI. An N-terminal Nuclear Export Signal Regulates Trafficking and Aggregation of Huntingtin (Htt) Protein Exon 1*. J Biol Chem. 2013;288(9):6063-71. doi: 10.1074/jbc.M112.413575.

[128] Bradley A. Production and analysis of chimeric mice. In "Teratocarcinomas and Embryonic Stem Cells, a Practical Approach". Robertson EJ, editor: IRL Press, Inc., Oxford; 1987.

[129] Klionsky D, Abdalla FC, Abeliovich H, Abraham RT, Acevedo-Arozena A, Adeli K, et al. Guidelines for the use and interpretation of assays for monitoring autophagy. Autophagy. 2012;8(4):445-544. doi: 10.4161/auto.19496.

[130] Kabeya Y, Mizushima N, Ueno T, Yamamoto A, Kirisako T, Noda T, et al. LC3, a mammalian homologue of yeast Apg8p, is localized in autophagosome membranes after processing. Embo j. 2000;19(21):5720-8. doi: 10.1093/emboj/19.21.5720.

[131] Tanida I, Tanida-Miyake E, Komatsu M, Ueno T, Kominami E. Human Apg3p/Aut1p homologue is an authentic E2 enzyme for multiple substrates, GATE-16, GABARAP, and MAP-LC3, and facilitates the conjugation of hApg12p to hApg5p. J Biol Chem. 2002;277(16):13739-44. doi: 10.1074/jbc.M200385200.

[132] Tanida I, Tanida-Miyake E, Ueno T, Kominami E. The human homolog of Saccharomyces cerevisiae Apg7p is a Protein-activating enzyme for multiple substrates including human Apg12p, GATE-16, GABARAP, and MAP-LC3. J Biol Chem. 2001;276(3):1701-6. doi: 10.1074/jbc.C000752200.

[133] Pankiv S, Clausen TH, Lamark T, Brech A, Bruun JA, Outzen H, et al. p62/SQSTM1 binds directly to Atg8/LC3 to facilitate degradation of ubiquitinated protein aggregates by autophagy. J Biol Chem. 2007;282(33):24131-45. doi: 10.1074/jbc.M702824200.

[134] Ciani B, Layfield R, Cavey JR, Sheppard PW, Searle MS. Structure of the ubiquitin-associated domain of p62 (SQSTM1) and implications for mutations that cause Paget's disease of bone. J Biol Chem. 2003;278(39):37409-12. doi: 10.1074/jbc.M307416200.

[135] Lippai M, Low P. The role of the selective adaptor p62 and ubiquitin-like proteins in autophagy. BioMed research international. 2014:832704. doi: 10.1155/2014/832704.

[136] Murphy KP, Carter RJ, Lione LA, Mangiarini L, Mahal A, Bates GP, et al. Abnormal synaptic plasticity and impaired spatial cognition in mice transgenic for exon 1 of the human Huntington's disease mutation. J Neurosci. 2000;20(13):5115-23.

[137] Brandt J, Shpritz B, Munro CA, Marsh L, Rosenblatt A. Differential impairment of spatial location memory in Huntington's disease. Journal of neurology, neurosurgery, and psychiatry. 2005;76(11):1516-9. doi: 10.1136/jnnp.2004.059253.

[138] Boland B, Kumar A, Lee S, Platt FM, Wegiel J, Yu WH, et al. Autophagy Induction and Autophagosome Clearance in Neurons: Relationship to Autophagic Pathology in Alzheimer's Disease. J Neurosci. 2008;28(27):6926-37. doi: 10.1523/jneurosci.0800-08.2008.

[139] Mizushima N, Yoshimorim T, Levine B. Methods in Mammalian Autophagy Research. Cell. 2010;140(3):313-26. doi: 10.1016/j.cell.2010.01.028.

[140] Gray DA, Woulfe J. Lipofuscin and aging: a matter of toxic waste. Science of aging knowledge environment : SAGE KE. 2005;2005(5):re1. doi: 10.1126/sageke.2005.5.re1.

[141] Brunk UT, Terman A. Lipofuscin: mechanisms of age-related accumulation and influence on cell function. Free radical biology & medicine. 2002;33(5):611-9. doi: 10.1016/S0891-5849(02)00959-0.

[142] Davies SW, Turmaine M, Cozens BA, Raza AS, Mahal A, Mangiarini L, et al. From neuronal inclusions to neurodegeneration: neuropathological investigation of a transgenic mouse model of Huntington's disease. Philosophical transactions of the Royal Society of London Series B, Biological sciences. 1999;354(1386):981-9.

[143] Wall NR, De La Parra M, Callaway EM, Kreitzer AC. Differential innervation of direct- and indirect-pathway striatal projection neurons. Neuron. 2013;79(2):347-60. doi: 10.1016/j.neuron.2013.05.014.

[144] Fremeau RT, Jr., Troyer MD, Pahner I, Nygaard GO, Tran CH, Reimer RJ, et al. The expression of vesicular glutamate transporters defines two classes of excitatory synapse. Neuron. 2001;31(2):247-60. doi: 10.1016/S0896-6273(01)00344-0.

[145] Herzog E, Bellenchi GC, Gras C, Bernard V, Ravassard P, Bedet C, et al. The existence of a second vesicular glutamate transporter specifies subpopulations of glutamatergic neurons. J Neurosci. 2001;21(22):Rc181.

[146] Okerlund ND, Schneider K, Leal-Ortiz S, Montenegro-Venegas C, Kim SA, Garner LC, et al. Bassoon Controls Presynaptic Autophagy through Atg5. Neuron. 2017;93(4):897-913.e7. doi: 10.1016/j.neuron.2017.01.026.

[147] Wang G, Liu X, Gaertig MA, Li S, Li XJ. Ablation of huntingtin in adult neurons is nondeleterious but its depletion in young mice causes acute pancreatitis. Proc Natl Acad Sci U S A. 2016;113(12):3359-64. doi: 10.1073/pnas.1524575113.

[148] Kegel KB, Sapp E, Yoder J, Cuiffo B, Sobin L, Kim YJ, et al. Huntingtin associates with acidic phospholipids at the plasma membrane. J Biol Chem. 2005;280(43):36464-73. doi: 10.1074/jbc.M503672200.

[149] Kassubek J, Juengling FD, Kioschies T, Henkel K, Karitzky J, Kramer B, et al. Topography of cerebral atrophy in early Huntington's disease: a voxel based morphometric MRI study. Journal of neurology, neurosurgery, and psychiatry. 2004;75(2):213-20. doi: 10.1136/jnnp.2002.009019.

[150] Kassubek J, Juengling FD, Ecker D, Landwehrmeyer GB. Thalamic atrophy in Huntington's disease co-varies with cognitive performance: a morphometric MRI analysis. Cerebral cortex (New York, NY : 1991). 2005;15(6):846-53. doi: 10.1093/cercor/bhh185.

[151] Ravikumar B, Vacher C, Berger Z, Davies JE, Luo S, Oroz LG, et al. Inhibition of mTOR induces autophagy and reduces toxicity of polyglutamine expansions in fly and mouse models of Huntington disease. Nat Genet. 2004;36(6):585-95. doi: 10.1038/ng1362.

[152] Sapp E, Schwarz C, Chase K, Bhide PG, Young AB, Penney J, et al. Huntingtin localization in brains of normal and Huntington's disease patients. Ann Neurol. 1997;42(4):604-12. doi: 10.1002/ana.410420411.

[153] Koga H, Martinez-Vicente M, Arias E, Kaushik S, Sulzer D, Cuervo AM. Constitutive upregulation of chaperone-mediated autophagy in Huntington's disease. J Neurosci. 2011;31(50):18492-505. doi: 10.1523/jneurosci.3219-11.2011.

[154] Kuhn A, Thu D, Waldvogel HJ, Faull RL, Luthi-Carter R. Population-specific expression analysis (PSEA) reveals molecular changes in diseased brain. Nature methods. 2011;8(11):945-7. doi: 10.1038/nmeth.1710.